

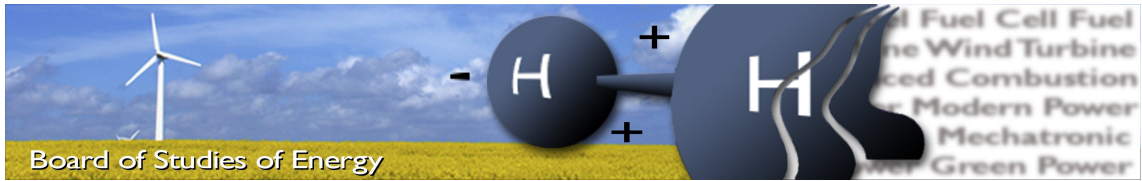
# Carbon Capture & Sequestration

## Integrating a MEA based CCS system at Nordjyllands Værket Unit 3

Mark Burgdorf Herskind & David Egede Fich, Group 1042, TEPE4

June 2, 2009





**Title:** Carbon Capture & Sequestration  
Integrating a MEA based CCS system at Nordjyllands Værket Unit 3

**Semester:** 4th, group 1042

**Semester theme:** Master Thesis

**Project period:** 01.02.09 to 03.06.09

**ECTS:** 30

**Supervisor:** Thomas Joseph Condra

---

David Egede Fich

---

Mark Burgdorf Herskind

#### SYNOPSIS:

This project concerns integration of a MEA based CCS cycle at a pulverized coal power plant, Nordjyllandværket Unit 3. The project consists of 3 parts. The first part concerns the state of the art, describing available technology and the state of the research. The second part addresses the formulation of models of the steam cycle and the CCS unit in EES. The last part concerns the integration of the models.

A study of the steam cycle confirms the outlet of the IP1 turbine as the most suitable for CCS addition, thus the integration proposal of the report is based on this stream. As the cooling water from a CCS unit represents vast quantities of heat, the solution proposal of this work includes a set of heat pumps utilizing the waste heat for district heating.

In conclusion, the models and the integration has been a success. The system with added heat pumps yields relatively low drops in plant output.

Copies: 2  
Pages, total: 132  
Appendices: 3

**By signing this document, each member of the group confirms that all participated in the project work and thereby all members are collectively liable for the content of the report.**



# Project summary

This project is an investigation of the feasibility of integrating a CCS unit at the pulverised coal fired unit 3 at Nordjyllandsværket. The project has been made in cooperation with the plants owner, Vattenfall. Vattenfall has a vision of being a low emission energy producer, and are investing in a multitude of technologies to decrease their carbon footprint. Part of this effort is decreasing CO<sub>2</sub> emissions from their existing fossil fuelled power plant fleet. One of the investigated approaches is to implement CCS systems in their plants. To gain experience in this field, Vattenfall is working with a number of the foremost companies in the world, as well as having their own engineers working to integrate a CCS unit at NJV Unit 3. Nordjyllandsværket has been chosen as the test site for this project, as the plant is one of the most efficient power plants in the world today, thus the CO<sub>2</sub>/MW rate is very low, resulting in a lower relative cost of capture.

The scope of this project has been to gather the necessary information on the state of the art, and evaluate the different technologies for potentials, create simplified models of the steam cycle and the CCS unit, and obtaining a feasible integration proposal.

The information gathering has been done through the available literature on the subject, including books, articles, and the internet, but even more through participation in the 8th Annual Conference of Carbon Capture and Sequestration in Pittsburgh, USA. This effort has resulted in a chapter describing the most promising technologies in terms of state of maturity. Furthermore the chapter tries to give a short introduction to how a given capture method works and how it affects the layout of a power plant. The conclusion of this chapter is, that even though Vattenfall is focused on a MEA based capture unit, which still is the only technology at a maturity level suitable for full scale integration, other solvents and technologies yields great potentials.

The models has been written in Engineering Equation Solver (EES). The modelling of the steam cycle has been an effort of creating a model as simple as possible, while still maintaining a sufficient level of accuracy both in full load and partial loads. Since a unit like NJV3 is a very complex unit, including 10 feed water heat exchangers, 9 turbines, district heating, and double steam re-heating, building a simple model is still a very tedious work, resulting in a very complex set of equations. As EES, as most other iterative solvers, is based on Newton-Raphson iteration, limits and guesses for the variables of the system is of high importance for a succesfull convergence. For a system of high complexity with only limited data available, guesses can be hard or even impossible to provide, thus hindering the convergence of the system. Despite this, the steam cycle converges at all load cases and predicts model behaviour with a high degree of precision. The CCS unit has been build on basis of information given by Jens Møller Andersen (Vattenfall). The information given only covers the full load case. Due to this, the model of the CCS is only valid for a full load simulation, and can not be expected to depict the system at other loads.

The integration phase of the project holds an analysis of the steam cycle. As the CCS unit needs a certain amount of heat at a given temperature, there are limitations as to where in the steam cycle the heat can be extracted. The purpose of the analysis is to extract steam three different places in the steam cycle while monitoring the energy penalty imposed on the system. The analysis yields a stream most suitable for extraction, while also revealing model vulnerabilities to extraction at certain points, as a result of insufficient guess values. On basis of the results of the analysis, the CCS unit is integrated into the steam cycle model, yielding a small loss in electricity production and a substantial loss in district heat production. While these results seem perfectly in order, the cost penalty on the system is far too high for an economically viable plant. Hence, further integration is needed in order to optimize plant performance. The approach of this work has been to utilize the waste heat, as a CCS unit of the type modelled for this project has a quite substantial waste heat, amounting to 309 MW. As this waste heat is of low temperature, it can not be used, as is, to increase the efficiency of the plant. The proposal of this project is to increase the quality of the heat by implementing a set of heat pumps. A heat pump is a system enabling transfer of heat from a low temperature to a high temperature reservoir, by utilizing that the saturation temperature of fluid changes with pressure. A crude heat pump model has been built in EES and implemented into the joined model. By using these simple models it is possible to recuperate a total of 195.33 MW of heat. The pressure difference of a heat pump is maintained by a pump. For the heat pumps of this project, the total energy required by the heat pumps amounts to 34.35 MW. Thus the loss in district heating output is minimized on expense of electric output.

In conclusion, the models of the project reasonably model the expected performance of Nordjyllandsværket Unit 3, and displays a feasible performance when integrating a CCS unit and a set of heat pumps. As expected, the unit will impose a severe cost penalty to the plant, but the integration attempt of this project reveals that a well designed integration can minimize the actual penalty of integration.

# Preface

This report is a Masters thesis from Aalborg University, Denmark, on the Thermal Energy and Process Engineering line at the Institute of Energy Technology. The topic of the report is integration of a Carbon Capture and Sequestration (CCS) unit at Nordjyllandsværket Unit 3. The report has been written on the basis of a project done in collaboration with Vattenfall A/S, who has provided the authors with data and information during the project period from 01/02 2009 to 03/06 2009.

The report comes with an additional CD containing the numerical models developed in this project as well as a pdf-version of the report. The authors would like to thank Jeppe Grue, Ph.D., and Jens Møller Andersen, M.Sc., both at Vattenfall A/S for their support.

The authors have during the project participated in the 8th Annual Conference on Carbon Capture and Sequestration in Pittsburgh, Pennsylvania, with great benefit and would like to thank Vattenfall A/S, Aalborg University and the Institute of Energy Technology for funding.

Contact information of the authors can be seen below.

- David Egede Fich, Tlf.: +45 27 12 80 99, email: davidfich@jubii.dk
- Mark Burgdorf Herskind, Tlf.: +45 22 38 80 67, email: mark@mark-h.dk

## Readers guide

This report comprises 3 major parts. The first part contains an introduction to the problem and a state of the art description. This results in a conclusion pertaining to the available CCS technologies. The second part contains a detailed description of the steam cycle model, which can be fairly heavy reading, and a description of the CCS model. The last part contains a study of the integration of the CCS unit in the plant through the steam cycle and CCS model and contains the kernel of the practical application of the project. Please note that the problem statement is not presented until chapter 5. Also in this report % point indicates relations between percentages, e.g. from 47 % to 42 % there is a drop of 5 % points. In the following an outline of the report can be seen with a short description of each chapter.

### **PART 1**

- Chapter 1: Introduction; Description of the problem presented to the authors.
- Chapter 2: The broad perspective; The broad motivation for CCS and CCS's role in mitigating CO<sub>2</sub> emissions.

- Chapter 3: State of the art; Description of available and future technologies and research activities in CCS with information obtained at the 8th Annual Conference on Carbon Capture and Sequestration.
- Chapter 4: The MEA process; Description of the MEA process chosen for CCS in this project.
- Chapter 5: Problem statement; Definition of the purpose and goals of the project and the method of fulfilling these.

## **PART 2**

- Chapter 6: The steam cycle at NJV 3; Description of the steam cycle as designed at NJV 3 when running in full district heating mode.
- Chapter 7: The component models; Detailed description of the modelling of each component in the steam cycle model. The detail level can make this chapter tedious reading.
- Chapter 8: The steam cycle model; Description of the integrated model of the steam cycle with simplifications and presentation of model results.
- Chapter 9: CCS model; Description of the MEA CCS unit model.

## **PART 3**

- Chapter 10: CCS integration; Analysis of the steam cycle sensitivity to heat removal, combining the models into a single steam cycle CCS model, analysis of the effects of CCS on steam cycle performance, presentation of a suggestion to integrate the CCS unit with minimum efficiency loss.
- Chapter 11: Conclusions.
- Appendix A: The boiler model: A model of the boiler at NJV 3 is presented which has multiple purposes not all used in this report.
- Appendix B: Numerical methods in EES: Presentation of the solver method used in Engineering Equation Solver (EES).
- Appendix C: Steam tables: Presentation of the historical differences between the steam tables used here and the state of the art steam tables today.

# Contents

<b>Preface</b>	<b>v</b>
Readers guide . . . . .	v
<b>List of figures</b>	<b>xiii</b>
<b>List of tables</b>	<b>xvi</b>
<b>Nomenclature</b>	<b>xvii</b>
<b>I Report</b>	<b>1</b>
<b>1 Introduction</b>	<b>3</b>
<b>2 The broad perspective</b>	<b>5</b>
2.1 Global CO <sub>2</sub> emissions . . . . .	5
<b>3 State of the art</b>	<b>9</b>
3.1 Overview of considered technologies . . . . .	9
3.2 Technology state and activity . . . . .	13
3.3 State of the art conclusion . . . . .	22
<b>4 The MEA process</b>	<b>23</b>
<b>5 Problem statement</b>	<b>27</b>
5.1 Problem definition . . . . .	27
5.2 Method and limitations . . . . .	27

---

<b>6</b>	<b>The steam cycle at NJV3</b>	<b>29</b>
6.1	The steam cycle . . . . .	29
<b>7</b>	<b>The component models</b>	<b>33</b>
7.1	The modelling strategy . . . . .	33
7.2	The turbine model . . . . .	34
7.3	The boiler model . . . . .	40
7.4	Heat exchanger models . . . . .	41
7.5	The pump model . . . . .	47
7.6	The tank model . . . . .	48
7.7	The condenser model . . . . .	49
7.8	The pipe model . . . . .	50
7.9	Component models conclusion . . . . .	51
<b>8</b>	<b>The steam cycle model</b>	<b>53</b>
8.1	Steam cycle simplifications . . . . .	53
8.2	Physical simplifications . . . . .	55
8.3	Model results . . . . .	57
8.4	Steam cycle model convergence . . . . .	59
8.5	Steam cycle model conclusion . . . . .	61
<b>9</b>	<b>CCS model</b>	<b>63</b>
9.1	The model in words . . . . .	63
9.2	The parameters of the model . . . . .	65
9.3	The mathematics . . . . .	67
9.4	CCS model conclusion . . . . .	69
<b>10</b>	<b>CCS Integration</b>	<b>71</b>
10.1	Sensitivity analysis . . . . .	71
10.2	Sensitivity discussion . . . . .	79
10.3	Integration of the models . . . . .	80
10.4	Integration in EES . . . . .	82

---

10.5 CCS Performance . . . . .	82
10.6 Integrated results . . . . .	83
10.7 Improvement idea . . . . .	84
10.8 Heat pumps . . . . .	84
10.9 Integration of the model . . . . .	86
10.10 Integration of heat pumps in EES . . . . .	88
10.11 Flexibility . . . . .	88
10.12 Chapter conclusion . . . . .	89
<b>11 Conclusion</b>	<b>91</b>
<b>II Appendices</b>	<b>93</b>
<b>A The boiler model</b>	<b>95</b>
A.1 The boiler characteristics . . . . .	95
A.2 Model overview . . . . .	96
A.3 The heat exchanger model . . . . .	97
A.4 Radiation heat exchange . . . . .	99
A.5 The flue gas side . . . . .	100
A.6 The boiler model results . . . . .	100
<b>B Numerical methods in EES</b>	<b>103</b>
<b>C Steam tables</b>	<b>107</b>
<b>Bibliography</b>	<b>108</b>



# List of Figures

2.1	Temperature anomaly development over the last century compared to the 1901-2000 average, (EPA, 2009b). . . . .	5
2.2	The global CO <sub>2</sub> emission over the last century, (EPA, 2009b). . . . .	6
2.3	Correlation between atmospheric CO <sub>2</sub> content and global temperatures, (EPA, 2009b). . . . .	6
2.4	The full portfolio effect on US CO <sub>2</sub> emissions according to the PRISM analysis, (EPRI et al., 2008). . . . .	7
3.1	Conceptual drawing of an oxyfuel system (Clarke et al., 2004) . . . . .	11
3.2	Sketch of a chemical absorption system (Herzog and Golomb, 2004) . . . . .	11
3.3	Schematic overview of an IGCC unit (EPRI et al., 2008) . . . . .	14
3.4	Diagram of energy demand versus cyclic capacity of solvents, (Northemann et al., 2009). . . . .	17
3.5	Technology Readiness Levels as posed by NASA, (Bhown, 2009). . . . .	19
3.6	Diagram of technology readiness level dependent on technology type, (Bhown, 2009). . . . .	20
3.7	Diagram of general progress in establishing larger test facilities. . . . .	21
3.8	The cost of development in development phases and the different technologies development level in 2008, modified from EPRI et al. (2008). . . . .	21
4.1	Sketch of the proposed system for NJV3 (Andersen and Köpcke, 2007) . . . . .	23
4.2	Cycle proposed by Vattenfall (Andersen and Köpcke, 2007) . . . . .	24
4.3	Fluegas temperature as function of flue gas temperature (Andersen and Köpcke, 2007) . . . . .	24
4.4	Minimum stripper energy as function of pressure (Andersen and Köpcke, 2007). . . . .	25

6.1	Diagram of the steam cycle with major components and flows. Thick lines signify steam flows. Based on Alstom (1993). . . . .	30
6.2	Diagram of the Rankine cycle used at NJV3 (Grue, 2009c). . . . .	31
7.1	Diagram of the energy balance over a heat turbine. . . . .	34
7.2	Diagram of a realistic turbine installation. . . . .	36
7.3	Diagram of the division of the steam turbines. Note that the LP turbines are not modelled and therefore not numbered. Steam sealing inlets and outlets are signified by small arrows. . . . .	36
7.4	Diagram of the steam inlets and outlets in the VHP turbine. . . . .	37
7.5	Diagram of preheater 10 with steam and feed water flow. . . . .	41
7.6	Diagram of the condenser heat exchanger. . . . .	44
7.7	Diagram of the doubleflow condensation model. . . . .	46
7.8	Diagram of pump with boundary variables. . . . .	47
7.9	Diagram of a feed water tank with inlet and outlet streams. . . . .	48
7.10	Diagram of the condenser model with boundary conditions. . . . .	49
8.1	The simplified steam cycle used in the steam cycle model. . . . .	54
8.2	The condensing chamber of the heat exchangers. . . . .	55
8.3	Diagram of free inlet to promote convergence. . . . .	60
9.1	Sketch of the cooling system. Edited drawing from Andersen and Köpcke (2007). . . . .	64
9.2	CCS unit with integrated district heating (Andersen, 2009a). . . . .	65
9.3	Proposals to the system at NJV3 (Andersen, 2009a). Only the configuration of the components is important in this figure. . . . .	65
9.4	Graph depicting specific boiler duty as a function of LG Ratio and pinch temperature (Andersen and Köpcke, 2007). . . . .	66
9.5	Pumping sketch . . . . .	68
10.1	Power loss in MW due to extraction of steam from the IP1 turbine as a function of steam pressure and mass flow rate, (Andersen, 2009a) . . . . .	72
10.2	The selected points for sensitivity analysis in the steam cycle. . . . .	73
10.3	Electricity production under varying heat removal at point 1. . . . .	74
10.4	Heat production as a function of heat removal at point 1. . . . .	74

10.5	The electric efficiency as a function of heat removal at point 1. . . . .	75
10.6	The thermal efficiency as a function of heat removal at point 1. . . . .	75
10.7	The electricity production and the electric efficiency as a function of heat removal in point 2. . . . .	76
10.8	District heating production as a function of heat removal in point 2. . . . .	76
10.9	Thermal efficiency as a function of heat removal in point 2. . . . .	77
10.10	Electricity production as a function of heat removal in point 3. . . . .	77
10.11	Production of district heating as a function of heat removal at point 3. . . . .	78
10.12	Electric efficiency as a function of heat removal in point 3. . . . .	78
10.13	Thermal efficiency as a function of heat removal at point 3. . . . .	79
10.14	NJV3 with CCS system . . . . .	81
10.15	Conceptual drawing of a heat pump (Aye, 2007) . . . . .	84
10.16	Conceptual drawing of the modelled system . . . . .	85
10.17	Sketch of the proposed system . . . . .	87
10.18	Sketch of plant with capability of switching of the CCS unit . . . . .	90
A.1	Diagram of the flow through the boiler, (Grue, 2009b). . . . .	96
A.2	An overview of the series of heat exchangers used in the boiler model 1st run. Steam flows from the left to the right. . . . .	97
A.3	The value of specific heat capacity for steam dependent on temperature. . . . .	98
A.4	Flow diagram of the flue gas through the boiler . . . . .	101
A.5	Graph depicting efficiency of the first boiler circuit. . . . .	102
B.1	Residual of $x^3 - 3.5x^2 + 2x = 10$ (Klein, 2009) . . . . .	105
C.1	The 5 regions in which the steam formulas are divided (IAPWS, 2007) . . . . .	108



# List of Tables

2.1	The global emission of CO <sub>2</sub> distributed on sectors, (WRI, 2009). . . . .	7
7.1	Table of thermal efficiencies of turbines from two calculation methods. . . . .	38
7.2	Average deviation of power output, output enthalpy and output pressure. The numbers indicate first or second part of the turbine. . . . .	39
7.3	Boiler efficiency for the primary heating and the two reheatings. . . . .	40
7.4	Table of thermal resistances of heat exchanger 10 based on load (mass flow rate) and deviation of output steam temperature in percent. . . . .	43
7.5	Table of thermal resistances of condenser 9 and 6 based on load (mass flow rate) and deviation of output feed water temperature and saturation temperature. . . . .	45
7.6	Table of thermal resistances of heat exchanger 8 based on load (mass flow rate) and deviation of output feed water temperature and saturation temperature. . . . .	46
7.7	$K_L$ -values for all 16 pipes. . . . .	51
8.1	Turbines share in electricity production in the model and in the Alstom heat balances. . . . .	58
8.2	Detailed view of steam cycle model predictions of selected variables at full load. . . . .	58
10.1	Key parameters for the steam cycle found by sensitivity analysis and extrapolated to a heat removal of 206 MW. . . . .	79
10.2	Results of the CCS unit . . . . .	83
10.3	Key variables of initial integration . . . . .	83
10.4	Key variables of heat pumps . . . . .	85
10.5	Key variables of second integration . . . . .	88
A.1	Comparison of predicted model values with nominal values from the boiler documentation. . . . .	100

A.2 Predicted first circuit boiler efficiency for varying load case. . . . . 102

A.3 Thermal resistance, R, for different load cases. All values are in K/W. . . . . 102

# Nomenclature

$CR$	Compression rate
$D$	Diameter [ $m$ ]
$I$	Tabulated coefficient
$J$	Tabulated coefficient
$L$	Length [ $m$ ]
$LHV$	Lower Heating Value [ $\frac{kJ}{kg}$ ]
$P$	Pressure [ $bar$ ]
$Q_H$	Heat transfer from working fluid [ $kJ$ ]
$Q_L$	Heat transfer to working fluid [ $kJ$ ]
$R$	Universal gas constant [ $\frac{kJ}{kg \cdot K}$ ]
$T$	Temperature [ $C$ ]
$V$	Velocity [ $\frac{m}{s}$ ]
$W$	Pump Work [ $W$ ]
$W$	Work and power output [ $W$ ]
$\Delta x$	Step size
$\Delta z$	Height difference [ $m$ ]
$\dot{m}$	Mass flow [ $\frac{kg}{s}$ ]
$\epsilon$	Residual
$\eta$	Efficiency
$\gamma$	Dimensionless number, [ $\frac{g}{RT}$ ]
$\pi$	Pressure ratio
$\rho$	Density [ $\frac{kg}{m^3}$ ]
$\tau$	Temperature ratio

$f$	Friction factor
$g$	Acceleration due to gravity [ $\frac{m}{s^2}$ ]
$g$	Gibbs Free Energy [ $\frac{kJ}{kg}$ ]
$h$	Enthalpy [ $\frac{kJ}{kg}$ ]
$n$	Stages (in compression)
$n$	Tabulated coefficient
$s$	Entropy [ $\frac{kJ}{kg \cdot K}$ ]

**Part I**

**Report**



# Chapter 1

## Introduction

One of the greatest challenges in modern times is global warming caused by anthropogenic carbon dioxide emissions. The CO<sub>2</sub> emissions primarily originates from three sectors; industry, transportation and power generation. The largest contributor is the power generation sector. In the United States power generation from fossil fuels represented approximately 40 % of the total CO<sub>2</sub> emissions in 2007, producing 2.4 billion tonnes (EPA, 2009a). Due to this, and the fact that the emissions by industry and transportation are spread over a lot of sources across the world, it makes sense to focus on the single large source; fossil fuelled power plants.

A variety of different approaches to decrease or even eliminate these emissions has been proposed. Most of the proposed technologies are still in their infancy and yield high cost penalties. Due to this, the environmental organisation Greenpeace deems Carbon Capture and Storage (CCS) as a "false hope", as CCS in their opinion is not able to affect CO<sub>2</sub> emissions soon enough, exploits potentially dangerous storage and has severe energy penalties (Rochen, 2008). Certainly there are problems to overcome.

Vattenfall has a promoted goal of being an environmentally responsible energy producer with the ambition of being CO<sub>2</sub> neutral by 2030. They mainly work in three areas; Optimization of existing technology to improve efficiency of power plants, increased use of zero emission energy sources, and carbon capture and storage systems for fossil fuelled power plants (Vattenfall, 2009). Nordjyllandsværket Unit 3 (NJV 3) has been chosen for a pilot project for carbon capture, as this plant has a high efficiency, thus the CO<sub>2</sub>/MW ratio is low, yielding lower relative cost penalty.

Vattenfall A/S has decided to design and construct a retrofitted CCS unit at NJV 3. The CCS unit has been chosen to be a fluid bed absorber system based on the well known solvent MonoEthanolAmine (MEA). The MEA CCS unit requires energy in the form of both heat and electricity to run, which will be extracted from the steam cycle and generators at NJV 3.

At the CASTOR test facility in Esbjerg, Denmark, DONG Energy has been experimenting with a CCS system operating of a small part of the flue gas stream. Through their best effort, they reduced the energy consumption to 3,7 *GJ* pr ton of CO<sub>2</sub> produced (Djursing, 2007). Yielding an approximate energy consumption of 286 *MW* for NJV 3, which is an absurdly high cost compared to the total capacity at 100 % load of 411 *MW* (Vattenfall, 2008).

Therefore it is necessary to conduct a study of integration of the CCS unit. This study proposes to perform such a study with limitations as described in Chapter 5.

In short, the initiating problem of the project therefore is:

*How can a MEA based carbon capture system be integrated at NJV 3, in order to minimize the cost penalties as much as possible?*

## Chapter 2

# The broad perspective

*The motivation for conducting studies of integration of a CCS unit at NJV 3 originates from issues of such a global nature that notions of world economics, global climate changes and conservation of polar regions is mentioned often in political debate. This chapter is a prelude to the rest of the report and aims to give a short description of the problem from the broadest point of view and to describe the role of carbon capture at NJV 3 in this context. This chapter is largely based on EPA (2009b) and EPRI et al. (2008).*

### 2.1 Global CO<sub>2</sub> emissions

Looking at the data collected over the past century temperatures seem to be rising across the world. This gives reason to concern since a continuous tendency of rising temperatures can have dire consequences for the world. Apart from rising sea level due to melting polar caps, extinction of certain animal species in the polar regions and severe draught in the third world due to local climate changes predictions has gone so far as to indicate that rising temperatures can set off a new ice age. In Figure 2.1 the global temperature development in this century can be seen.

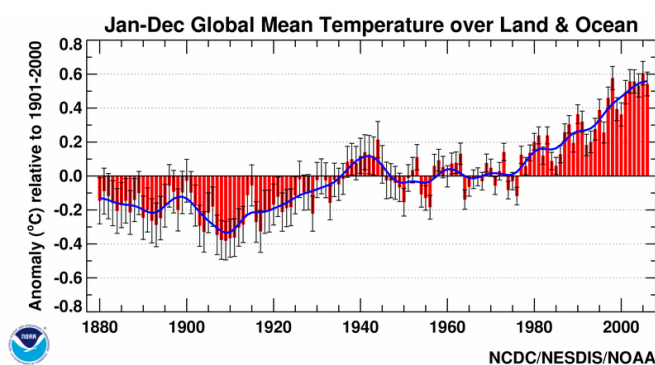


Figure 2.1: Temperature anomaly development over the last century compared to the 1901-2000 average, (EPA, 2009b).

The theory of climate researchers is that there is a connection between anthropogenic CO<sub>2</sub> emissions and globally rising temperatures. It is known that green house gasses such as CO<sub>2</sub> traps heat in the atmosphere, (EPA, 2009), but it is still unproven that the human emissions of green house

gases are the reason for increasing temperatures at this moment. However, this hypothesis seem to be supported by the development of CO<sub>2</sub> emissions over the last century, see Figure 2.2.

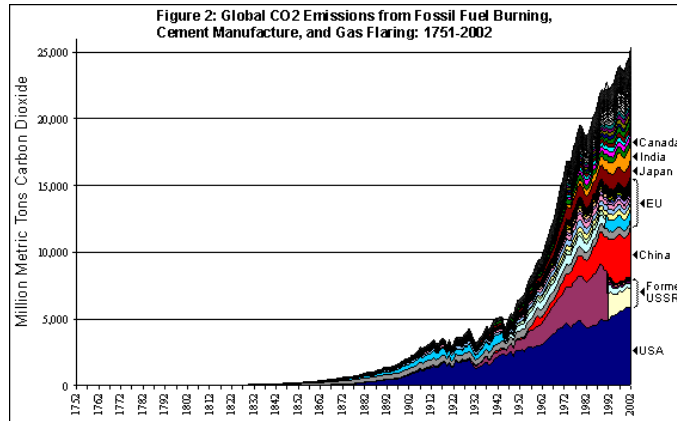


Figure 2.2: The global CO<sub>2</sub> emission over the last century, (EPA, 2009b).

Even more outspoken is the connection between CO<sub>2</sub> content in the atmosphere and global temperature when it is studied over a longer period. In Figure 2.3 the correlation between CO<sub>2</sub> content in the atmosphere and global temperatures can be seen over a period of several hundred thousand years.

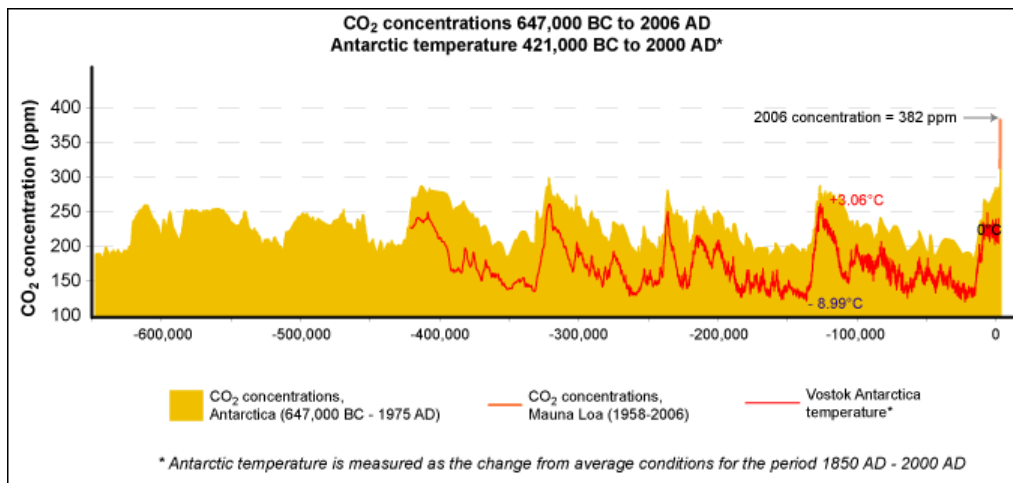


Figure 2.3: Correlation between atmospheric CO<sub>2</sub> content and global temperatures, (EPA, 2009b).

The proposed list of consequences of continued global warming is almost endless. EPA (2009b) states that negative effects of global warming extends into public health, agriculture and food supply, ecosystems and biodiversity, forests, water resources, energy production and use, extreme weather and coastal zones and sea level among others. With such a wide area of effect of global warming it is impossible to put a price on the effects and a whole range of economic models are used to predict the overwhelming economic consequences of continued global warming (EPA, 2009b). It should be noted here that not all effects of global warming is negative but it is generally agreed upon that the negative effects will influence areas that are already economically weak.

The global CO<sub>2</sub> emissions in 2001 reached 27898.6 million metric tons distributed on several different sectors, as can be seen in Table 2.1.

Sector	Electricity and heat	Other energy industries	Manufacturing & construction	Transportation	Residential	Agricultural & other
Share %	37.2	4.7	16.8	18.4	7.8	5.6

Table 2.1: The global emission of CO<sub>2</sub> distributed on sectors, (WRI, 2009).

As can be seen in Table 2.1 the electricity and heat production sector is the largest of the contributors to global CO<sub>2</sub> emissions. Considering that this sector also holds the largest single point sources, as opposed to the many small sources of for example transportation or residential, it is the obvious place to begin mitigation of CO<sub>2</sub> emissions.

The electricity and heat sector is, however, to expect large increases in demand over the next decades. EPRI et al. (2008) states that while the worlds population is expected to increase by 36 % from 6.1 to 8.3 billion people by 2030, the worlds electric power generation is expected to climb 110 % from 14426 billion kWh in 2000 to 30364 billion kWh in 2030. If the electricity and heat sector is to mitigate CO<sub>2</sub> releases, while still being able to respond to the growing standard of living, drastic measures must be taken in the near future.

According to EPRI et al. (2008) no single technology will be able to meet the necessary CO<sub>2</sub> emission mitigation. They work with a so-called "full portfolio" of technologies that together can comprise a solution to the problem of meeting demands of electricity while still mitigating CO<sub>2</sub> emissions in the US. In Figure 2.4 the effect of implementing a full portfolio of advanced technologies on CO<sub>2</sub> emissions can be seen.

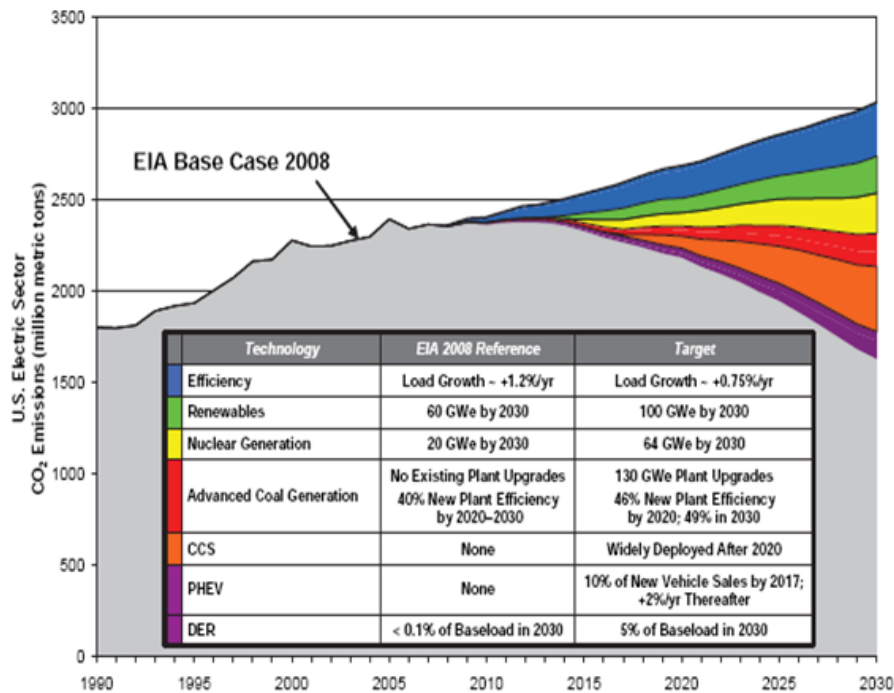


Figure 2.4: The full portfolio effect on US CO<sub>2</sub> emissions according to the PRISM analysis, (EPRI et al., 2008).

The full portfolio includes an increase in efficiency of the electrical grid that reduces the load increase from 1.2 % per year to 0.75 % per year, an increase in use of CO<sub>2</sub> neutral renewables from 60 GWe to 100 GWe in 2030, an increase in nuclear production from 20 GWe to 64 GWe, an increase in plant efficiency from 40 % to 49 %, 36 % Plug-in Hybrid Vehicles on the road, an increase in DER from below 0.1 % to 5 % of the baseload and finally a wide deployment of CCS by 2030. This should enable the US electrical sector to reduce the CO<sub>2</sub> emissions by 45 % as compared to the EIA base case to approximately 1990 levels.

As can be seen CCS is only one of the necessary technologies necessary to mitigate CO<sub>2</sub> emissions from the electric sector while the electric sector is only part of the total emission of CO<sub>2</sub>. Considering that the MEA technology considered in this project is only one of the technologies necessary to implement CCS in the electrical sector it becomes apparent what a challenge the electrical sector as well as society in general faces over the next decades.

## Chapter 3

# State of the art

*The purpose of this chapter is to give the reader an overview of the available techniques on the market for CO<sub>2</sub> capture along with an insight into the current advances and lines of development. This is done in two ways; firstly an overview of CO<sub>2</sub> capture techniques based on a number of articles is given, and secondly further insight into active areas of development and state of progress in CO<sub>2</sub> capture technology is given, based on several articles and lectures given at the 8th Annual Conference on Carbon Capture and Sequestration held in Pittsburgh, Pennsylvania on the 4th to 7th of May, 2009. It has been chosen to separate the information found in articles and the information from the conference in this way. Also this chapter aims to provide the means to draw a conclusion as to whether the MEA absorption process chosen by Vattenfall is prudent for Carbon Capture at Nordjyllandsværket Block 3.*

### 3.1 Overview of considered technologies

In this section an overview of potential technologies to mitigate CO<sub>2</sub> emissions is given based on articles published between 1997 and 2008. The technologies presented are not necessarily suitable for CO<sub>2</sub> reduction at Nordjyllandsværket or even realistically applicable but merely an indication of the possibilities considered by researchers so far.

#### 3.1.1 Phytoremediation

Phytoremediation is the process of removing pollutants utilizing vegetation. The idea of this technique is to use a plant with a high CO<sub>2</sub> removal rate to extract the pollutant from the flue gas. The technique is still at the development state, currently aiming at establishing knowledge on removal rates of plants. An investigation has been carried out by Rhee and Iamchaturapatr (2008) dealing with CO<sub>2</sub> uptake in five different wetland plants. The investigation was performed in an environment with a controlled rate of CO<sub>2</sub>, nutrition for the plants, ambient air, water and light. Through a series of tests, both with continuous CO<sub>2</sub> flow and a batch approach, the uptake of these species has been determined.

The investigations yield removal rates between 0.76 and 1.21 g/m<sup>2</sup>h with better removal rates for the batch experiments, owing to better time for reactions since the CO<sub>2</sub> is not swept away from the

plant by the continuous mass flow. These values are estimated to rise to approximately 24 g/m<sup>2</sup>h for a full scale system exposed to sunlight radiation rather than a fluorescent lamp of 40 W.

The information gathered from investigations like this will eventually provide the data needed to assess whether phytoremediation may be a feasible alternative for CO<sub>2</sub> removal.

### 3.1.2 Membranes

Membranes that can separate CO<sub>2</sub> from the flue gas is a known possibility for Carbon Capture. There is currently a selection of membranes being tested for CO<sub>2</sub> capture. Favre et al. (2008) describes how these can be integrated in a biogas plant and presents some pros and cons throughout the article. For a membrane to work efficiently, a high CO<sub>2</sub> concentration (> 30 %) and a considerable pressure is recommended. For a typical power plant the CO<sub>2</sub> concentration in the flue gas is expected to be between 3 and 20 % (Favre et al., 2008; Hultman, 2007; Marion et al., 2008) and the pressure close to atmospheric. This calls for implementation of further preprocessing to raise the concentration and the pressure in the flue gas. The common way to do so is a pre-combustion measure, such as using an oxygen rich mixture for the combustion (Favre et al., 2008), which may increase the CO<sub>2</sub> concentration to above 80 % (Gupta et al., 2003). Of course, increasing the oxygen level also consumes energy, and this energy consumption must be taken into account, when evaluating the efficiency of the membranes. In the work done by Favre et al. (2008) an oxygen concentration of approximately 40 % was used.

Since the oxy-fuel combustion process is quite costly due to the cryogenic method used today, a number of other methods are being developed to lower the expense (Gupta et al., 2003). For more on oxy-fuel see Section 3.1.3 and Section 3.2.1.

The conclusion of the text by Favre et al. (2008) is that the method of using membranes for carbon capture seems feasible and that membranes may play a decisive role in carbon capture technology when concentrated streams of CO<sub>2</sub> needs to be treated. Furthermore the text states that the use of membranes seems most reasonable for medium scale units from 1-100 MW. In conclusion the authors recommends that further studies are conducted on the subject.

Membranes, as they are today, does not allow for an effective capture process using a single membrane. Hence the technology calls for multiple passes through the same membrane or multiple membranes in series (Hultman, 2007), inevitably increasing the capital cost of the unit.

### 3.1.3 Oxy-fuel combustion

The method of increasing the oxygen content in the combustion air to raise the concentration of CO<sub>2</sub> is not only useful when considering membranes but can also be used as part of a CO<sub>2</sub> capturing system in itself. There are a number of ways being investigated, as of how to separate the oxygen from the ambient air. Currently, the method of cryogenic separation is the method of choice (Clarke et al., 2004). As such, cryogenic separation of nitrogen would be used to produce an almost pure oxygen stream which, in combustion, would only produce H<sub>2</sub>O and CO<sub>2</sub> along with some SO<sub>x</sub>'s. The SO<sub>x</sub>'s can be removed in conventional manner leaving only H<sub>2</sub>O and CO<sub>2</sub> where H<sub>2</sub>O could easily be removed through condensation leaving a stream of almost pure CO<sub>2</sub> (EPRI et al., 2008), see Figure 3.1.

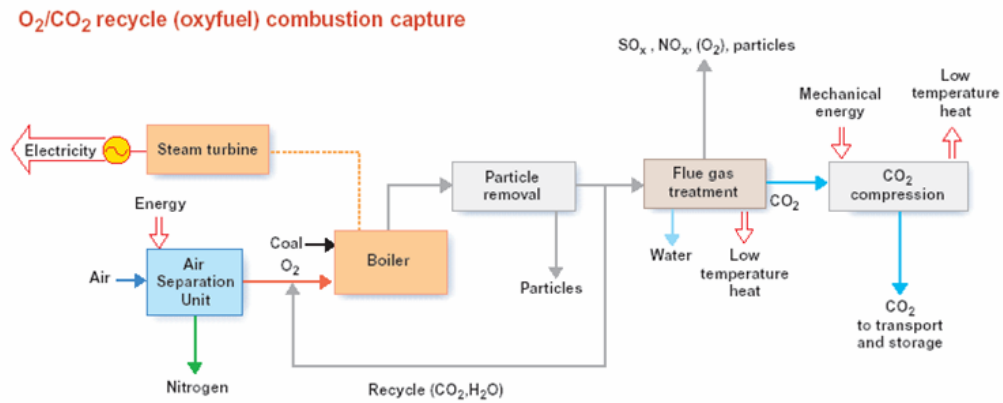


Figure 3.1: Conceptual drawing of an oxyfuel system (Clarke et al., 2004)

This method demands more changes to conventional plant lay-out than immediately obvious because of higher temperature in the boiler. This would require either recirculation of CO<sub>2</sub> or changes to the boiler or even a combination of both. As already mentioned cryogenic removal of nitrogen is a relatively expensive method of separating CO<sub>2</sub>, yielding a cost penalty of up to 15 % (Herzog and Golomb, 2004) of the electricity production of the plant.

### 3.1.4 Chemical absorption

Absorption, in the context of Carbon Capture, is the process of transferring a pollutant from the gas stream to a solvent. The process occurs when the partial pressure of the pollutant in the gas stream is greater than the vapour pressure of the pollutant in the solvent. Hence the transfer relates to the pressure gradient of the pollutant. Due to this, the absorption process is generally counterflow, allowing maximum transfer of the pollutant (Liu and Lipták, 1997). A sketch of a typical chemical absorption process can be seen in Figure 3.2.

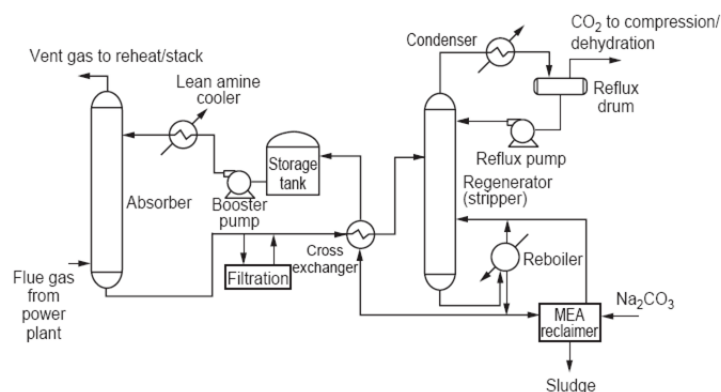


Figure 3.2: Sketch of a chemical absorption system (Herzog and Golomb, 2004)

In short, the flue gas enters the absorber and is bubbled through or scrubbed by the solvent. The CO<sub>2</sub> rich solution is transported through a heat exchanger to the regenerator (or stripper), where it is heated causing the CO<sub>2</sub> to evaporate from the mixture. The evaporated CO<sub>2</sub> is lead to a

compressor and hereafter leave the system for storage. The solvent is reclaimed and recycled (Herzog and Golomb, 2004). According to Andersen and Köpcke (2007) cooling the flue gas prior to entering the absorber will lower the energy consumption in the stripper.

The chemical absorption method is the type of separation also considered for this project using the MEA solvent. A more thorough presentation of the MEA absorption system can be found in Chapter 4.

A study performed by David and Herzog (2000) has established the estimated cost of introducing a MEA based system to an existing plant to be 0.0216 \$/kWh, with an energy penalty of approximately 15 %. Furthermore the total investment cost is estimated to be in the vicinity of 1319 \$/kW for a system that will be able to remove 90 % of the CO<sub>2</sub> from the flue gas and down to approximately 540 \$/kW for 30 % (Ciferno et al., 2007). This means a total investment cost for Nordjyllandsværket Unit 3 of approximately 2.9 billion Dkk.

Ammonia has also been suggested as a solvent alternative. The technique is somewhat similar, with a few changes. An ammonia based system seems to promise greater performance than MEA of up to 8 percent points on the overall plant efficiency (Zachary, 2008). This technology however has some drawbacks. The absorption rate of ammonia is slow, yielding a need for larger absorption units and as ammonia is a volatile substance it can be harder to contain without leakage (Zachary, 2008).

### 3.1.5 Adsorption

Closely related to the absorption process is the adsorption. The adsorption process is based on using solids instead of liquids to extract the pollutant. Adsorption is mainly used when the pollutant is insoluble in liquid (Liu and Lipták, 1997). Adsorption can be categorized as either chemical or physical. The process of physical adsorption binds the pollutant to a solid using the van der Waals forces. In chemical adsorption, also referred to as chemisorption, the pollutant reacts with the surface of the solid thus binding the pollutant to the solid (Liu and Lipták, 1997).

### 3.1.6 Cryogenic separation

Cryogenic separation is the process of freezing the flue gas, thus separating the CO<sub>2</sub> from the stream. This method is mainly used for streams of higher CO<sub>2</sub> concentrations (> 50 %), hence it would require integration of an oxygen rich combustion. An advantage of using cryogenic separation is, that the separated CO<sub>2</sub> is in liquid form and therefore suitable for transport (Gupta et al., 2003).

### 3.1.7 Fuel Decarbonization

Fuel Decarbonization is a pre-combustion approach, utilizing well known methods for removing H<sub>2</sub> from the fuel. These processes release both CO<sub>2</sub> and H<sub>2</sub>. The CO<sub>2</sub> can then be captured and the H<sub>2</sub> combusted (Marion et al., 2008). There are a number of other methods to extract the CO<sub>2</sub> from the fuel, including steam reforming, gasification and partial oxidation (Marion et al., 2008). The advantages of using the pre-combustion approach, is higher CO<sub>2</sub> concentration and lower mass

flow (Marion et al., 2008). A system of this type is often referred to as an Integrated Gasification Combined Cycle (IGCC). More details on this type of power plant can be found in Section 3.2.2.

## 3.2 Technology state and activity

This section pertains to the state of the different technologies as well as their research activity level. The overview given is based on information gathered at the 8th Annual Conference on Carbon Capture and Sequestration. The information is gathered from a mixture of articles, booklets, reports and lectures given at the conference.

The challenge of presenting material collected at a conference is separating the relevant from the irrelevant and presenting the relevant in an organised form. To make a meaningful and systematic division of the research fields is difficult both due to interconnections between different technologies and to highly varying activities in the different areas. However, in this report a division between post-combustion and pre-combustion technologies is attempted. Some technologies are, though, not exclusively pre- or post-combustion and can be used in combinations of different technologies. Some technologies have already been presented in this chapter and will not be repeated except to describe the research activity in the respective areas.

Beginning with the pre-combustion technologies a set of technologies are in active research. The majority of pre-combustion technologies are by no means purely pre-combustion but require additional separation after combustion has taken place.

### 3.2.1 Oxy-fuel

According to EPRI et al. (2008) oxy-fuel combustion is an emerging technology with the largest running test facility currently at 30 MW. Some developers are planning to build demonstration scale units of 50 MW but these will not be ready for use for several years. Currently Alstom has built two pilot scale facilities, one at the Schwarze Pumpe plant in Germany and one at Lacq in France (Alstom, 2009). For an explanation of the different scales of test facilities see Section 3.2.6.

Furthermore two pilot scale plants of 30 MW, owned by Babcock and Wilcox, are operating along with an Australian-Japanese collaboration pursuing 30 MW in Queensland, Australia (EPRI et al., 2008).

### 3.2.2 The Integrated Gasification Combined Cycle

A technology that holds great attention, due to its potential for CCS in an economically efficient way, is the so-called IGCC with enhanced water gas shift (EWGS). This technology is based on the pre-combustion technologies of IGCC and EWGS along with an additional technology for CCS. The reason for its popularity is that this technology combination provides smaller mass flow rates to handle and therefore less expensive CO<sub>2</sub> removal.

The Integrated Gasification Combined Cycle (IGCC), Figure 3.3, is a power plant design based on firing a synthetic gas, originating from gasification of for example coal, oil or biomass. The

gasification process is a high temperature process controlled by oxygen and steam. When the raw carbonaceous material is heated pyrolysis occurs. In this process the material releases volatiles and leaves char. The volatiles are dependent on the material. The carbon in the volatiles can react with both the oxygen and the steam, yielding the reactions seen in (3.1) and (3.2), (Mahajan et al., 1977).

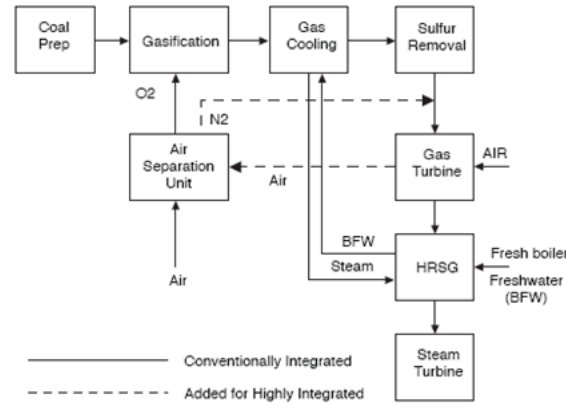


Figure 3.3: Schematic overview of an IGCC unit (EPRI et al., 2008)



Furthermore a water-gas shift reaction will occur between the water and the carbon monoxide, (3.3) (Turns, 2006)



Once the gas has been generated, it is cleaned and filtered to remove sulfur species and particles before it is used to fuel a Brayton cycle. The Brayton process is a system of a compressor feeding high pressure air to a combustion chamber, where it is combusted with the syngas. The combusted gas then drives a gas turbine generating the mechanical work to drive a generator.

Modern IGCC units are equipped with a heat recovery steam generator. This is a steam cycle fed by the excess heat from the gasification process, the waste heat from the gas turbine along with hot streams from the gas cleaning system. The heated steam drives steam turbine providing the mechanical energy to drive another generator.

According to EPRI et al. (2008) the thermal efficiency of an IGCC plant is in the range of 38-41 % HHV based.

It should be noticed that the IGCC technology is only in use today in four commercial units in the U.S. (EPRI et al., 2008) and IGCC with CCS is therefore mainly an option for new power plant building. It is therefore not likely that CCS at an IGCC plant will be demonstrated for a while since retrofitted test facilities with other technologies are easier and cheaper to build.

The IGCC technology is combined with the enhanced water gas shift technology to force the syngas to find an equilibrium as far to the CO<sub>2</sub>-H<sub>2</sub> side as possible. This is done by adding a catalyst and temperature control in the reactor. The EWGS would normally be done in the gas cooling phase because the water gas shift reaction tends to find the wanted equilibrium at low temperatures (Turns, 2006). The need for a catalyst arises because the reaction rate is lower at low temperatures.

CO<sub>2</sub> removal would take place after the sulfur removal depending on the type of CO<sub>2</sub> removal used. The benefits of the IGCC with EWGS are low mass flow rates, a high CO<sub>2</sub> concentration and in the case of MEA CCS the low temperature. Separation technologies that can be considered are membranes, solvents and solid bed adsorption.

IGCC with CCS is considered to be more cost efficient for bituminous coals, but for lignite and sub-bituminous coals pulverised coal combustion with post-combustion CCS is competitive (EPRI et al., 2008).

### 3.2.3 Solvents

Turning to the post-combustion technologies these are to a higher degree purely post-combustion and therefore more suitable for retrofitting to existing power plants. Amongst the technologies that are potentially pure post-combustion are membranes, adsorption and of course solvent absorption.

The majority of technologies in existence used for carbon capture are absorption based, (Bhown, 2009) although the technological processes used for absorption in different solvents are very alike. Apart from a few differences in component design due to solvent behaviour the general concept seen in Figure 3.2 is the same from solvent to solvent.

A given solvent has certain key attributes that are important for its performance in CCS. First of all it needs to have low regenerative energy. It is not feasible to use not regenerable solvents since CCS introduction at a commercial scale would quickly deplete world resources of any given solvent (Bhown, 2009). Secondly, fast absorption is naturally a beneficial attribute as well as a high loading capacity. Also a low degradation of the solvent as it is circulated in the system is required and of course issues as toxicity, flammability and corrosivity are important.

In the following a series of solvents are presented and their level of commercialisation and research activity described.

#### MEA

Amine based CCS is a technology already commercial below 20 MW equivalent from CO<sub>2</sub> production in the food and beverages industry and from enhanced oil recovery. Extensive RD&D is being done to improve solvent abilities and system design to reduce the high energy penalty for implementing MEA CCS, (EPRI et al., 2008). MEA is considered toxic, flammable and corrosive.

The solvent manufacturer Fluor has a 30 % aqueous solution of monoethanolamin with proprietary additives named Econamine FG. This is deployed at approximately 20 plants in the chemical, food and EOR industry. None of these places process coal derived flue gas, (EPRI et al., 2008).

Also, Econamine FG Plus, which is an improved version of the former has been deployed at a site burning lignite coal with a reduction in energy consumption of about a third as compared to Econamine FG.

Several test facilities for MEA has been built even in northern Europe among which are the Sleipner project, the CASTOR project and the CESAR Project.

### KS-1

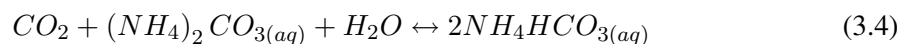
KS-1 is an amine based solvent developed by Mitsubishi Heavy Industries and Kansai Electric Power CO., Inc. Mitsubishi themselves state that KS-1 has lower regeneration energy than conventional MEA, as well as lower absorbent degradation and consumption, a low corrosiveness and lower circulation rate (Holton, 2009; Mitsubishi, 2009). Mitsubishi proposes to use this solvent as part of their KM-CDR process in which they have developed the components needed to exploit the benefits of KS-1 in a 50-3000 tons/day CO<sub>2</sub> recovery plant.

As already mentioned Mitsubishi has used KS-1 commercially in a recovery plant in Keda, Malaysia that started in October 1999. This 160 metric ton/day plant is by no means the only KS-1 CO<sub>2</sub> absorption unit in the world today. Also in Fukuoka (Japan, 283 metric ton/day), Aonla (India, 450 metric ton/day) and Phulpur (India, 450 ton/day) the KS-1 solvent has been in use since 2005-6. Furthermore new recovery plants are being established in Abu Dhabi (United Arab Emirates, 400 metric ton/day), Bahrain (450 metric ton/day), Kakinada (India, 450 metric ton/day), Ghotki (Pakistan, 340 metric ton/day) and Phu My (Vietnam, 240 metric ton/day) for start-up in 2009 or 2010 (Mitsubishi, 2009).

Apart from experience with the mentioned commercial plants the KS-1 solvent also undergoes long term research at a bench scale plant of 0.3 metric ton/day, two pilot plants of 1 and 2 metric ton/day at Hiroshima and Nanko respectively and at a demonstration scale plant of 10 metric ton/day.

### Chilled ammonia

The process of a chilled ammonia cycle is in essence the same as for a MEA based cycle. The cleaned flue gas enters an absorber column, where it is introduced to a solution of ammonia carbonate. The CO<sub>2</sub> react with the ammonia carbonate, forming ammonia bicarbonate following the equation seen in (3.4) (McLarnon, 2009). The ammonia bicarbonate solution is pumped to a stripper column where the solution is heated under pressure, reversing the process, releasing the CO<sub>2</sub> (EPRI, 2009a). As the reversed process is operated at elevated pressures, the compression rate for the CO<sub>2</sub> is less (EPRI et al., 2008) yielding lower compression energy consumption.



The chilled ammonia as a sorbent is a technology licensed by Alstom. In Cooperation with We Energies, EPRI and a consortium of 37 utility companies, Alstom has build a pilot scale unit at the Pleasant Prairie power plant in southern Wisconsin, USA. The plant treats a 1.7 MW equivalent flue gas stream, capturing up to 15000 tons per year of CO<sub>2</sub> (EPRI, 2009a), at a capture rate of

87 % (Hammond, 2009). A series of test has been and will be performed on the unit to establish empirical knowledge of how a chilled ammonia system will operate under given conditions.

One of the challenges when operating a plant based on chilled ammonia is the volatility of ammonia. At Pleasant Prairie Alstom has achieved a ammonia slip of less the 10 ppm (Ericson, 2009).

Alstom has a total of 5 pilot projects. Besides Pleasant Prairie, there are plants in Karlshamn, Mountaineer, Mongstad and Edmonton, located in Sweden, USA, Norway and Canada respectively (Alstom, 2009). Besides these existing project, Alstom is building a 100000 Tons per year plant (Hammond, 2009).

The chilled ammonia technology holds, as mentioned earlier, a potential for lower energy consumption compared to MEA, making the research in this field of high interest.

### No-Escape

BASF SE has screened approximately 400 substances with the potential to be an efficient solvent for CO<sub>2</sub> capture. Based on the criteria already mentioned a few substances has been selected for further study. Among one of these substances one is selected and will bear the name of No-Escape for CO<sub>2</sub>.

At this point it is possible to predict some of the attributes the No-Escape solvent will have compared to conventional MEA. First of all a lower energy consumption in regeneration will result in a lower plant efficiency loss (Northemann et al., 2009). Secondly the capital expenses will be lower as well as product losses will be significantly lower. In Figure 3.4 a diagram of some of BASF's results can be seen.

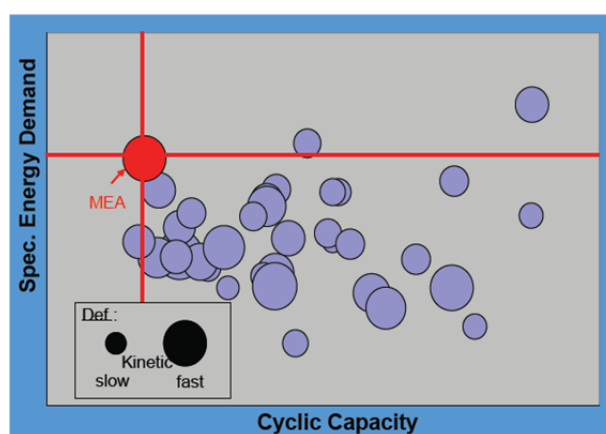


Figure 3.4: Diagram of energy demand versus cyclic capacity of solvents, (Northemann et al., 2009).

In Figure 3.4 it can be seen that several substances display lower energy demand, higher cyclic capacity and competitive kinetics to conventional MEA. Among the remaining candidates for the No-Escape solvent are some that display significantly better stability than MEA keeping the solvent content well above 90 % after 600 hours of stress testing. BASF expects to start pilot testing during July 2009 and begin to collect the earliest results in 2010.

### Ionic liquids

Some organic compounds has a high selectivity for CO<sub>2</sub> as compared to N<sub>2</sub> and O<sub>2</sub>. Instead of reacting with the CO<sub>2</sub> they form weak ionic bonds and therefore has a lower requirement for regeneration energy, (EPRI et al., 2008). DOE-NETL is providing funding for further development at the University of Notre Dame. Luebke (2009) presents a ionic liquid named Solexol which is "reasonably" kinetically fast and states that ionic liquids in general are at a low development stage and that the potential of these is therefore largely unknown.

### 3.2.4 Membranes

Membranes are useful for both pre-combustion and post-combustion separation. Among the membrane technology tested is the Ion Transport Membrane (ITM) with the purpose of reducing power consumption and capital expenses for separating oxygen for gasification or oxy-fuel combustion, (Ciferno et al., 2007; EPRI et al., 2008). The ITM unit uses heated, pressurised air, for example taken from the combustion turbine in an IGCC cycle. No information has been obtained concerning the development progress for the ITM unit.

Regarding membranes in general Barillas (2009) states that the advantage of membranes naturally are that no moving parts are necessary and that the technology therefore is relatively compact and that less energy is needed for separation. However, membranes need to be highly selective to produce the quality of streams necessary and also highly permeable to the desired compound. However, according to Barillas (2009) high permeability also means low selectivity. This of course constitutes a problem with utilizing membranes as a separation method.

### 3.2.5 Solid sorbents

The solid sorbent technology as mentioned bases its potential on adsorption. Much as for solvents, several sorbents are being tested for CCS. Park et al. (2009) has tested a potassium-based dry sorbent capture process, using a slip stream of the flue gas of a coal-fired power plant. The chemistry of the reaction is presented in (3.5).



The adsorption takes place at 70-80 °C while regeneration of the sorbent occurs at above 150 °C. Conclusions after testing were that long term operation of the adsorption system was done, capable of removing above 80 % of the CO<sub>2</sub>. Regeneration generated a stream of CO<sub>2</sub> with a purity of up to 96 %.

Also a sodium-based sorbent has been tested by RTI International, (Ciferno et al., 2007). The chemistry of this sorbent can be seen in (3.6).

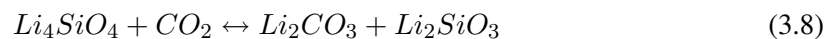


The adsorption, with this sorbent, takes place at 60 °C and the regeneration at 120 °C. 90 % CO<sub>2</sub> removal has been achieved at large lab scale and a 1 ton/day facility has been planned at EPA for start-up in 2009.

Sorbents can also be used for enhancing Water Gas Shift reactions in IGCC cycles. By adding solid sorbents to the steam in the WGS reactor CO<sub>2</sub> will immediately be absorbed forcing the equilibrium further toward the H<sub>2</sub> side, thus achieving enhanced water gas shift with CCS in one reactor (Siriwardane, 2009). The solid sorbent tested is CaO for which the chemical reaction utilized can be seen in (3.7).



According to Turk (2009) the chemical reaction seen in (3.8) can be used for the same purpose.



In general it can be said that solid sorbents are mainly carbonates which have chemical processes occurring at temperatures similar to those found using aqueous solvents. The advantage lies in lower heat of regeneration but it is a relatively untested technology and it is therefore not known what technical difficulty lies in designing an adsorption system. Also carbonates have good loading capacity and are still being developed in capture rate (Thomas, 2009).

### 3.2.6 Technology readiness level

The Electric Power Research Institute (EPRI) uses a NASA developed method of evaluating technology readiness level (TRL). In Figure 3.5 a diagram can be seen of the different levels of readiness.

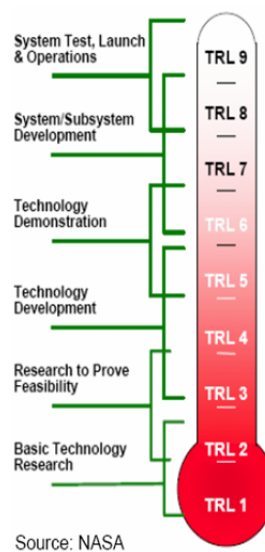


Figure 3.5: Technology Readiness Levels as posed by NASA, (Bhown, 2009).

Along with this division of different stages of technology progress there is a parallel division of different scales of test facilities for CCS at power plants. Wildgust (2009) states that there are the following scales of test facilities.

- Bench/Lab scale, <1 ton/day
- Pilot scale, 1-10 ton/day
- Demonstration scale, 10-100 ton/day
- Commercial scale, >100 ton/day

These divisions of technology progress and test facility scale are as mentioned parallel in the sense that test facilities of pilot scale is necessary to reach TRL 3 and demonstration scale facilities are necessary to reach TRL 6. Therefore climbing the TRL ladder is, among other things, a question of constructing larger and larger CCS facilities.

On the basis of the TRL scale Bhowan (2009) has presented the following diagram of TRL in different technology areas, see Figure 3.6.

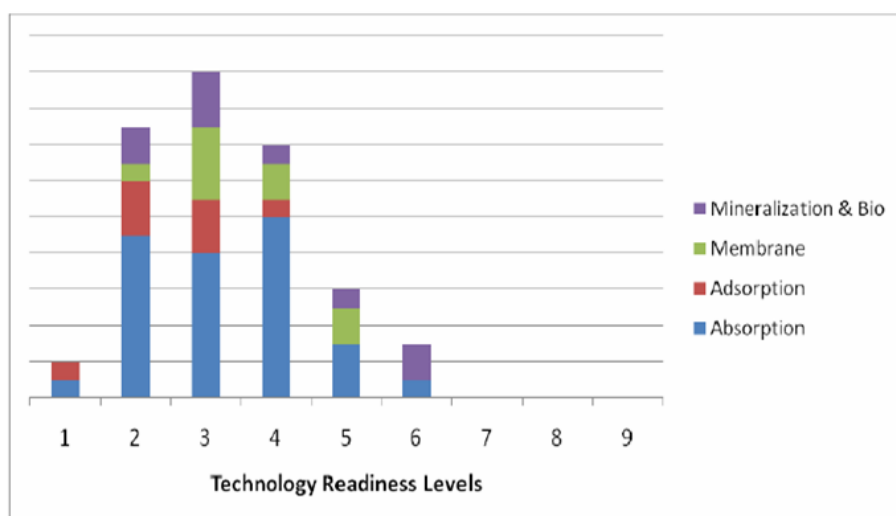


Figure 3.6: Diagram of technology readiness level dependent on technology type, (Bhowan, 2009).

It is apparent from Figure 3.6 that absorbent technologies are dominating in the TRL ladder. Apparently the technology area which has the most technologies closest to commercialization is mineralization and bio which is a technology area that attracts less attention from researchers in the CCS field. Membrane and adsorption technologies are also climbing the TRL ladder but has so far not achieved the same level of commercialization or attention as the absorption technologies. The lack of presence of precombustion technologies on Figure 3.6 has to do with the fact that testing of these technologies has only developed slightly from the bench scale testing facilities as there is no more than a handful of IGCC and Oxy-fuel testing facilities in the US.

The key to increased commercialization lies in increasing experience with larger scale CCS (EPRI et al., 2008). Boer (2009) presents a diagram of how far along establishment of larger scale test facilities are in general. In figure Figure 3.7 this diagram can be seen.

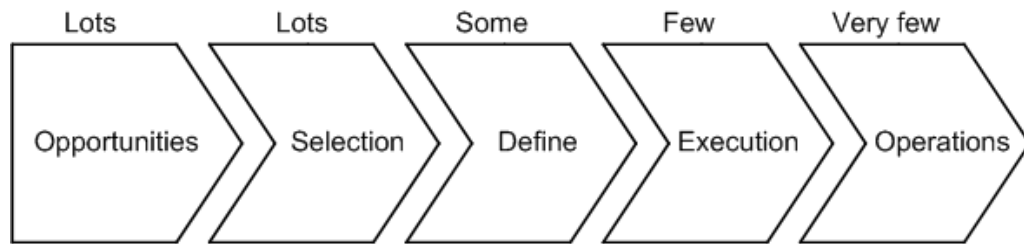


Figure 3.7: Diagram of general progress in establishing larger test facilities.

The phase arrows, seen in Figure 3.7, signifies different phases of CCS test facility implementation. In short they can be presented as reviewing the opportunities, selecting the most feasible, defining the design, building and running the facility. As can be seen immediately above the phase arrows it has been vaguely indicated how many test facilities has reached the phase. To specify the indications it can be said that lots means 50-100 facilities.

In Figure 3.7 it can be seen that lots of test facilities are in the planning phase where opportunities are screened and selected as is also the case with the CCS unit at NJV 3. Some facilities are so far as to being defined in the design phase while few are in the actual building phase. Even fewer are actually operating and the few that are, are relatively small scale units.

In general it can be said that while extensive planning is being done in many companies and government institutions, very few are actually collecting experience from construction or running a larger scale CCS test facility. Whether this is a result of lack of economical will or merely a question of being early in the process is unknown. However if one looks at Figure 3.8 an explanation can be offered.

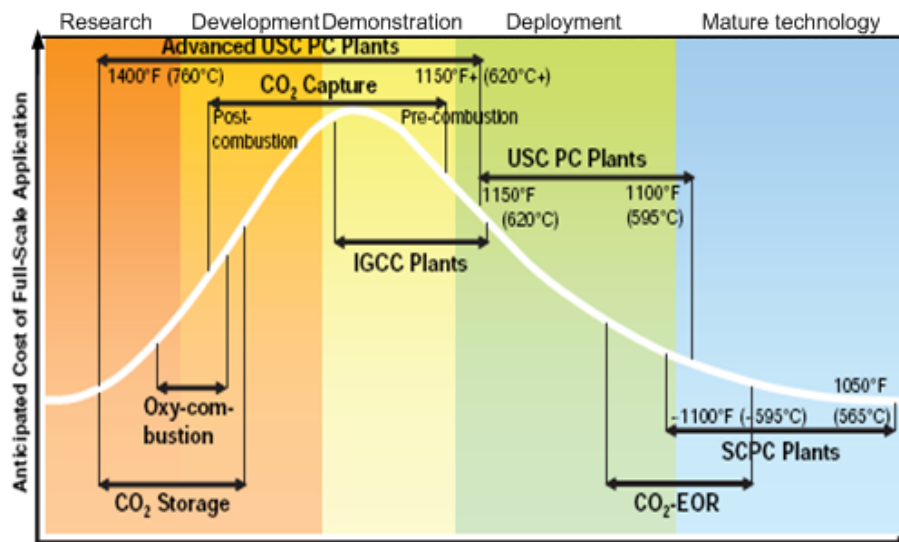


Figure 3.8: The cost of development in development phases and the different technologies development level in 2008, modified from EPRI et al. (2008).

As can be seen in Figure 3.8 only three technologies are in the latter phases of commercialization. Furthermore these technologies are not exactly CCS technologies but enhanced oil recovery (EOR) which has been used since the 1980's, the super-critical pulverised coal (SCPC) technology

which is used at NJV 3 today and the ultra super-critical pulverised coal technology which is in deployment at this time.

Neither the IGCC technology is an actual CCS technology but merely a plant type that facilitates a higher energy efficiency with CCS than conventional combustion with CCS, according to EPRI et al. (2008). The actual CO<sub>2</sub> capture technologies are currently in the development and demonstration phase with the pre-combustion capture technologies in the forefront, again according to EPRI et al. (2008). Oxy-combustion and CO<sub>2</sub> storage are still in the research and development phase.

The postulate that IGCC with CCS is a more mature technology than post-combustion CCS is not necessarily the case, as seen in Figure 3.8, since there is a need to develop integration technology between pre-combustion CCS and IGCC plants before moving into the deployment phase. Therefore the representation of the pre-combustion capture and IGCC technology as separately ready to enter the deployment phase does not necessarily mean that IGCC plants with integrated pre-combustion CCS are ready for deployment. Indeed, no IGCC plants currently operate with CCS in any form (EPRI, 2009b).

The white line in Figure 3.8 signifies the cost of development in the different phases of commercialization. As can be seen the true CCS technologies lie in the region where the cost of development is highest. Therefore more care is taken in designing and constructing the pilot and demonstration scale plants needed to move further along the development phases. Therefore also, even though the motivation is unchanged, more time is passing between initiatives in this phase than later on. As experience begins to build up an increase in construction activity can be expected.

### 3.3 State of the art conclusion

A range of technologies has the potential to play a role in CCS for coal-fired power plants in the future. According to EPRI et al. (2008) a full portfolio of technologies will be necessary to ensure mitigation of CO<sub>2</sub> emissions from the electric sector.

Among the technologies that attracts the most attention from researchers and companies are the absorption technology with a wide variety of solvents, the IGCC with CCS technology with vigorous promotion from certain institutions, and the solid sorbent technology in which a variety of sorbents are being tested at lab scale. Other technologies exist and shows promise but are not object to the same activity of research.

The most mature technology is the absorption technology with conventional MEA as the most commercial solvent. This is the main reason for choosing MEA as the solvent for CCS at NJV 3. Other solvents show greater promise and would likely have economical benefits if chosen but these solvents would require additional time for R&D and design, extending the time frame of the CCS at NJV 3 project.

It should be noticed that, even though an abundance of information and expertise is available at a conference like the 8th Annual Conference on CCS, the information gathered is still only a sample of the total research activity, and as such can be subject to bias and therefore not convey the correct image of the state and activity of a given technology.

## Chapter 4

# The MEA process

*The MEA process is described in Section 3.1.4. This chapter aims to give a more detailed presentation of the process, and the work done by Vattenfall so far.*

MEA is weak base, that will react with a weak acid such as  $\text{CO}_2$ . It is produced by reacting ethylene oxide with aqueous ammonia (Weissermel and Arpe, 2003). MEA is used in a variety of industries and is described as a toxic, flammable, colourless liquid with an ammonia like odour (OSHA, 2009).

As presented, the MEA process is based on an absorber and a stripper. In Figure 4.1, the proposed system for Nordjyllandsværket is presented.

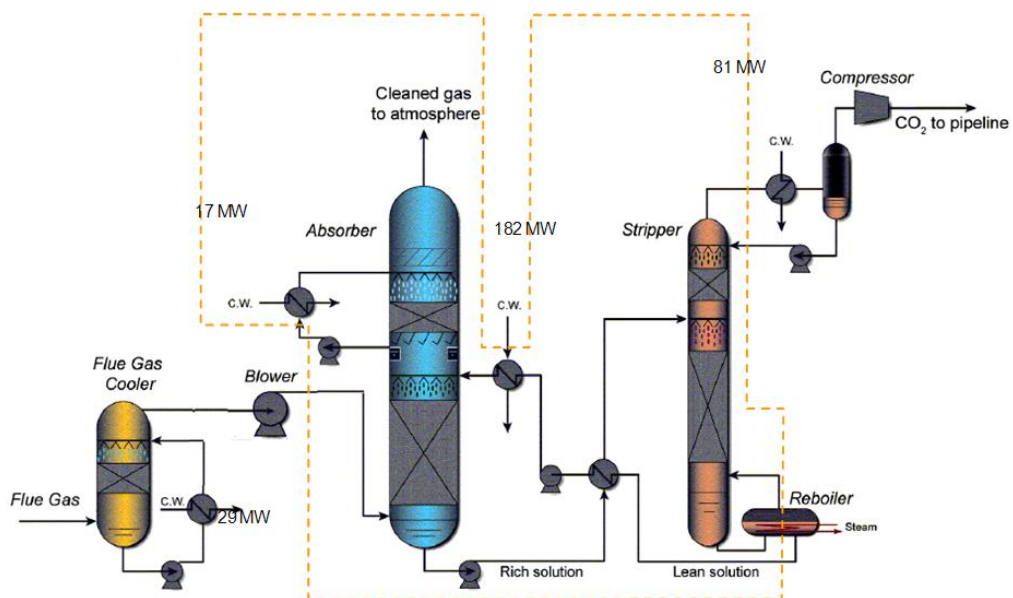


Figure 4.1: Sketch of the proposed system for NJV3 (Andersen and Köpcke, 2007)

The sketch shows the flue gas cooler on the left, the absorber in the centre and the stripper on the right. In the top right, the compressor and vapour condenser is seen.

The proposal so far by Vattenfall is to implement the CCS unit at the point shown in Figure 4.2, the IH stream on Figure 6.1, which is split into a stream, I, for the district heating and a stream H, which goes to tank 1.

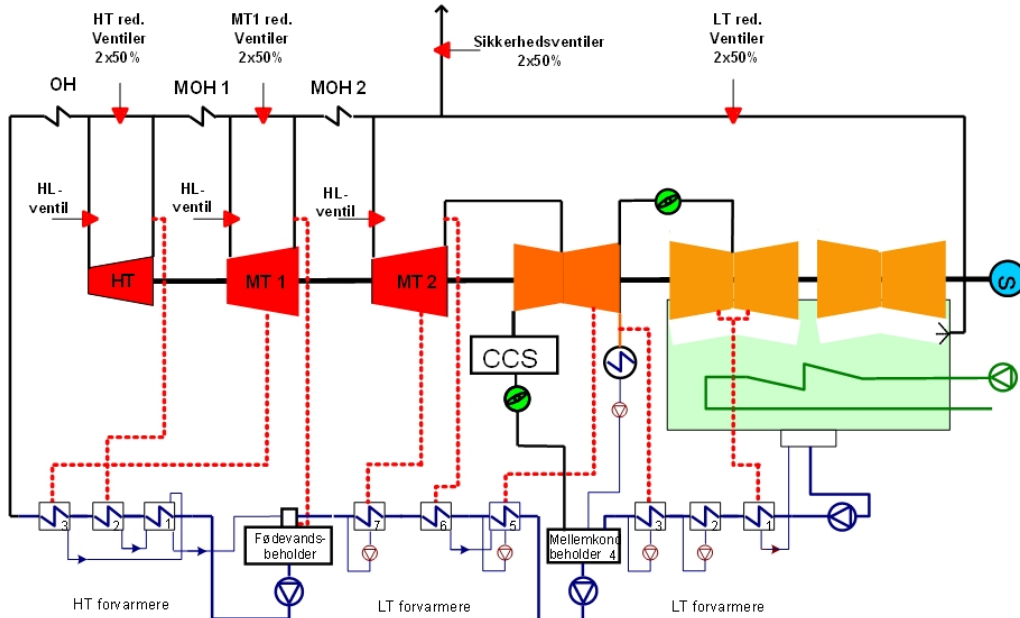


Figure 4.2: Cycle proposed by Vattenfall (Andersen and Köpcke, 2007)

The setup sketch has a flue gas cooler, which as mentioned in the Section 3.1.4 will decrease the energy consumption in the stripper. This can be seen in Figure 4.3. However, it has been proposed by the engineers at Vattenfall to use the energy contained in the flue gas and the MEA solution for district heating (Andersen, 2009b).

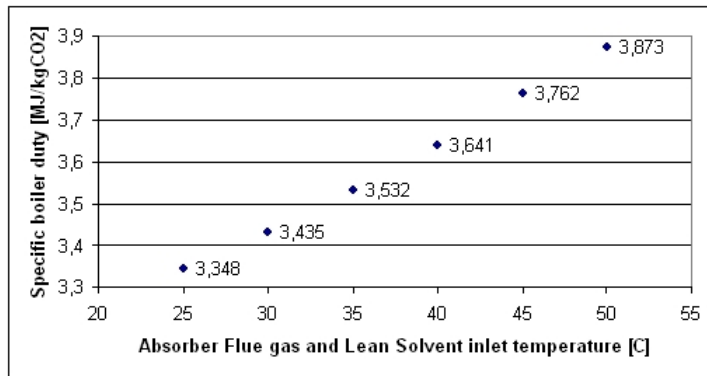


Figure 4.3: Fluegas temperature as function of flue gas temperature (Andersen and Köpcke, 2007)

When using MEA, the flue gas stream containing CO<sub>2</sub> is typically either bubbled through or showered by the MEA dissolved in water causing the CO<sub>2</sub> and the solvent to react according to equation (4.1) (Herzog and Golomb, 2004). The reaction forms a weakly bonded compound called carbamate (Rubin and Rao, 2002).



Though the method of full contact between the flue gas and the solvent is widely used, new technologies separating the flue gas stream and the MEA solution are being researched which seems to allow lower pressure drop through the absorber, lower evaporation of the MEA and generally smaller equipment (Clarke et al., 2004).

The  $\text{CO}_2$  rich MEA solution is transported to the stripper and the cleaned flue gas is led to the chimney. In the stripper, the pressure is the main parameter determining the energy consumption. As can be seen in Figure 4.4, higher pressure yields lower energy consumption for boiling the MEA. However, raising the pressure also raises the required temperature, thus increasing the quality demand for the supply steam, Figure 4.4. Furthermore, the MEA/ $\text{CO}_2$  ratio has a dramatic effect on the energy consumption, allowing approximately 30 % energy savings from worst to best (Andersen and Köpcke, 2007).

The process of evaporating the  $\text{CO}_2$  is a chemical process, designed to break the bonds in the carbamate. As carbamate is a fairly stable compound, a substantial amount of energy is required for this process (Rubin and Rao, 2002). At high temperatures, the salts on the right hand side of equation (4.1) will dissociate, and the  $\text{CO}_2$  will be liberated (Schatz, 1978). The  $\text{CO}_2$  will form in its gaseous state, and as the temperature in the boiler is very near the saturation temperature of water at 2 bars pressure, much of the water will evaporate as well. The stream of  $\text{CO}_2$  and water will by natural buoyancy be forced upwards, once again entering the stripper, where most of the steam once again will condense, due to heat exchange with the colder rich MEA/ $\text{CO}_2$  solution. The  $\text{CO}_2$  and some water vapour will continue towards the stripper outlet for  $\text{CO}_2$ , where a heat exchanger will cool the gasses, condensing the remaining water vapor, and bringing the  $\text{CO}_2$  to a temperature more suitable for compression. The condensed water will be led back to the stripper column.

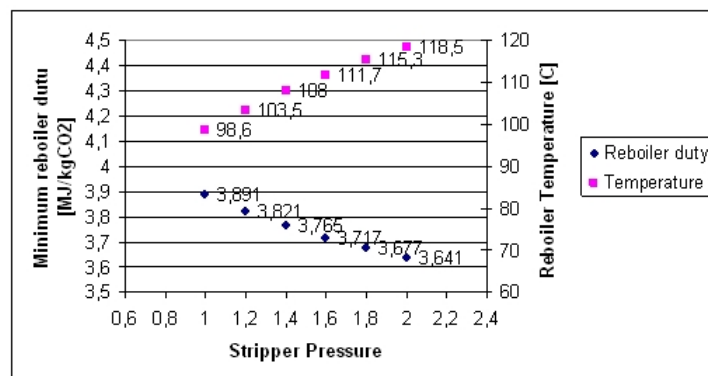


Figure 4.4: Minimum stripper energy as function of pressure (Andersen and Köpcke, 2007).

Once separated in the stripper, the concentrated  $\text{CO}_2$  is cooled and compressed to be sent to storage.

The complete system contains a number of pumps, fans, coolers and a heater. The aim of this project is, in a simplified manner, to implement the system in the complete model of NJV3. That is to obtain the heat for boiling from a stream, where it is least costly, and to use the excess heat from the coolers elsewhere in the system.



## Chapter 5

# Problem statement

*At this point the first part of the project, described in the preface, is being concluded. In this chapter the purpose of this study, based on the information presented so far, will be defined. The limits of the study and the method of conducting the study will also be presented before embarking on the remaining 2 parts of the project.*

### 5.1 Problem definition

Even though other solvents holds higher promise for energy efficiency the benefits of MEA such as easy accessibility and known technology makes it the first choice of Vattenfall. Therefore the use of MEA as the solvent for the retrofitted CCS unit is a given condition from Vattenfall A/S from the beginning of the project. This condition leaves no reason to make changes to the initiating problem which will be investigated further in the remainder of this project.

Therefore the problem to be studied further is as also found in Chapter 1:

*How can a MEA based carbon capture system be integrated at NJV 3, in order to minimize the cost penalties as much as possible?*

### 5.2 Method and limitations

The problem defined is going to be studied through numerical modelling. A model of the steam cycle at NJV 3 will be formulated along with a model of the proposed MEA CCS unit. An attempt to integrate the models, so as to perform an integration study through the models, will be done.

The steam cycle model will be constructed as a system model with the system components being the components of the steam cycle at NJV 3. Therefore a model will be constructed for each of the components at NJV 3 and described independently of each other. The steam cycle model consisting of the integrated component models will be described and the results of this model presented.

The CCS model will be based on information given by Andersen and Köpcke (2007) and Andersen (2009b). The CCS model will not be as detailed as the steam cycle model since it has not yet been completely designed. Therefore the internal processes of the MEA CCS unit will not be modelled but only simple transfers of heat and power. As another consequence this will not be a stand alone model. No presentation of results from the CCS model can be done until integration with the steam cycle model has been successfully performed.

Upon combination of the two models the integration study will be performed and information will be obtained to form a basis for conclusions pertaining to energy efficient CCS retrofitting.

The limitations of this study are, besides limitations done during the modelling, that the study will only be performed at full district heating production of NJV 3. There are many other ways to run the plant dependent on district heating and electricity demand but to model them all and consider integration effects for all of them would be outside the time frame of this project. Furthermore the integration study will be performed at full load since this is the only case where information on the CCS unit has been obtained. The steam cycle model will function at all loads but below full load this will only be used for verification.

## Chapter 6

# The steam cycle at NJV3

*In this chapter the reader is introduced to the steam cycle at NJV3. This is necessary for the reader to appreciate the reasons for the many choices and simplifications it is necessary to make in the formulation of the steam cycle model in the following chapters. The layout of the steam cycle will be described and the working principles will be explained. This chapter is based on Alsthom (1993).*

### 6.1 The steam cycle

The steam cycle at Nordjyllandsværket Unit 3 basically consists of a boiler, a condenser, 2 feed water pumps, 7 turbines and 10 preheaters. Other major components are the two feed water tanks and the two district heating heat exchangers. In Figure 6.1 a diagram of the steam cycle with major components can be seen.

When referring to the 10 heat exchangers individually a numbering convention will be used for those component types that are multiply present. This convention will be to number the components clockwise so that the first heat exchanger after the condenser is named preheater 1. The same convention is of course used for the turbines so that the first turbine after the boiler corresponds to turbine 1. However, in practice the turbines are referred to by the names corresponding to the range of pressure in which they work. As such turbine 1 is referred to as the Very High Pressure turbine (or VHP turbine), turbine 2 is the High Pressure turbine (HP), turbine 3, 4 and 5 are the Intermediate Pressure 0, 1 and 2 turbines (IP0, IP1, IP2), while the remaining two turbines are the Low Pressure turbines 1 and 2 (LP1, LP2).

In the steam cycle there is a mass flow rate of 265 kg/s at full load. In the boiler the steam is heated to 580 °C at 280 bar before entering the VHP turbine where it is expanded to a pressure of 78 bar and therefrom stepwise down to below 1 bar. Between the VHP and the HP turbine and again between the HP and the IP0 turbines reheating of the steam to 580 °C occurs. Two reheating processes are an advantage often used in a Rankine steam cycle to improve the power output as well as the overall thermal efficiency. In Figure 6.2 a T-s diagram of the Rankine cycle used at NJV3 can be seen. The diagram shows that reheating makes it possible to run the condenser at low pressure while maintaining a high steam quality, thus increasing the area inside the cycle line and thereby also the power output and the thermal efficiency.

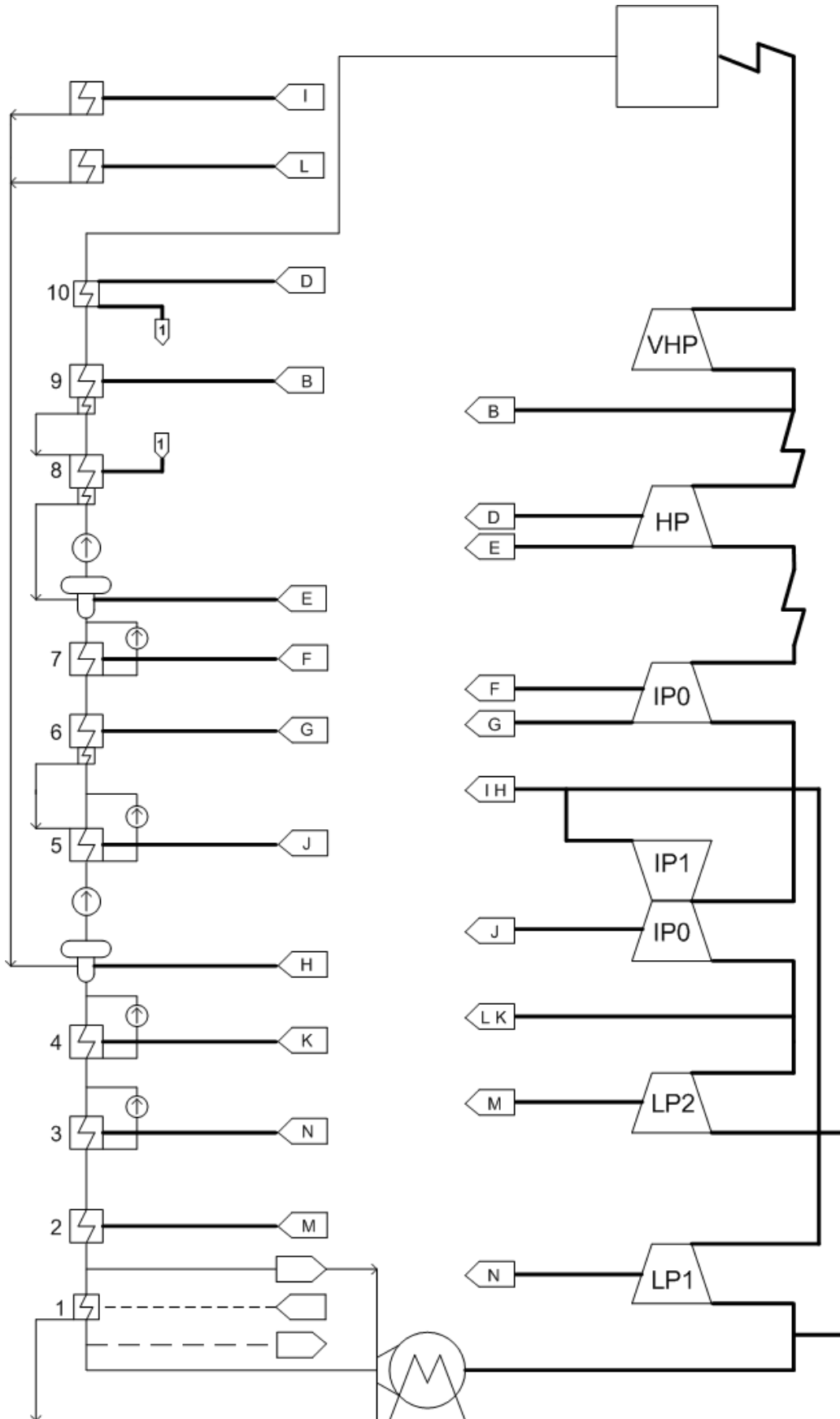


Figure 6.1: Diagram of the steam cycle with major components and flows. Thick lines signify steam flows. Based on Alstom (1993).

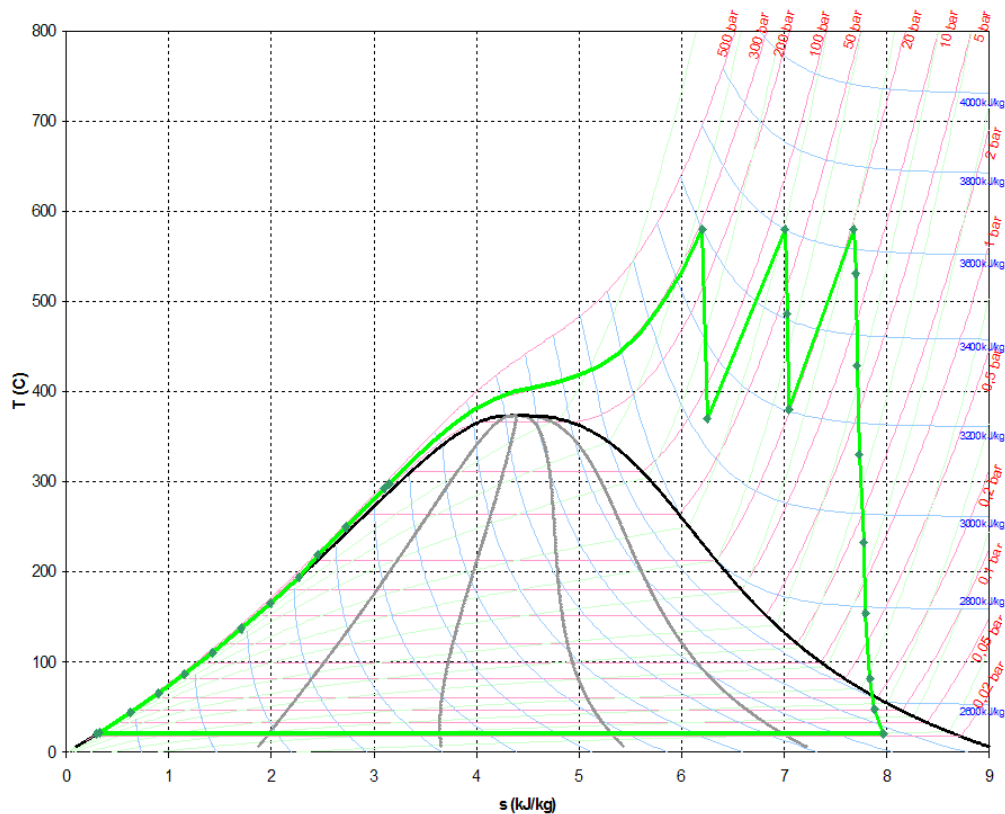


Figure 6.2: Diagram of the Rankine cycle used at NJV3 (Grue, 2009c).

As the steam is expanded through the turbine series several outlets from the conventional Rankine steam cycle can be seen. These are marked on Figure 6.1 by small arrows with letters. These outlets are used for preheating the feed water through the 10 preheater heat exchangers. Depending on the condition of the heat exchangers they will pull more or less steam from the overall cycle, use it to preheat the feed water and recirculate it into the system either in the feed water tanks or immediately after the heat exchange has taken place.

When the steam has been expanded to the condensation pressure the steam is condensed in the condenser or in the district heating system depending on the load configuration of the plant. In this report the notion of loads is separated from the notion of load configurations. The load merely describes how "fast" the plant is running in a specific load configuration, or more specifically, what the value of the mass flow of steam in the steam cycle is relative to the maximum load. The notion of the load configuration pertains to different setups in which the plant can function in order to vary the production of electricity relative to the production of district heating. In the situation in which the plant produces maximum district heating, the two low pressure turbines are shut down and produces no electricity, as opposed to when the plant produce no district heating. The cases of for example 80 % load in these two load configurations are not immediately comparable, which is the reason for the introduction of the mentioned concepts.

When district heating is done only approximately 4,4 kg/s flows through the condenser, while the rest flows through the district heating heat exchangers and recirculated into the steam cycle at the first feed water tank.



## Chapter 7

# The component models

*The steam cycle model is comprised of a series of smaller models of each component in the steam cycle. In this chapter each component model is described and tested. The chapter begins with some general comments on the strategy used in developing the component models and then moves on to describe each type of model and testing them.*

### 7.1 The modelling strategy

The basic information source used to construct the component models is the GEC Alsthom heat balances (Alsthom, 1993). The heat balances provide point values of steam properties around the steam cycle for different loads and load configurations. The Alsthom heat balances are very useful when formulating the component models since the point values of steam property can be used as boundary conditions for the components. It should be noted that the Alsthom heat balances uses an outdated version of steam tables, namely the IFC 1967 steam tables. In this project the same tables are used for consistency even though the IAPWS steam tables would be more up-to-date. For differences between the IAPWS tables and the 1967 tables see Appendix C.

The component models all have in common that their performance is dependent on several variables making the construction of an integrated steam cycle model complicated. The boundary conditions of temperature, pressure and mass flow determines the ability of the fluids in the components to convey heat or work. However, to determine the dependence of the component models on all of the variables would require models based on the actual geometrical and material design, which would require extensive modelling and knowledge of material constants and construction which is considered outside the scope of this project. In this report it has been chosen to use the boundary conditions, given by Alsthom, on each component to determine a dependence on a single variable. The variable chosen is the mass flow rate which is also the variable determining the load case.

Thus the models are simplified component models, for the sake of convergence in EES, which require determination of efficiencies or thermal resistances dependent on the mass flow rate. To obtain these values the models are first run in reverse with the boundary conditions fixed, also yielding indications of the models precision, which in this report functions as model testing. The calculated efficiencies and thermal resistances are taken from each load case and approximated by

a curve dependent on the mass flow rate. When the component models are integrated into the steam cycle model the boundary conditions are released and the thermal resistances and efficiencies are determined solely by the mass flow rate.

When modelling the components it is useful to consider, that there are several models in which there need be very few differences except for boundary conditions and thereby the thermal resistances or efficiencies. This is especially the case for the turbine models, but also to a large extent for the pumps and tanks and to some extent for the heat exchangers. This means that it is possible to mathematically formulate similar models for the components mentioned which reduces the work needed significantly. This, along with the preliminary reverse run, is the main strategy of the model formulation and reduces the modelling needs to a single turbine model, a single tank model, a single pump model, a boiler model, a condenser model and four different heat exchanger models. The reason for the amount of heat exchanger models has to do with the flow configuration of the steam cycle and will be clarified later.

## 7.2 The turbine model

The basic turbine model is based on a simple heat balance over an arbitrary turbine. In Figure 7.1 a diagram of an arbitrary turbine can be seen.

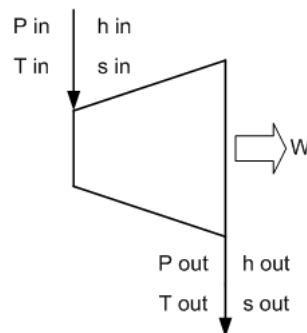


Figure 7.1: Diagram of the energy balance over a heat turbine.

In Figure 7.1 a number of variables can be seen, that along with an efficiency,  $\eta$ , comprise the number of variables that the model system of equations must determine. The variables that are known from the Alstom heat balances can be considered boundary conditions.

When formulating the model in EES the system of equations becomes a mixture of ordinary mathematical equations and table lookups. The turbine component model needs to be able to determine temperature and pressure of the steam in the outlet possibly via the enthalpy. Therefore a simple energy balance is not sufficient and must be supported by additional equations. In this case the formula originally formulated by Aurel Stodola, in the form presented in Bohl (1994), is chosen. The system of equations that comprise the turbine model is presented in the following, see equations (7.1) to (7.7).

$$\frac{\dot{m}_{last}}{\dot{m}_{nom}} \approx \frac{P_{in,last}}{P_{in,nom}} \cdot \sqrt{\frac{1 - \left(\frac{P_{in,last}}{P_{out,last}}\right)^2}{1 - \left(\frac{P_{in,nom}}{P_{out,nom}}\right)^2}} \cdot \sqrt{\frac{T_{out,nom}}{T_{out,last}}} \quad (7.1)$$

$$W = \dot{m}_{last} \cdot (h_{in} - h_{out}) \quad (7.2)$$

$$\eta = \frac{h_{in} - h_{out}}{h_{in} - h_{out,s}} \quad (7.3)$$

$$h_{in} = f(T_{in,last}, P_{in,last}) \quad (7.4)$$

$$s_{in} = f(T_{in,last}, P_{in,last}) \quad (7.5)$$

$$h_{out} = f(T_{out,last}, P_{out,last}) \quad (7.6)$$

$$h_{out,s} = f(s_{in}, P_{out,last}) \quad (7.7)$$

In the turbine model system of equations, equation (7.1) is the additional equation proposed by Stodola to determine the outlet pressure and temperature. This equation is based on a nominal known load case of the turbine, and the outlet pressure and temperature at other loads is determined based upon an approximation of the turbine behaviour. This formula works quite well for all load cases with a high degree of precision. Equations (7.2) and (7.3) arise from the energy balance and the final four equations are simple table lookups performed by EES.

### 7.2.1 Thermal efficiency

As mentioned in Section 7.1 the first thing to be done with this model is to run it in "reverse", meaning with fixed boundary conditions, to obtain the efficiency,  $\eta$ , of the turbine at different mass flow rates. However, the general turbine installation in NJV3 is more complicated than shown in Figure 7.1. In reality the turbine installations are all variations of the one seen in Figure 7.2.

In Figure 7.2 it can be seen that there are multiple inlets and outlets to each turbine in the steam cycle. In Figure 7.2 the longer arrows correspond to inlets or outlets of main steam cycle flows, while the smaller arrows correspond to inlets and outlets from the turbine steam sealing system. While the main flow steam properties are given there is less information available for the steam sealing inlets and outlets.

The main flow outlet in the middle of the turbine is found in all the turbines except for the VHP and IP1 turbines. This means that it is necessary to divide the turbines into two turbines in series with an outlet in between. With the two LP turbines taken out of the steam cycle model, due to the fact that no production of power takes place in these at full production of district heating, this

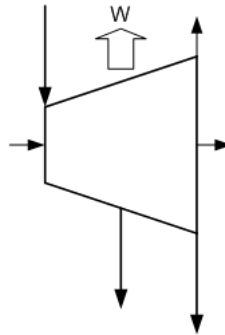


Figure 7.2: Diagram of a realistic turbine installation.

yields 6 half-turbines plus the VHP and IP1 turbines which will be dealt with later. It is therefore necessary to establish efficiencies for each of the half-turbines. In Figure 7.3 a diagram of the division of the turbines into half-turbines can be seen.

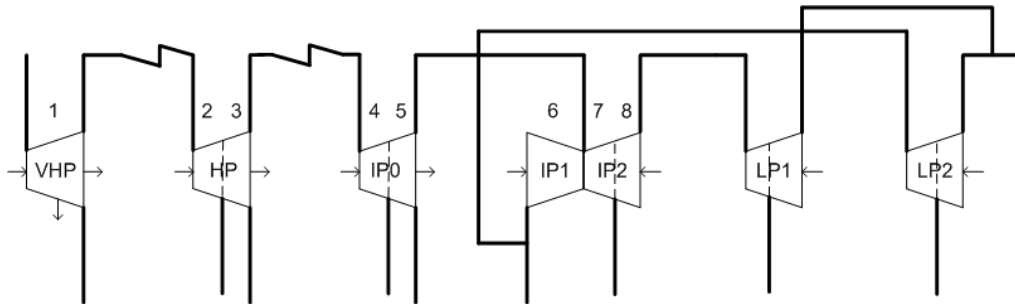


Figure 7.3: Diagram of the division of the steam turbines. Note that the LP turbines are not modelled and therefore not numbered. Steam sealing inlets and outlets are signified by small arrows.

The steam sealing inlets and outlets found at the end of most turbines are also necessary to take into account. Even though the mass flow rate through them are small, they are still large enough to affect the efficiency noticeably. In general the temperatures, the mass flow rates and the pressures of the different inlets and outlets of the steam sealing system are known. The temperatures and the mass flow rates are given everywhere, while the pressure in every case, but one, can be determined from the position of the inlets and outlets. The pressure of the general steam sealing system is 1.15 bar but in the cases of the HP and the IP0 turbines steam is taken directly from the VHP turbine and fed into them to ensure the intended flow. In Figure 7.3 it is possible to see which inlets and outlets there are for the sealing system on each turbine.

Based on the boundary conditions given by the main flows and the steam sealing flows it is possible to calculate the efficiencies of all of the turbines except the VHP turbine. However, only the nominal load case of the sealing system is known and it therefore becomes a challenge to determine the temperatures and pressures at the outlets to the sealing system. In the case of the pressures it is natural to set the steam sealing pressures at the inlets and outlets at the ends of the turbines to the same as the inlet and outlet pressure of the turbine. In case of the temperatures, these are only known at nominal load. Therefore, there is nothing to do except to find an acceptable assumption on the temperatures of the other load cases. Studying the Alstom heat balances it is evident that the inlet and outlet temperatures of the turbines change very little with the load case. This naturally leads to the assumption that the temperatures of the steam sealing inlets and outlets are constant and therefore the temperature given by the nominal load case is used as such.

The VHP turbine offers a unique problem, as the steam extracted from the outlet in the middle of the turbine is lead to the steam sealing system, see Figure 7.4. In this case the pressure of the outlet in the turbine cannot be determined by the Alsthom heat balances.

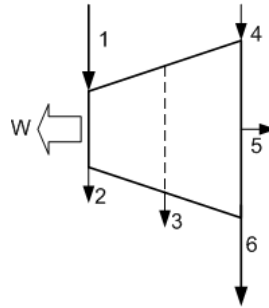


Figure 7.4: Diagram of the steam inlets and outlets in the VHP turbine.

Therefore it becomes a problem to determine where the turbine is to be divided. Fortunately, at nominal load, a pressure of the outlet of the steam to the sealing system is known from Grue (2009a). Studying the Alsthom heat balances it is possible to see that the pressure at the inlets and outlets of the VHP turbine decline approximately proportionally with mass flow rate, so that the pressure at 80 % mass flow rate or load is approximately 80 % the pressure at nominal load also. Therefore it is assumed that the pressure at the steam sealing outtake displays the same behaviour and decreases linearly with the mass flow rate. This assumption enables us to determine the required amount of boundary conditions and thereby also the efficiency.

Using the model and the described assumptions at the necessary places it becomes possible to determine the efficiency of the turbines as predicted by the Stodola formula, equation (7.1). However, there is another, more direct way, to determine the efficiency of the turbine. Merely looking at the inlet and outlet state of the steam at each turbine allows us to compare the enthalpy decrease over the turbine with the isentropic enthalpy decrease to determine an efficiency as seen in equation (7.3). This method is possible to use merely by excluding the Stodola formula from the model and applying an extra boundary condition. This has been done and the isentropic efficiencies are known to the authors of this report. They are, however, not presented here due to reasons of confidentiality.

Both models with applied boundary conditions result in a series of thermal efficiencies along with predictions of boundary variables that are not fixed. In Table 7.1 thermal efficiencies for all modelled turbines and load cases can be seen compared for both calculation methods.

Studying Table 7.1 the first thing to notice is the efficiencies above 1. This only happens in the Stodola efficiencies where it is immediately explainable since the Stodola formula is an approximation of the behaviour of the turbine. Therefore when turbine efficiencies approach 1 there is a possibility that the constraint, that the Stodola formula puts on the system of equations, forces the thermal efficiency above 1. This is what happens in the 6 cases in Table 7.1 in which the Stodola efficiency becomes larger than 1. It should be noted that the overshoots in these cases are relatively small consistent with the reason given for them.

When using the thermal efficiencies in the turbine models it becomes necessary to choose if the Stodola or isentropic efficiencies should be used. Here, it is important to notice that the isentropic efficiencies are the physically correct efficiencies to use in the turbine models. However, the Stodola efficiencies are calculated with the model it is intended to use in the steam cycle model

Turbine	load case	$\eta_{Stodola}$	Turbine	load case	$\eta_{Stodola}$
	%			%	
VHP 1	100	0.9278	IP0 1	60	0.8921
VHP 1	80	0.9747	IP0 1	40	0.8741
VHP 1	60	1.006	IP0 2	100	0.9652
VHP 1	40	1.035	IP0 2	80	0.9667
VHP 2	100	0.8585	IP0 2	60	0.9646
VHP 2	80	0.7326	IP0 2	40	0.9526
VHP 2	60	0.5421	IP1	100	0.9489
VHP 2	40	0.2225	IP1	80	1.004
HP 1	100	0.9265	IP1	60	1.038
HP 1	80	0.9254	IP1	40	0.9009
HP 1	60	0.9231	IP2 1	100	0.9504
HP 1	40	0.9189	IP2 1	80	0.96
HP 2	100	0.9579	IP2 1	60	0.9633
HP 2	80	0.9579	IP2 1	40	0.9258
HP 2	60	0.9581	IP2 2	100	0.965
HP 2	40	0.9551	IP2 2	80	1.01
IP1 1	100	0.9014	IP2 2	60	1.008
IP1 2	80	0.8968	IP2 2	40	0.8771

Table 7.1: Table of thermal efficiencies of turbines from two calculation methods.

with fixed boundary conditions. Therefore choosing the efficiencies calculated with the Stodola formula would most likely yield more precise results when calculating output temperatures and pressures. This is important in this study since this influences the heat exchange with the MEA carbon capture unit. Choosing these efficiencies would however also mean that the prediction of the power output of the turbines would be less precise but studying the results from the two efficiency calculation methods this is only very slightly. Therefore it is chosen to use the unmodified thermal efficiencies from the Stodola calculations for the turbines throughout this study.

The chosen efficiencies are used to determine the coefficients in a third degree polynomial that are to be used as an extra equation in the Stodola model system, equations (7.1) to (7.7). The use of a third degree polynomial ensures that the approximation has  $R^2 = 1$ , since only 4 heat balances are given for this load configuration, but also limits the range of precise approximation to between 100 % and 40 % load since no extrapolation can be done without reducing precision significantly. In (7.8) the additional equation to the model, used when running as a part of the steam cycle model can be seen. It should be noted here that the dangers with applying third degree polynomials to approximate 4 points are known and that all such approximations in this project has been checked to ensure that no "bulges" or the like is found.

$$\eta = a \cdot \dot{m}^3 + b \cdot \dot{m}^2 + c \cdot \dot{m} + b \quad (7.8)$$

## 7.2.2 Model precision

Considering the turbine model used to simulate turbine behaviour as a function of mass flow rate it is prudent to estimate the precision that can be expected from the component model used in the

steam cycle model. When the boundary conditions are applied the model calculates the power output, the input and output enthalpy and the output pressure as auxiliary variables to the thermal efficiency. These variables can be compared to the same variables in the Alstom heat balances to see what sort of precision is achieved. In Table 7.2 the average variable precision for each turbine can be seen.

<b>Turbine</b>	<b>Average power deviation</b>	<b>Average enthalpy deviation</b>	<b>Average pressure deviation</b>
	<i>%</i>	<i>%</i>	<i>%</i>
VHP	4.058	-	-
VHP 1	-	-	-
VHP 2	-	0.193	3.531
HP	2.654	-	-
HP 1	-	0.0093	0.1157
HP 2	-	0.03132	0.1245
IP0	2.1	-	-
IP0 1	-	0.0173	0.2055
IP0 2	-	0	0.346
IP1	1.876	0.02696	12.43
IP2	1.828	-	-
IP2 1	-	0.01771	0.838
IP2 2	-	0.03171	14.49

Table 7.2: Average deviation of power output, output enthalpy and output pressure. The numbers indicate first or second part of the turbine.

In Table 7.2 it can be seen that the power output has an average deviation between 1.828 % and 4.058 % which is noticeable. On the other hand the enthalpy has average deviations in the vicinity of 0.1 %. The pressure deviations are somewhat more varying. The HP, IP0 and the IP2 part 1 has average deviations of below 1 %, which is as expected for the Stodola model. The VHP part 2 turbine has an average deviation of 3.5 % on the pressure and is also more deviating in the enthalpy and power output. This is of course due to the artificial way the turbine was divided at the steam sealing outlet. Had there been sufficient boundary conditions to avoid the assumptions made here, it would most likely have produced results with the same precision as the other turbine models. Another effect of the lack of information on the steam sealing outlet in the VHP turbine is that there is no basis of comparison for the outlet of the VHP turbine part 1. Therefore no information on the precision of this can be found in the table.

The final thing to draw attention in Table 7.2 is the large deviations in pressure for the IP1 and IP2 part 2 turbines. These deviations are most likely the result of the fact, that these turbines are the only turbines with outlet pressure below 1 bar. The fact that the pressure is below 1 bar means that even slight absolute variations in outlet pressure results in large deviations in terms of percent.

The lower precision on the power output than on the enthalpy and pressure in general is considered acceptable here since it is important to have correct conditions where the CCS unit heat exchange is placed. It is of course also important to have the correct thermal efficiency of the steam cycle model, but since this efficiency in principle only needs to be compared to the same efficiency in other steam cycle configurations it is less of a problem. It is, however, important to know that less precision on the steam cycle efficiency makes it less comparable with the plant efficiency as given

by Vattenfall. However, a method of comparing model efficiency with efficiencies based on the Alstom heat balance is later devised.

### 7.3 The boiler model

The boiler model is a very simple model since it is possible to consider the temperature output of the boiler as independent of the load case as long as the boiler is able to heat the steam sufficiently. What is actually done is that no matter the temperature of the feed water, the boiler always heats the steam to  $580^{\circ}\text{C}$ . Provided with a value of boiler efficiency the boiler model can then calculate the amount of heat generated when burning the coal and thereby the amount of coal burned given an average LHV.

It is of course not given that the boiler is actually able to transfer the necessary heat to heat the steam sufficiently and this will reveal itself through a requirement of more coal than it is possible to burn in the boiler. There are 3 points in the steam cycle in which the boiler model is used each with a different value of boiler efficiency or "amount of the total generated heat transferred into this part of the boiler". These efficiencies dependent on load case can be obtained in two different ways. First of all it is possible to obtain the boiler efficiency by considering the heat transfer at the feed water inlet and the steam outlet compared to heat generated much in the way the isentropic efficiencies are obtained for the turbines. The other way is to construct a somewhat larger boiler model that is able to predict boiler behaviour dependent on the mass flow. A large boiler model has been constructed and can be seen in Appendix A. However the efficiencies have been obtained by adjusting the efficiencies in the entire steam cycle model until the total efficiency was above 90 % and the returned boiler heat value from the burning of coal equal for each heating. The efficiencies can be seen in Table 7.3.

Run	1	2	3	Total
$\eta$	0,68	0,1565	0,1152	0,9517

Table 7.3: Boiler efficiency for the primary heating and the two reheatings.

The boiler model equations used in the steam cycle model can be seen in the following, (7.9) to (7.11).

$$c_{steam} = \frac{h_{steam,out} - h_{steam,in}}{582^{\circ}\text{C} - T_{steam,in}} \quad (7.9)$$

$$\dot{Q}_{boiler} = c_{steam} \cdot \dot{m}_{steam} \cdot (582^{\circ}\text{C} - T_{steam,in}) \quad (7.10)$$

$$\eta_{boiler} = \frac{\dot{Q}_{boiler}}{\dot{Q}_{burned}} \quad (7.11)$$

## 7.4 Heat exchanger models

In this section the four different types of heat exchanger models used will be presented. The need for four different heat exchanger models arise because the heat is taken from the steam at different temperatures to heat the feed water. Heat exchanger 10, which is the last preheater before the boiler is merely a de-superheater, while others both de-superheat, condensate and sub-cool. Also there are heat exchangers where two flows of condensed steam are mixed during the sub-cooling to heat the feed water. All the models are based on different versions of the  $\epsilon$ -NTU heat exchanger model. Therefore it is necessary to run the models in reverse with fixed boundary conditions in order to obtain the thermal resistances,  $R$ , see Section 7.4.1, that determine the overall conductivity of the heat exchanger as a function of the mass flow rate when running as a part of the steam cycle model. In the case of the heat exchangers there are two mass flows to choose from, when talking about the mass flow rate, but in this case the mass flow rate of the feed water is chosen since this is the largest flow in the heat exchangers.

### 7.4.1 De-superheating

The first type of heat exchanger model is one of the most simple of the heat exchanger models. This model is merely a single heat exchanger between superheated steam and feed water discharging a flow of still superheated steam and a flow of preheated feed water. In Figure 7.5 a diagram of the heat exchanger as can also be seen as a part of Figure 6.1 is shown.

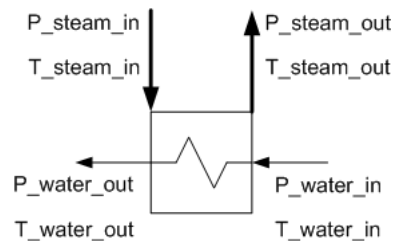


Figure 7.5: Diagram of preheater 10 with steam and feed water flow.

The model needed to simulate this heat transfer is merely a single  $\epsilon$ -NTU model. In the following the system of equations comprising this model can be seen, see equations (7.12) to (7.21).

$$c_{feed} = \frac{h_{out} - h_{in}}{T_{out} - T_{in}} \quad (7.12)$$

$$c_{steam} = \frac{h_{in} - h_{out}}{T_{in} - T_{out}} \quad (7.13)$$

$$C_{feed} = c_{feed} \cdot \dot{m}_{feed} \quad (7.14)$$

$$C_{steam} = c_{steam} \cdot \dot{m}_{steam} \quad (7.15)$$

$$C_{min} = MIN(C_{feed}; C_{steam}) \quad (7.16)$$

$$\dot{Q} = C_{feed} \cdot (T_{feed,out} - T_{feed,in}) \quad (7.17)$$

$$\dot{Q} = \epsilon \cdot C_{min} \cdot (T_{steam,in} - T_{feed,in}) \quad (7.18)$$

$$\dot{Q} = C_{steam} \cdot (T_{steam,in} - T_{steam,out}) \quad (7.19)$$

$$NTU = HX('crossflow'_{oneunmixed}; \epsilon; C_{feed}; C_{steam}; 'NTU') \quad (7.20)$$

$$R = \frac{1}{C_{min} \cdot NTU} \quad (7.21)$$

The  $\epsilon$ -NTU model equations consists of a number of heat balance equations combined with a calculation of the efficiency of the heat exchanger based on heat exchanger geometry and overall heat transfer coefficient, U, times the heat exchanger area, A. The reciprocal product of the overall heat transfer coefficient and the heat exchanger area is treated as a single variable named the thermal resistance, R, in this model. This allows us to determine the resistance to heat transfer dependent on both geometry and material as a single variable. This variable is as mentioned obtained as a function of the mass flow rate by running the model with fixed boundary conditions under varying load.

In the  $\epsilon$ -NTU model, equations (7.12) and (7.13) are calculations of the average specific heat capacity of the feed water and the steam. In equations (7.14) and (7.15) these specific heat capacities are converted to heat capacities of the two flows respectively so that they can be compared in equation (7.16) to determine which flow has the lowest heat capacity and as so is the limiting flow on the heat exchange.

Equations (7.17) to (7.19) are determining equations for the heat transfer and when running in reverse the boundary conditions will determine the heat transfer through these. When running "normally" as a part of the steam cycle model equation (7.18) will determine the heat transfer through the efficiency,  $\epsilon$ , based on calculations involving the thermal resistance and the "Number of Transfer Units" (NTU).

Equations (7.20) determines the NTU based on the efficiency and on the type of heat exchanger. In this case it is merely a function in EES that is used for heat exchangers with the highest heat capacity flow unmixed. The equation used to determine NTU based on  $\epsilon$  can be seen in (7.22).

$$NTU = - \frac{\ln[c \cdot \ln(1 - \epsilon) + 1]}{c} \quad (7.22)$$

In equation (7.22)  $c = C_{Min}/C_{Max}$ . Equation (7.21) determines the thermal resistance, R, of the heat exchanger when running with fixed boundary conditions but is a part of the iterative process when running the model as intended.

The result of running the model with fixed boundary conditions can be seen in Table 7.4. In this table the obtained thermal resistances can be seen along with the deviation of the output temperature of the steam after desuperheating.

<b>Load</b>	<b>R</b>	<b>T<sub>steam,out</sub> dev.</b>
%	K/W	%
100	0.,000008571	0.957
80	0.000008196	0.1053
60	0.0000106	1.054
40	0.0000132	0.5349

Table 7.4: Table of thermal resistances of heat exchanger 10 based on load (mass flow rate) and deviation of output steam temperature in percent.

In Table 7.4 it is possible to see that the deviation of the output steam temperature is between 0.1 and 1.1 %. This is quite acceptable and gives a reasonable credibility of the thermal resistances. However it should be noticed that the thermal resistances are not only dependent on the mass flow rate of the feed water. They are of course also dependent on inlet temperatures and pressures but in the very least it would be more correct to make the thermal resistance dependent on both mass flow rates. This is however not done and is considered a source of error in the steam cycle model.

Using the thermal resistance dependent on mass flow rate of the feed water when running the model as a part of the steam cycle model demands an extra equation in the de-superheater model system of equations. In equation (7.23) the extra equation determining the thermal resistance can be seen. It should be noted that the equation used in the model uses significantly more decimals.

$$R = 3 \cdot 10^{-12} \cdot \dot{m}_{feed}^3 - 10^{-9} \cdot \dot{m}_{feed}^2 + 2 \cdot 10^{-7} \cdot \dot{m}_{feed} + 9 \cdot 10^{-6} \quad (7.23)$$

## 7.4.2 Condensation

The condenser model is used for heat exchanger 6 and 10 in the steam cycle, since here the steam from the turbine side of the system is not only desuperheated, as in Section 7.4.1, but also condensed and subcooled. This makes it necessary to add two additional heat exchanger phases to the de-superheating. The second phase is naturally condensation and the third is sub-cooling. Therefore the condensation heat exchanger model consists of a series of three heat exchangers where the first and third are  $\epsilon$ -NTU models while the second is merely transfer of the amount of enthalpy needed to convert steam to water at saturation temperature. A diagram of this heat exchanger model can be seen in Figure 7.6.

In Figure 7.6 the feed water flows through the heat exchanger diagram horizontally taking on the temperatures from  $T_1$  to  $T_4$  while the superheated steam flows through the other paths taking on the temperatures  $T_{in}$ ,  $T_{sat}$  and  $T_{out}$ .  $T_{sat}$  is of course the saturation temperature for the steam.

In this model the input temperature and pressure of the steam is known along with the input temperature and pressure of the feed water. This is enough information for the system of equations to be able to solve the problem and provide thermal resistances for the first and third phase. A thermal resistance in the second phase is not necessary since it is assumed that the steam always condensates fully. In equations (7.24) to (7.26) the equations comprising the second phase, or the actual condensation, can be seen.

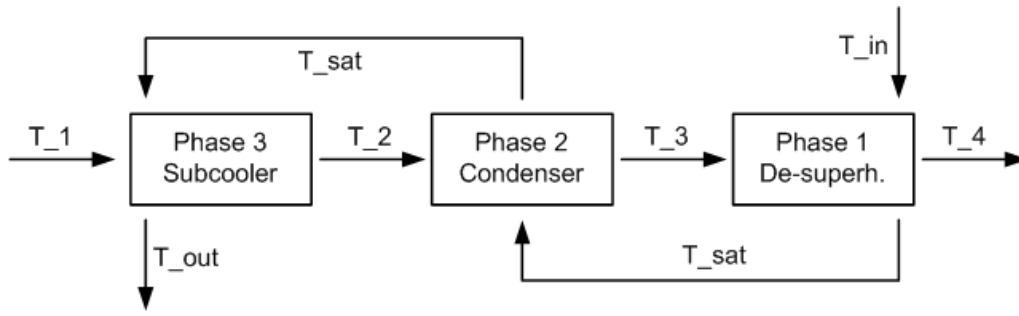


Figure 7.6: Diagram of the condenser heat exchanger.

$$c_{p,feed} = Cp(Steam; T = (T_3 + T_2)/2; P = P_{feed}) \quad (7.24)$$

$$\dot{Q} = \dot{m}_{steam} \cdot (h(Steam; x = 1; P = P_{steam}) - h(Steam; x = 0; P = P_{steam})) \quad (7.25)$$

$$\dot{Q} = c_{p,feed} \cdot \dot{m}_{feed} \cdot (T_3 - T_2) \quad (7.26)$$

These equations comprise the connection between the two very similar  $\epsilon$ -NTU models in phase 1 and 3, whose set of equations are similar to the set of equations seen in equations (7.12) to (7.21). Equation (7.24) is merely a table lookup of the constant pressure heat capacity at average feed water temperature and pressure. It should be noted here that it is assumed that there is no significant pressure loss over the heat exchangers. In equation (7.25) the heat flux from the condensation of the steam is calculated and thus equation (7.26) will return the outlet temperature of the feed water when the condensation phase has finished.

When running the condenser model in reverse, to obtain the thermal resistances of phase 1 and 3, an additional boundary condition is fixed so that the model returns the saturation temperature of the steam without an actual table lookup. This is done to ensure that the model behaves correctly and the solution returned for saturation temperature can be used as a measure of precision. Also the temperature  $T_4$  is used to measure precision of the condenser model.

In Table 7.5 the resulting thermal resistances can be seen along with measures of precision of the condenser model.

As can be seen in Table 7.5 the deviation of the output feed water temperature,  $T_4$ , from the Alstom data ranges between 0 and 0.15 %. Also the deviation of the saturation temperature at steam pressure ranges between 0 and 0.07452 %. This precision is considered satisfactory. In reality also heat exchanger 1 is a condenser type heat exchanger and therefore results for this heat exchanger should be presented here. These results exist but are not presented here due to simplifications made in the construction of the steam cycle model.

The polynomial expressions used as approximations for the thermal resistance in heat exchanger 6 and 9 can be seen in equations (7.27) to (7.29).

Heat exchanger	Load	$R_1$	$R_3$	$T_4$ dev.	$T_{sat}$ dev.
	%	K/W	K/W	%	%
10	100	0.000003034	0.000003652	0.06838	0.03418
10	80	0.000004221	0.000004797	0.07138	0.03586
10	60	0.000006403	0.000006974	0.15123	0
10	40	0.00001137	0.00001152	0.08231	0.0418
6	100	0.0000136	0.0000131	0.06087	0
6	80	0.00001729	0.00001566	0	0
6	60	0.00002411	0.00002025	0	0
6	40	0.00004023	0.00003007	0.07824	0.07452

Table 7.5: Table of thermal resistances of condenser 9 and 6 based on load (mass flow rate) and deviation of output feed water temperature and saturation temperature.

$$R_{1,6} = -2.004 \cdot 10^{-12} \cdot \dot{m}_{feed}^3 + 1.451 \cdot 10^{-9} \cdot \dot{m}_{feed}^2 - 3.714 \cdot 10^{-7} \cdot \dot{m}_{feed} + 0.00003682 \quad (7.27)$$

$$R_{3,6} = -1.496 \cdot 10^{-12} \cdot \dot{m}_{feed}^3 + 1.135 \cdot 10^{-9} \cdot \dot{m}_{feed}^2 - 3.068 \cdot 10^{-7} \cdot \dot{m}_{feed} + 0.00003307 \quad (7.28)$$

$$R_{1,9} = -1.600 \cdot 10^{-11} \cdot \dot{m}_{feed}^3 + 9.050 \cdot 10^{-9} \cdot \dot{m}_{feed}^2 - 0.18 \cdot 10^{-5} \cdot \dot{m}_{feed} + 0.0001402 \quad (7.29)$$

$$R_{3,9} = -8.190 \cdot 10^{-12} \cdot \dot{m}_{feed}^3 + 4.769 \cdot 10^{-9} \cdot \dot{m}_{feed}^2 - 9.905 \cdot 10^{-7} \cdot \dot{m}_{feed} + 0.00008629 \quad (7.30)$$

### 7.4.3 Doubleflow condensation

The doubleflow condensation heat exchanger model is much like the condenser model only slightly more complicated. In heat exchanger 5 and 8 the subcooled water from flow B and G, that streams from the condenser heat exchangers is mixed with the condensed steam from flow 1 and J, see Figure 6.1. This creates a condenser with two input flows on the hot side. One flow of superheated steam and another of subcooled water. What happens in reality is that the subcooled water inlet streams directly into the saturated condensate from the superheated steam, mixes with this and exchanges heat with the feed water side before exiting the heat exchangers.

In the doubleflow heat exchanger model the system of equations is almost exactly the same as in the condenser model. The only difference is that between the condensation equations in phase two and the  $\epsilon$ -NTU model equations in phase three, a set of equations is placed, determining the enthalpy and the mass flow rate of the combined flows from the two inlets. This new flow then exchanges heat in the third phase. In equations (7.31) and (7.32) the mixing equations can be seen.

$$\dot{m}_{condensate} = \dot{m}_{steam} + \dot{m}_{auxiliary} \quad (7.31)$$

$$h_{condensate} = \frac{\dot{m}_{steam} \cdot h_{steam} + \dot{m}_{auxiliary} \cdot h_{auxiliary}}{\dot{m}_{condensate}} \quad (7.32)$$

In Figure 7.7 a diagram of the doubleflow condenser model can be seen. Notice that the model consists of three phases, with  $\epsilon$ -NTU models in phase 1 and 3, and condensation in phase 2, just as in the normal condensation model. In this model, however, there is an additional inlet that mixes with the main steam flow between phase 2 and 3.

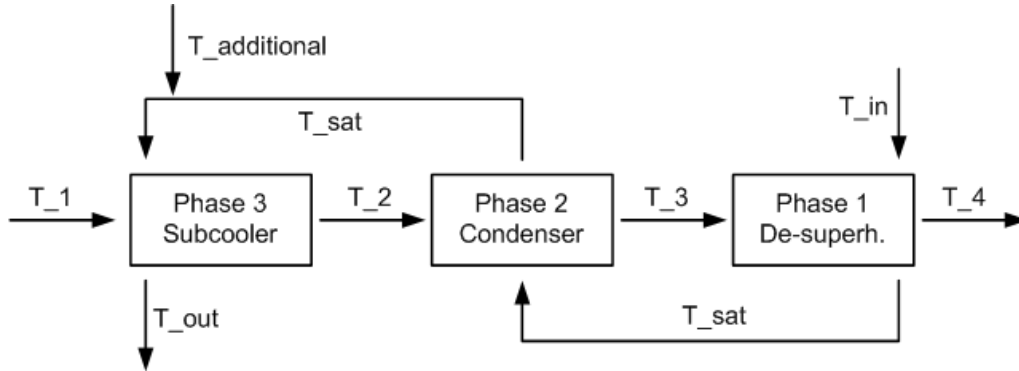


Figure 7.7: Diagram of the doubleflow condensation model.

It should be noticed that the temperature of the additional inlet is approximately the same as the saturation temperature and that the extra heat exchange obtained by adding the water is primarily due to a higher mass flow rate. In Table 7.6 the thermal resistances and the relative precision of the predicted parameters can be seen.

Heat exchanger	Load	$R_1$	$R_3$	$T_4$ dev.	$T_{sat}$ dev.
	%	K/W	K/W	%	%
8	100	0.000007035	0.000001936	0	0
8	80	0.000009033	0.000002511	0	0
8	60	0.00001245	0.000003551	0	0.044
8	40	0.00001961	0.000005866	0	0

Table 7.6: Table of thermal resistances of heatexchanger 8 based on load (mass flow rate) and deviation of output feed water temperature and saturation temperature.

With these results the polynomial approximations used in the doubleflow condenser model can be seen in equations (7.33) and (7.34).

$$R_{1,8} = -2.602 \cdot 10^{-12} \cdot \dot{m}_{feed}^3 + 1.907 \cdot 10^{-9} \cdot \dot{m}_{feed}^2 - 5.017 \cdot 10^{-7} \cdot \dot{m}_{feed} + 0.00005446 \quad (7.33)$$

$$R_{3,8} = -9.068 \cdot 10^{-13} \cdot \dot{m}_{feed}^3 + 6.595 \cdot 10^{-10} \cdot \dot{m}_{feed}^2 - 1.700 \cdot 10^{-7} \cdot \dot{m}_{feed} + 0.00001756 \quad (7.34)$$

#### 7.4.4 Mixing

In the case of heat exchangers 1 to 5 and 7 the steam is condensed and flows into the feed water stream immediately after condensation. In this case there is no need to model the actual heat exchange and a weighted average of the specific enthalpies of the stream therefore suffice. The mixing model is therefore very simple. The two equations, that can be seen in (7.35) and (7.36), are merely the mentioned weighted average and a simple mass conservation.

$$\dot{m}_{out} = \dot{m}_{in,1} + \dot{m}_{in,2} \quad (7.35)$$

$$h_{out} = \frac{h_{in,1} \cdot \dot{m}_{in,1} + h_{in,2} \cdot \dot{m}_{in,2}}{\dot{m}_{out}} \quad (7.36)$$

Thus the mixing model along with the other presented heat exchanger models comprise the needed set of models necessary to model the preheating of the feed water as it flows from the condenser to the boiler.

### 7.5 The pump model

There are two pumps in the steam cycle that serve the purpose of raising the pressure to boiler level and to balance the pressure loss. In Figure 7.8 a diagram of the pump with boundary variables can be seen.

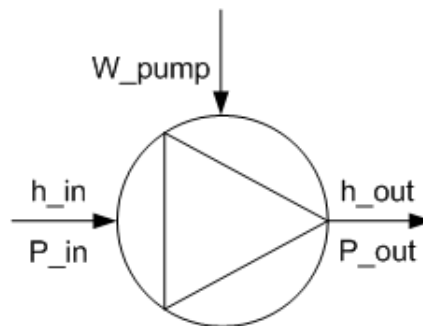


Figure 7.8: Diagram of pump with boundary variables.

The pump model has some of the same problems as the turbine models. An energy balance over the pump is insufficient to determine the outlet pressure and temperature. The obvious solution to this problem would be the pump performance curve but this has not been provided for this study. Instead the boundary conditions provided by the Alstom heat balances are used to determine a dependency of the pressure increase on the mass flow rate. The equation describing this dependency together with an energy balance comprise the system of equations used to model the pump. The pressure rise is approximately linearly dependent on the mass flow rate and therefore the component model system of equations for the pump is as seen in equations (7.37) to (7.40).

$$W_{pump} = (h_{out} - h_{in}) \cdot \dot{m}_{pump} \quad (7.37)$$

$$W_{pump} = \left( \frac{P_{out}}{\rho_{out}} - \frac{P_{in}}{\rho_{in}} \right) \cdot \dot{m}_{pump} \quad (7.38)$$

$$\Delta P_{pump} = a * \dot{m}_{pump} - b \quad (7.39)$$

$$\Delta P_{pump} = P_{out} - P_{in} \quad (7.40)$$

In equation (7.39) the constants  $a$  and  $b$  are to be determined for each pump via the boundary conditions. This means that this component model also needs to be run in reverse to obtain these values before it can be put to use in the steam cycle model.

## 7.6 The tank model

The steam cycle at NJV3 contains two feed water tanks. These feed water tanks contains a mixture of steam and saturated water ready to be pumped through the steam cycle. These tanks serve the purpose of a buffer so that variation of the pump work is possible without negative effects of transient behaviour in the steam cycle. The two tanks have several inputs of steam or water and a single outtake to the pumps placed immediately after them in the steam cycle. A diagram of a tank with boundary variables are shown in Figure 7.9.

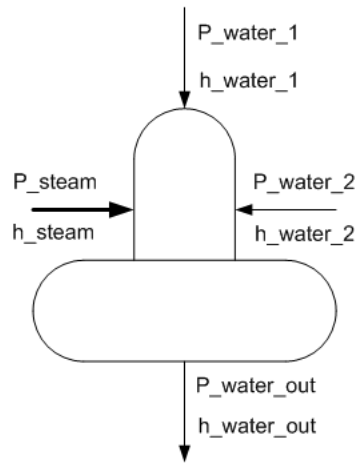


Figure 7.9: Diagram of a feed water tank with inlet and outlet streams.

To determine the enthalpy of the outlet and mass flow through the tank is simple. The mass flow through the tank, when in steady state, which is an assumption throughout this report, is merely the sum of the mass flows of the three input streams. The enthalpy of the water taken out of the tank is taken as a mass flow weighted average of the enthalpies of the inlet streams.

Thus the major problem of the tank model is to determine the pressure of the water at the outlet. This is a problem since the inlet streams possibly are of different pressures. The Alsthom heat balances indicate only the inlet pressure of the steam inlet at both tank models. The inlet pressures from either the district heating in tank 1 or the inlet from the doubleflow condenser in tank 2 are

not specified and neither are the inlets from the main steam cycle. From Grue (2009a) it is known that the pressures at these inlets are always higher than the steam inlets and that these streams are therefore throttled down to steam pressure. Therefore the pressure of the tanks are taken to be the pressures of the steam inlets from stream H and E respectively. In equations (7.41) to (7.43) the equation set comprising the tank model can be seen.

$$\dot{m}_{tank} = \dot{m}_1 + \dot{m}_2 + \dot{m}_3 \quad (7.41)$$

$$h_{outlet} = \frac{h_1 \cdot \dot{m}_1 + h_2 \cdot \dot{m}_2 + h_3 \cdot \dot{m}_3}{\dot{m}_1 + \dot{m}_2 + \dot{m}_3} \quad (7.42)$$

$$P_{outlet} = P_{steam} \quad (7.43)$$

## 7.7 The condenser model

The final actual component of the steam cycle is the condenser. In this component the leftover heat in the steam is taken out at low pressure and the steam is condensed and cooled to a certain temperature before entering the feed water side. In Figure 7.10 a diagram of the condenser model can be seen.

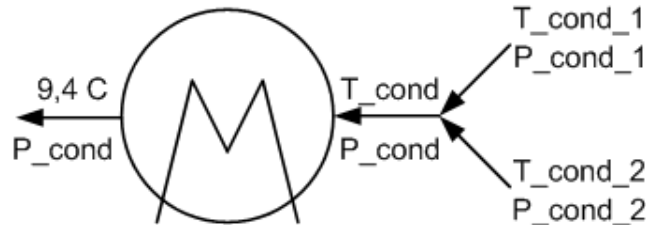


Figure 7.10: Diagram of the condenser model with boundary conditions.

The condenser takes flow inputs from both the two low pressure turbines along with some steam from the sealing system entering the low pressure turbines. This constitutes a problem when modelling the condenser since the outlet pressure of the low pressure turbines are not equal and since it is not known at what pressure they combine. Therefore the pressure in the condenser is calculated as an average of the outlet pressures of the LP turbines (or in reality of the IP1 and IP2 turbines since the LP turbines are idle). This is only a possible solution to the pressure problem since the outlet pressures are very close to each other and the error of averaging is therefore negligible. The inlet state of the condenser is therefore determined from this pressure and a weighted average of the specific flow enthalpies as can be seen in (7.44) to (7.47).

$$h_{cond} = \frac{\dot{m}_{cond,1} \cdot h_{in,1} + \dot{m}_{cond,2} \cdot h_{in,2} + 0.440[\text{kg/s}] \cdot h(\text{Steam}; T = 150; P = 1.15)}{\dot{m}_{cond,1} + \dot{m}_{cond,2} + 0.440[\text{kg/s}]} \quad (7.44)$$

$$\dot{m}_{cond} = \dot{m}_{cond,1} + \dot{m}_{cond,2} + 0.440[\text{kg/s}] \quad (7.45)$$

$$P_{cond} = \frac{P_{cond,1} + P_{cond,2}}{2} \quad (7.46)$$

$$T_{cond} = \text{temperature}(\text{Steam}; P = P_{cond}; h = h_{cond}) \quad (7.47)$$

$$T_{sat,cond} = T_{sat}(\text{Steam}; P = P_{cond}) \quad (7.48)$$

$$\begin{aligned} \dot{Q}_{cond} = & \dot{m}_{cond} \cdot Cp(\text{Steam}; T = (T_{cond} + T_{sat,cond})/2; P = P_{cond}) \cdot (T_{cond} - T_{sat,cond}) \dots \\ & + \dot{m}_{cond} \cdot (h(\text{Steam}; x = 1; P = P_{cond}) - h(\text{Steam}; x = 0; P = P_{cond})) \dots \\ & + \dot{m}_{cond} \cdot Cp(\text{Steam}; T = (9.4[C] + T_{sat,cond})/2; P = P_{cond}) \cdot (T_{sat,cond} - 9.4[C]) \end{aligned} \quad (7.49)$$

In equation (7.48) the saturation temperature of the condenser is found based on the condenser pressure. This is done so that the heat transferred out of the steam cycle in the condenser can be calculated in (7.49). As the reader may have noticed the condenser model merely calculates the waste heat rejected in the condenser based on a fixed temperature, (Alstom, 1993), of the feed water as it leaves the condenser. This temperature is the 9.4 ° C seen in equation (7.49).

## 7.8 The pipe model

The steam cycle at NJV3 of course contains several pipes in which steam or water flows from one component to another. Depending on the velocity of the stream and the length and diameter of the pipe the stream will experience a pressure loss as it travels through the pipe. This pressure loss can be determined as can be seen in equation (7.50) (Çengel and Turner, 2005).

$$\Delta P = f \frac{L}{D} \frac{\rho V^2}{2} \quad (7.50)$$

In equation (7.50) it can be seen that the pressure loss depends on several parameters. It can be seen that (7.50) contains two types of variables, variables that depend on the pipe and variables that depend on the stream. The variables that depend on the stream are of course the velocity,  $V$ , and the density,  $\rho$ . The friction factor,  $f$ , models the roughness of the pipe wall while the length,  $L$ , and the diameter,  $D$ , models the geometry of the pipe.

The pipe parameters are combined into one parameter,  $K_L$ , since these are not known. It is then possible to determine  $K_L$  by running the model with boundary conditions as done with many of the other models.  $K_L$  should have the same value regardless of the load case. Therefore the equation used to calculate the pressure loss over the pipe can be seen in (7.51).

$$P_{in} - P_{out} = K_L \cdot \text{density}(\text{Steam}; T = T_{in}; P = P_{in}) \cdot \frac{V^2}{2} \quad (7.51)$$

In this equation the density is found via a table lookup in EES based on inlet temperature and pressure.

It is necessary to determine the velocity of the stream to calculate the pressure loss. This value is not known anywhere in the steam cycle but since the mass flow rate is, it is possible to determine an imaginary velocity by assuming a pipe diameter of one meter. When running the model with boundary conditions  $K_L$  will adjust itself so that it fits to the imaginary velocity. Therefore the remaining equations in the tube model can be seen in equations (7.52) and (7.53).

$$r = 0,5 \quad (7.52)$$

$$V = \frac{\dot{m}_{steam}}{\text{density}(\text{Steam}; T = T_{in}; P = P_{in})} \frac{1}{\pi r^2} \quad (7.53)$$

With these equations the resulting values for  $K_L$  is presented in Table 7.7.

<b>Pipe</b>	1	2	3	4	5	6	7	8
$K_L$	860.7	53.66	5.171	0.5236	4796	3816	17815	$1.12 \cdot 10^6$
<b>Pipe</b>	9	10	11	12	13	14	15	16
$K_L$	$4.664 \cdot 10^6$	1864	662.5	143	111.7	1379	2190	13401

Table 7.7:  $K_L$ -values for all 16 pipes.

## 7.9 Component models conclusion

The series of models presented in this chapter comprise the needed models to build an integrated model of the steam cycle. Each model has been kept as simple as possible to further convergence in the integrated steam cycle model. The most complicated models are the heat exchanger models which are therefore the most likely to cause difficulty when being integrated into a steam cycle model. The most unprecise models are the turbine models which therefore will contribute negatively to the precision in predicting the thermal and electric efficiency of the steam cycle as well as the power output.



## Chapter 8

# The steam cycle model

*In this chapter the component models developed in the previous chapter are combined into a single integrated steam cycle model. Some simplifications on the original steam cycle are necessary and will be presented in the following. Furthermore the ability of EES to obtain a converged solution limits the model complexity and therefore other simplifications to the steam cycle model are necessary. Selected parameters of the finished steam cycle model will be presented and model predictions of the value of these parameters will be compared to the Alstom heat balances.*

### 8.1 Steam cycle simplifications

The original steam cycle as found in NJV3 has a few features that implies significant difficulty for the convergence in EES. A few major simplifications on the steam cycle are therefore necessary to ensure convergence. First of all the two low pressure turbines are removed since their contribution to the electric efficiency is zero or even slightly negative when running in full district heating mode. This of course also means that heat exchanger 2 and 3 are also removed since no steam enters these. That is, apart from the LK and IH outtakes, the steam flows directly from the IP1 and IP2 turbines and into the condenser.

Also there is a loop of 40 kg/s of feed water immediately after the condenser, as can be seen in Figure 6.1 plus an outtake from the sealing system that exchanges heat with the feed water in heat exchanger 1 and then flows into the condenser. These two features are dealt with simultaneously. The 40 kg/s loop is only handled in the sense that mass balance is ensured. That is, 40 kg/s is taken out of the feed water stream between heat exchanger 1 and 2 and put back into the stream after the condenser assuming that it has the same specific enthalpy as the feed water it flows into. This is of course not correct due to the heat exchange in heat exchanger 1. To ensure that the feed water, between the 40 kg/s loop inlet and heat exchanger 1, has the correct enthalpy the stream in heat exchanger 1 is separated into two streams where one is mixed into the feed water immediately after the condenser and the other is mixed in at the position of heat exchanger 1. The mass flow rates are adjusted so that enough steam flows into the feed water after the condenser to ensure the correct enthalpy between the condenser and heat exchanger 1. The rest of the steam flows into the feed water at heat exchanger one and ensures the correct enthalpy after this point. This of course means that the mass flow rate between the condenser and heat exchanger 1 is slightly overestimated.

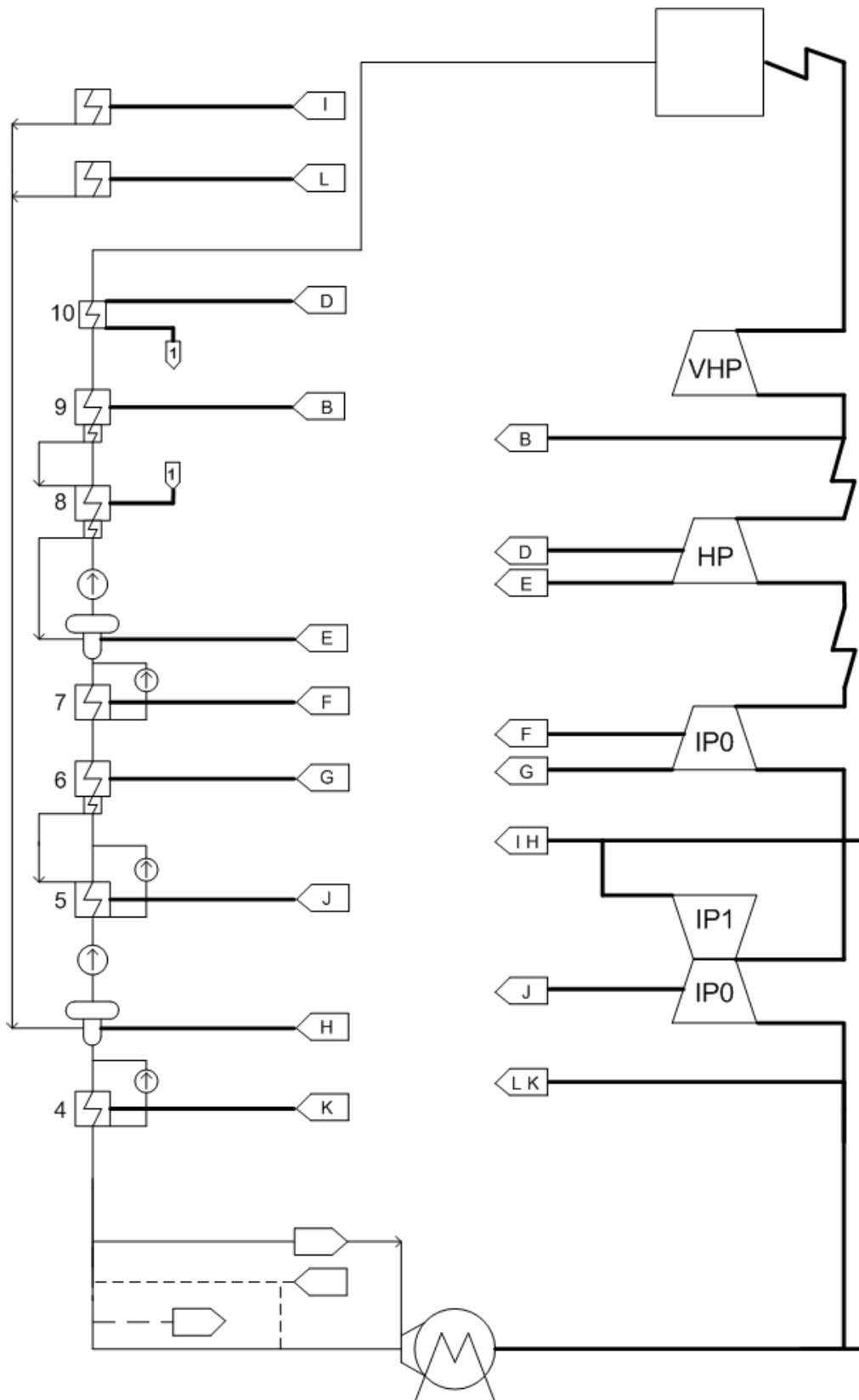


Figure 8.1: The simplified steam cycle used in the steam cycle model.

It should be noted that the reason for the loop of feed water is the necessity to supply sufficient water to the pump after the condenser. This pump is designed for a load configuration where no district heating is produced and therefore has difficulty in pumping a mere 4,44 kg/s of water. Since this pump has very little information on pressure difference across it and since it uses significantly less energy than the two major feed water pumps it has been removed from the simplified steam cycle. The result of these simplifications can be seen in Figure 8.1.

## 8.2 Physical simplifications

The flow in the steam cycle at NJV3 is almost completely selfregulating. The mass flow rate of the steam or feed water in the cycle depends solely on the pressure drop over the different components and tubes in the system. This creates one of the major difficulties of the model when considering convergence and in turn also one of the most significant simplifications done to the way the model works.

The problem arises from the heat exchanger side where the steam from the turbines are condensed in the multiple feed water preheaters. A simplified scetch of the method of condensation used at NJV3 can be seen in Figure 8.2.

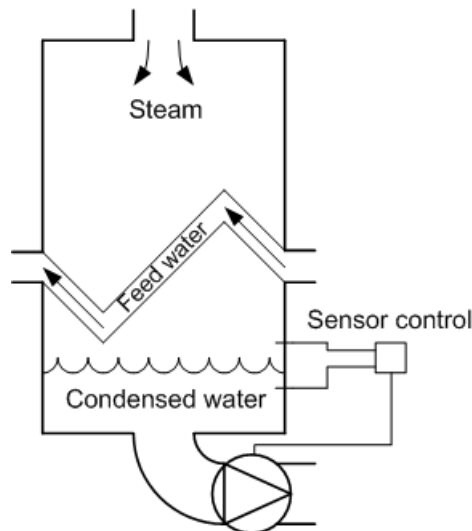


Figure 8.2: The condensing chamber of the heat exchangers.

Steam flows into the condensation chamber as can be seen in the top of Figure 8.2. The steam condenses on the surface of the feed water pipes and falls into the condensed water pool at the bottom of the condensation chamber. Two simple sensors keeps the water level between two marks by adjusting the load on the pump at the water outlet. The water pressure is then throttled down to the pressure level of the point at which it is inserted into the feed water stream.

This behaviour is mathematically no problem to model. However, this creates a complicated interdependency of pressure, mass flow rate, and temperature everywhere in the steam cycle. This is of course due to the many loops that arise in the system with the steam feeding flows to the preheaters. In the simplified steam cycle there are 8 such flows that create a loop in the steam

cycle. Taking into consideration that these loops share certain flows it is obvious that this is something that increases the complexity of the system.

The reason that this looping structure is a problem for the EES solver to handle lies in the fact that the solver, before actually solving the equations, groups them into blocks that can be solved separately. That is, a system with fifty equations can be broken down into perhaps ten blocks of five equations where, after solving one block of equations, it is possible to solve the next and so on. The more broken down the system of equations is the more easy it is for EES to solve the system.

Obviously the more interdependent the system is the harder it is to group into blocks and therefore harder to solve. This, combined with the fact that pressure, mass flow rate and temperature are also mutually dependent, means that using the pressure drops throughout the steam cycle to regulate mass flow rate (and thereby temperature and pressure again and so on...) implies much larger blocks to solve and therefore greater difficulty gaining in convergence.

The problems with convergence that arise from this are so severe that it has proven to time consuming to adjust the model until it converges and a different solution has therefore been applied. Instead of regulating the flow with pressure drops a forced flow has been used dependent on the load case being modelled. That is, we know that at 80 % load, or a mass flow through the boiler of 232.2 kg/s, a certain amount of steam flows through stream B. At 60 % load this value is 25 % lower and so on. To ensure that steam can be taken out of the system and used in the Carbon Capture unit without error the mass flow rate at each stream is determined by the mass flow rate at the stream immediately before instead of by the overall load case.

This simplification means that pressure drop is only modelled from the entrance of the boiler and until the steam enters either the heat exchangers or the condenser. At the feed water side pressure is constant except across the pumps where the pressure increase is modelled as a function of load as can be seen in Chapter 7.

Since the reality is that the pressure, mass flow rate and temperature is mutually dependent, this way of modelling mass flow of course has negative implications. If, for example, a certain stream is used to heat the MEA there will be a pressure drop over the pipes and reboiler which will propagate through the system. This is however solved simply by assuming that any pressure drop due to interactions with the CCS unit is counteracted by a pump or compressor. Of more interest is the fact that removing heat from the steam means lower temperatures which also propagates through the system. This especially would create problems in the condenser chambers where a colder feed water stream would mean more efficient condensation and therefore a higher mass flow through the steam streams for the feed water preheaters. This is a source of error in the steam cycle model and should be taken into consideration when interpreting the model results.

The same looping tendency is present at other places in the cycle. The district heating system has the same effect on the ability to obtain converging solutions as has connecting the system ends into a cycle at the condenser outlet. To ensure convergence the state of the steam is defined at certain points in the steam cycle. After each passing of the steam through the boiler the temperature of the steam is set to 580 °C. The large boiler model presented in Appendix A makes it possible to check if the boiler is actually able to deliver the amount of heat needed. At the inlet of the stream with residual heat from the district heating the steam state is also defined as is also the case after the condenser.

### 8.3 Model results

The finished steam cycle model consists of 577 equations in 577 variables. These equations draw on 6 lookup tables with values for thermal resistances, turbine efficiencies and  $K_L$ -factors. The model code itself can be separated into two major parts. A part in which the code for each component is introduced in the form of an EES module or procedure and another part in which calls of each component is stated along with equations describing the relationship between each component. The component call part of the code is again divided into two parts, one on each side of the boiler. The entire code can be seen on the enclosed CD.

Running the steam cycle model at full load the following electrical efficiency is returned.

$$\eta_{el} = 44.23\% \quad (8.1)$$

This value of electrical efficiency should be compared to an electric efficiency calculated on the basis of Alstom (1993) of approximately 43.5 % in full district heating mode. This is based on a method of calculating electric efficiency that takes the heat input into the steam cycle (as opposed to the heat generated in the boiler) plus the work input from the major feed water pumps and relates this to the power output as can be seen in equation (8.2).

$$\eta_{el} = \frac{P_{total}}{\dot{Q}_{boiler} + W_{pumps}} \quad (8.2)$$

The value returned by the steam cycle model is slightly higher than would be expected since mechanical losses and losses in the generator are not included in the steam cycle model. Removing these losses from the Alstom electrical efficiency returns an efficiency of 44.17 %, only 0.06 % points lower than the predicted value from the model.

Evaluating the thermal efficiency with district heating at full load in the model yields a value of

$$\eta_{therm} = 97.95\%. \quad (8.3)$$

This value should be compared to a value of 97.52 % found via Alsthoms heat balance (or 98.2 % without losses). Looking at the actual district heating output the model returns values of 422 MW which is precisely the district heating output stated by Alstom. The total electrical power output predicted by the steam cycle model is seen in equation (8.4).

$$P_{electric} = 347.5MW \quad (8.4)$$

This value is 2.3 % higher than the total power output stated by Alstom. The heat intake of 775.5 MW in the boiler predicted by the model is 0.8 % higher than the value found in the Alstom heat balance.

Looking at the distribution of electrical production on the turbines, a comparison between model predictions and the Alstom heat balance can be seen in Table 8.1.

<b>Turbine</b>	VHP	HP	IP0	IP1	IP2	Sum
	%	%	%	%	%	%
<b>Model</b>	25.40	25.55	18.97	12.61	17.47	100.00
<b>Alsthom</b>	25.42	25.46	19.01	12.69	17.60	100.18
<b>Difference</b>	-0.02	0.09	-0.04	-0.08	-0.13	-0.18

Table 8.1: Turbines share in electricity production in the model and in the Alsthom heat balances.

The differences between the model results and the Alsthom heat balances in Table 8.1 are very small. This leads to the conclusion that the turbines of the system behaves in the same manner as in reality. It should be noted here that the extra 0.18 % in the Alsthom values are used to rotate the LP turbines.

Finally it is possible to study the precision of the model predictions at a detailed level by inspecting predictions of pressure, temperature, mass flow rate and enthalpy throughout the system. In Table 8.2 a comparison between selected model variables and their counterparts from the Alsthom heat balance can be seen.

<b>h</b>	<b>Prediction</b>	<b>Deviation</b>	<b>P</b>	<b>Prediction</b>	<b>Deviation</b>	<b>T</b>	<b>Prediction</b>	<b>Deviation</b>
	kJ/kg	%		bar	%		° C	%
$h_2$	3056	0.1	$P_1$	285	0	$T_{19}$	163.9	0.24
$h_{7,1}$	2860	0.02	$P_{VHP}$	279.3	0	$T_{21}$	211.2	0.28
$h_{7,2}$	2671	0.01	$P_2$	78.03	0	$T_{22}$	216.5	1.00
$h_{14}$	65.67	0.16	$P_3$	74.12	0.013	$T_{23}$	247.5	0.76
$h_{15}$	311.9	0.02	$P_{HP}$	72.93	0.014	$T_{24}$	290.7	0.62
$h_{16}$	422.5	0.01	$P_4$	20.61	0	$T_{25}$	296.2	0.61
$h_{17}$	425.8	0.27	$P_5$	18.96	0	$T_2$	370.4	0.08
$h_{18}$	569.0	0.25	$P_{IP0}$	18.58	0	$T_4$	379.6	0.08
$h_{19}$	693.9	0.27	$P_6$	7.123	0.07	$T_6$	426.7	0
$h_{20}$	825.3	0.20	$P_{IP12}$	7.051	0.07	$T_{7,1}$	192.7	0
$h_{21}$	902.9	0.35	$P_{7,1}$	1.078	0.19	$T_{7,2}$	93.45	0.16
$h_{22}$	938.6	1.05	$P_{IP2_{out}}$	0.3908	0.31	$T_B$	369.8	0.11

Table 8.2: Detailed view of steam cycle model predictions of selected variables at full load.

In Table 8.2 values of enthalpy, pressure and temperature has been given at selected points in the steam cycle model along with their deviations in percent from the Alsthom heat balance. An almost continuous sequence of values has been chosen for each variable except for the temperature where two continuous sequences has been chosen.

Looking at the enthalpy, the first three values are taken at the VHP turbine outlet and at the IP1 and IP2 outlets. The remaining enthalpy values are a series of values starting after heat exchanger 1,  $h_{14}$ , and continuing until after the second feed water pump,  $h_{22}$ . Noticeable in the first three values is merely that the outlet values of the IP1 and IP2 turbines are not identical since the turbines are different. Going over the values from  $h_{14}$  to  $h_{22}$  the enthalpy is slowly climbing corresponding to addition of heat from the steam side. Looking at the deviation from the same values in the Alsthom heat balance these are in general very small. However there is a tendency for the deviations to slowly rise as we move up in enthalpy. Between  $h_{21}$  and  $h_{22}$  the deviation experiences a sudden increase. The explanation for this is found in the way the feed water pumps are modelled. Since no

pump characteristics were available the pump models are based on an interpolation of the pressure difference over the pump, based on the mass flow rate. This pressure difference is converted into an enthalpy difference via equation (7.38) and this is where the enthalpy is lost.

Turning to the pressures, a series of pressures from the boiler outlet,  $P_1$ , and to the outlet of the IP1 and IP2 turbines,  $P_{7,1}$  and  $P_{IP2,out}$  respectively, is chosen. It is noticeable that the predictions are very precise but that the deviations increase slightly at low pressures. This is merely because they are stated in percentages, meaning that a small difference appears larger in percent when the compared variables are also small.

The temperatures are, as mentioned, taken in two series, one from before heat exchanger 7,  $T_{19}$  and until after heat exchanger 10,  $T_{25}$ , and one from after the VHP turbine and until after the IP1 and IP2 turbines. In addition, there is also a value for the output temperature of the first cross-stream, stream B. The temperature deviations are in general the largest in Table 8.2. This is especially the case on the heat exchanger side even though it has been concluded that the turbine models are more unprecise than the heat exchangers.

Taking an overview of the results presented in this section it is possible to conclude that the model works and predicts steam cycle behaviour well at full load. This is important since it is at full load the integration study with the CCS unit is going to take place. Whether the model provides results of a similar quality at partial load is a question of convergence and can be used as a tool of verification. In the next section the matter of convergence is studied in more detail.

## 8.4 Steam cycle model convergence

In this section a number of discussions pertaining to steam cycle model convergence will be conducted. Several different subjects are interesting in this context and will be treated individually.

### 8.4.1 The open loop control method

The steam cycle model is not a closed loop as normally seen in a steam cycle. In order to promote convergence of the system an additional stream has been made and the mass flow rate and specific enthalpy of this steam set free. This means that the solver can vary the mass flow rate and specific enthalpy of this free inlet in order to make the system converge. In Figure 8.3 a diagram of the method can be seen.

In order for the system to have converged correctly it is necessary for the free inlet to have nearly zero mass flow rate and nearly zero total enthalpy. In equations (8.5) and (8.6) the values of the mass flow rate of the inlet and the total enthalpy can be seen.

$$\dot{m}_{free} = 0.004306 \text{ kg/s} \quad (8.5)$$

$$H_{free} = 0.108 \text{ kJ/s} \quad (8.6)$$

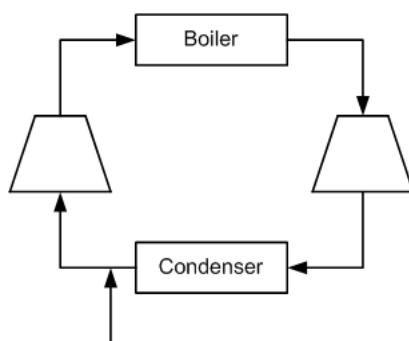


Figure 8.3: Diagram of free inlet to promote convergence.

These values are certainly small enough to consider the model converged satisfactorily. It is a confirmation that conservation of mass and energy is kept throughout the steam cycle.

#### 8.4.2 Partial load convergence

In order to verify the model it is, as mentioned, necessary for it to converge to a correct solution also at partial load. This has been tested by running the model at 80 % load since a heat balance for this load case is provided. This report will not include a lengthy presentation of model results from the 80 % load case but merely convey the conclusion that the model converges fully at partial load also. The precision of the model predictions are slightly less accurate but this is merely due to the interpolations, controlling the mass flow rates around the cycle, being slightly off at this load. An adjustment of these interpolations would have the model return as accurate results as at full load.

Heat balances for load case 40 %, 60 %, 80 % and 100 % are provided, which means that it is possible to give EES precise guesses on the correct solution at these loads. Therefore EES is able to converge to tolerance in these cases. When running the model between these discrete loads it is not possible to provide guesses for the variables unless one does an almost insufferable amount of tedious calculations. Therefore EES has problems converging to tolerance between the discrete loads. It is, however, very close and the results returned by EES shows that the model precision drops slightly when moving away from the 100 % load case. Again this is contributed to the mass flow rate interpolations which by a rough count will amount to approximately 30 interpolated equations. The mass flow rate interpolations are often dependent on each other and therefore small uncertainties in each interpolation will propagate into the others and yield unpredictable fluctuations in model precision. An adjustment of the mass flow rate interpolations to higher precision will improve the precision of the model at partial load.

#### 8.4.3 Convergence with heat loss

The purpose of the steam cycle model is not only to function as a mathematical replica of the steam cycle at NJV3 but also to model the change in the steam cycle as heat is taken out and used in the reboiler of a MEA CC unit. Due to the demands for amount and quality of energy for the reboiler (approximately 200 MW at 120 °C) it is only possible to extract the heat from certain places in the steam cycle. The areas in which the steam holds enough enthalpy and high enough

temperature are after the boiler through the turbines until the end of the IP1 turbine where the IH district heating outlet provides the lowest feasible combination of temperature and enthalpy content.

Taking heat out of the steam cycle of course makes the solution diverge from the untouched steam cycle model. It is not possible to provide new guesses for the solution with the outtake of heat without embarking on tedious hand calculations of the effect on the steam cycle. Therefore it is not necessarily certain that the steam cycle will converge under these conditions.

This matter has been tested in three more or less feasible locations in the area of the steam cycle where the steam has sufficient attributes. Immediately after the boiler where the steam holds the most enthalpy and where there is the maximum possible mass flow, the maximum possible heat transfer, while maintaining convergence, was 86.7 MW. Above this point the VHP turbine model and heat exchanger 9 experience so large deviations from the original guesses that they cease to converge. At the district heating stream I heat has also been removed and here it is quite possible to extract 200 MW of heat without losing the ability to converge. This is of course due to the fact that this stream delivers more than 200 MW to the district heating system so that removing this heat means only less district heating and no change in the steam state at the inlet of the first feed water tank. Finally heat extraction has been tested between the IP0 and the IP1 and IP2 turbines. This is the place in the steam cycle where the effects of extraction on the steam cycle are most complicated. In this location, it has been found, that the steam cycle model is only able to accept a heat extraction of 14 MW which is hardly enough to use in combination with the MEA CC model.

This behaviour has fundamental implications on the use of the model. Combining the steam cycle model with a model of carbon capture with MEA seems only feasible when extracting the heat at the I stream and a full integration study is therefore not an option. This is due to the inherent dependency on correct guesses for convergence in EES which will be further discussed in the next section. However, there are other options for conducting an integration study on the basis of the results of both the steam cycle model and the MEA CC model. These options will be explored in Chapter 10.

It should be noted that it is most likely the heat exchanger models that are restraining convergence since these hold the highest complexity. A possible measure to promote convergence would be to replace the heat exchanger models with other more simple models. This is actually possible since there exists explicit methods of modelling heat exchanger which would be an option for further iterations on the steam cycle model.

## **8.5 Steam cycle model conclusion**

Upon construction and testing of the integrated steam cycle model it has been found that the model predicts steam cycle behaviour well at full load. It has been verified that the model also predicts results well at partial load also, even though slight adjustments of the mass flow rate equations are necessary to achieve equal precision to predictions at full load. The results of such adjustments are not presented here since there is little use of model results at partial load further in this report.

The model has been found to have certain limitations due to convergence issues in EES. First of all assumptions have been made to eliminate looping structures in the mass flow rate and pressure equations to promote convergence. This limits the possibility of introducing additional pressure

loss in the steam cycle since this would have an effect on the mass flow rates that this model would not be able to predict. Also mass flow rates are independent of temperatures in condenser chambers which is an approximation. Secondly solver instability in EES limits the possibility of removing heat from the steam cycle. This constitutes a problem for the integration study which must be adjusted to these circumstances.

In general it can be said that solver instability in EES puts major limitations on the model. Convergence issues forces a number of assumptions restraining the natural dynamics of the system as well as limits the use of the finished model. It is possible to conclude that EES is not necessarily the right choice of software for this type of modelling. For an introduction to the EES unlinear equations solver see Appendix B.

## Chapter 9

# CCS model

*This chapter will describe the CCS model as to how the real system is operating, which parameters has been used and how the model has been built mathematically. The model has been based on design information from Vattenfall and makes no attempt at modelling the actual thermodynamics and chemics internally in the CCS unit. Instead, heat transfer to and from the model, heat generation within the CCS unit and certain model temperatures are given in the design information. Therefore the model merely accepts inputs from the steam cycle model and the surroundings and returns values for use in the steam cycle model.*

### 9.1 The model in words

The proposed CCS system for NJV 3 can be seen in Figure 4.1. A relatively simplified model of this system has been build to mimic the behaviour of the system, with respect to heating needs of the reboiler, the utility cooling and excess heat of compression. The word simplified should be interpreted as meaning that the model is limited to the full load case and no further, due to insufficient system data. Also the model does not predict any internal processes but only interactions with its surroundings.

The model takes the flue gas, a cooling and a heating stream from the plant as input. The flue gas enters the flue gas cooler, where the hot fluegas is chilled to 40 °C by the cooling stream from the plant and, if needed, utility cooling. The cooled flue gas enters the absorber. Inside the absorber a chemical process occurs releasing heat when the CO<sub>2</sub> reacts with the MEA. This heat amounts to 17 MW that is removed using utility cooling.

The CO<sub>2</sub> rich MEA solution is then pumped through a heat exchanger to the stripper. In the heat exchanger, the rich solution recieves energy from the lean solution that has been stripped. In the stripper column, the rich solution is heated in a heat exchanger. This heating allows the CO<sub>2</sub> to evaporate along with some of the water. The lean MEA solution is pumped back to the absorber, first exchanging heat with the rich solution and then cooled to 40 °C through utility cooling. The evaporated CO<sub>2</sub>/water is cooled. In this project this cooling has been assumed to fully condense the water out of the mixture, leaving pure CO<sub>2</sub> for the compression. The compression is done in stages, which are intercooled, and eventually reach 110 bar.



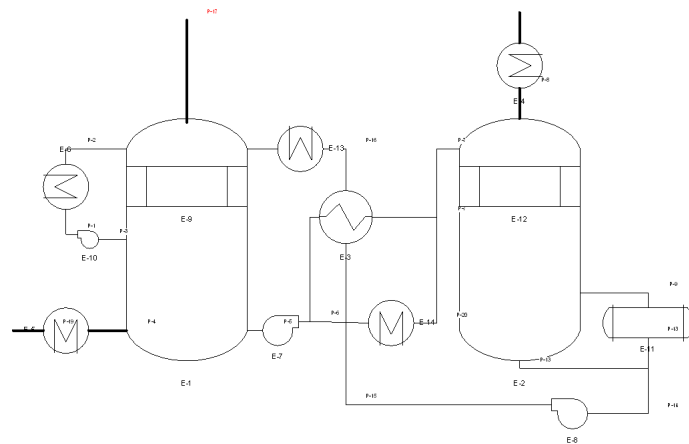


Figure 9.2: CCS unit with integrated district heating (Andersen, 2009a).

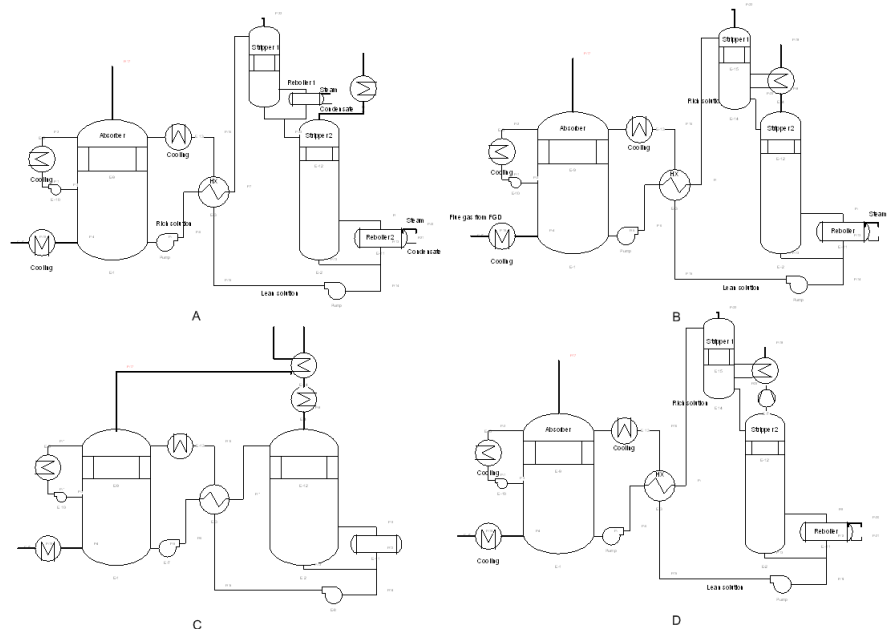


Figure 9.3: Proposals to the system at NJV3 (Andersen, 2009a). Only the configuration of the components is important in this figure.

may seem futile. There are two reasons for heating the flue gas. From an engineering point of view, the gas has to be hot enough to travel up the chimney and a rapid condensation once released is unwanted, due to small amounts of sulfur that may react and form sulfuric acid. Secondly there is an image problem for the power plant owners if too much smoke is released, regardless of the fact that it is mainly water vapor in this case.

## 9.2 The parameters of the model

For this model a number of parameters has been determined and treated as constants during the modelling. These have been selected based on the CASTOR project in Esbjerg, but slightly mod-

ified according to Andersen and Köpcke (2007) and Andersen (2009b). The parameters that has been selected is a solvent/gas temperature in the absorber of 40 °C, a system pressure of 2 bar, a liquid/gas ratio of 6.581 and a pinch temperature of 2 K between the rich and the lean MEA/CO<sub>2</sub> mixture. This yields a MEA flow of 2326 kg/s and a reboiler duty of 3.03 MJ/kg(CO<sub>2</sub>), according to Figure 9.4. In this model the liquid/gas (LG) ratio is slightly higher than in the CASTOR project according to Andersen (2009b).

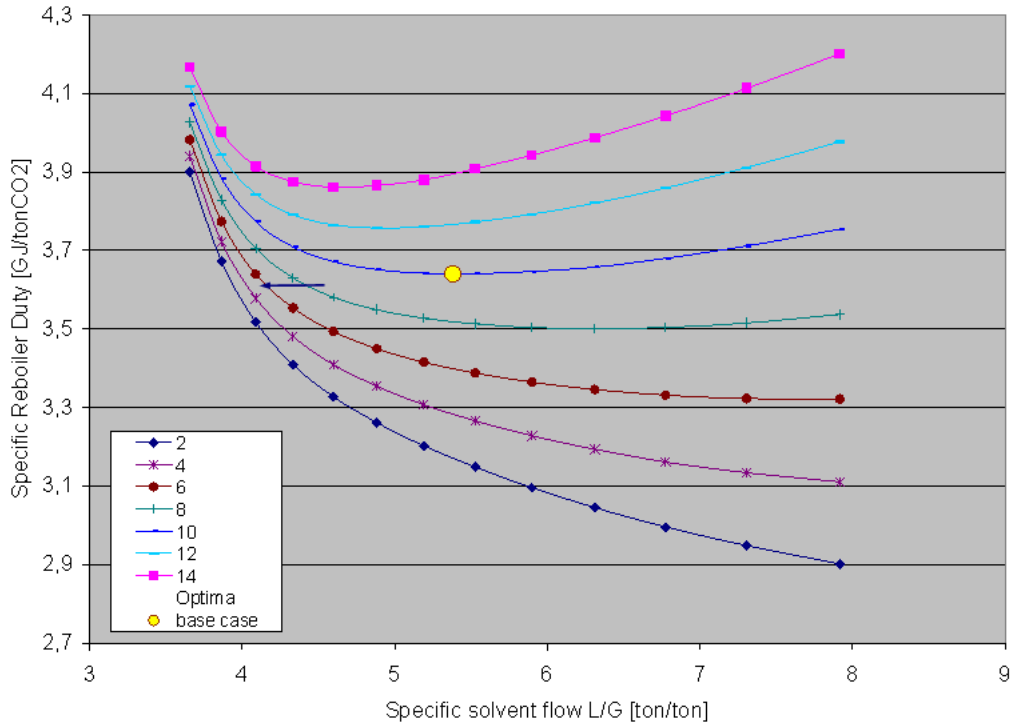


Figure 9.4: Graph depicting specific boiler duty as a function of LG Ratio and pinch temperature (Andersen and Köpcke, 2007).

As can be seen in Figure 9.4 lower pinch temperature in the heat exchanger between lean and rich solvent improves performance. The behaviour of the dark blue line, depicting the 2 K pinch, furthermore shows an improved performance with higher LG-ratio. The yellow dot on the graph indicates the CASTOR project.

For the compression a 4 stage intercooled compression has been selected, to minimize work load. For multistage compression an equal compression rate is usually preferred. To find the compression rate, the general practice follows (9.1).

$$CR = \sqrt[n]{\frac{p_2}{p_1}} \quad (9.1)$$

Where CR is the compression rate, n is the number of stages, p<sub>1</sub> and p<sub>2</sub> is the pressure before and after the compression respectively. Applying the values for the model, this yields (9.2).

$$CR = \sqrt[4]{\frac{110}{2}} = 2.723 \quad (9.2)$$

### 9.3 The mathematics

The model has been build as simple and crude as possible while still maintaining a sufficient accuracy. The heat exchangers has been modelled as "perfect" heat exchangers with an added pinch temperature, to imply reasonable temperature relations. That is to say, that the stream with the highest relative energy difference does not, mathematically, transfer heat with a stream of the opposite streams temperature, but with a temperature altered by the value of the pinch. This means, that if two streams of 40 °C and 120 °C respectively were to transfer heat with a 5 K pinch, one of them would in fact be matched with a stream of either 45 °C or 115 °C, yielding a lower heat transfer thus mimicing the behaviour of a true heat exchanger. The heat exchanger set up of an exchange of two streams can be seen in equation (9.3), (9.4) and (9.5).

$$T_{2,out} = T_{1,in} - 5 \quad (9.3)$$

$$Q = (\text{enthalpy}(\text{water}; T = T_{1,out}; P = P_1) - \text{enthalpy}(\text{water}; T = T_{1,in}; P = P_1)) \cdot \dot{m}_1 \quad (9.4)$$

$$Q = (\text{enthalpy}(\text{water}; T = T_{2,in}; P = P_2) - \text{enthalpy}(\text{water}; T = T_{2,out}; P = P_2)) \cdot \dot{m}_2 \quad (9.5)$$

It should be noted, that these three equations are part of a larger set of equations solved simultaneously, yielding both temperatures and mass flows. Furthermore, it is important to bear in mind, that EES is an iterative solver, that does not need the equations listed chronologically or explicitly.

The given code will eventually, in cooperation with the remaining code, yield an outlet temperature of stream 1 and 2 including a mass flow of stream 2, when given information on inlet conditions as well as massflow of stream 1.

When only a heat flux from a hot stream is given, an even simpler model is used. In these cases, the heat is simply added to the coolant stream, again using a pinch temperature relative to an assumed temperature of the source. A part of the model can be seen in equation (9.6), (9.7) and (9.8).

$$T_{1,out} = 40 - 5K \quad (9.6)$$

$$Q = 50MW \quad (9.7)$$

$$Q = (\text{enthalpy}(\text{water}; T = T_{1,out}; P = P_2) - \text{enthalpy}(\text{water}; T = T_{1,in}; P = P_1)) \cdot \dot{m}_2 \quad (9.8)$$

In this example, the source stream is estimated to be 40 °C, with a cooling need of 50 MW. The coolant stream is allowed to be heated to 5 K below this temperature. By defining an inlet temperature of the coolant stream, these lines will return the needed mass flow of coolant in the system.

The compression has also been modelled as simple as possible. As the isentropic efficiency of a compressor is relatively high, the compressors has been modelled isentropically. The model can be seen in equation (9.9) and (9.10).

$$s = \text{entropy}(\text{CarbonDioxide}; T = T_1; P = P_1) \quad (9.9)$$

$$T_2 = \text{temperature}(\text{CarbonDioxide}; s = s; P = P_2) \quad (9.10)$$

These two lines will, when supplied with a temperature and pressure for state 1 and a target pressure, return the temperature in state 2.

The main mass flow, that is the MEA solution, is governed by two single variables based on the LG-ratio of the system. In this project the LG ratio has been set to 6.581, based on Andersen (2009b). With a CO<sub>2</sub> mass fraction of 0.2137, a flue gas mass flow of 353.4 kg/s (Vølund A/S et al., 2001) and a CO<sub>2</sub> caption rate of 90 %, this yields a captured CO<sub>2</sub> flow of 67.97 kg/s. From the LG ratio, which relates to the flue gas mass flow, the lean MEA solution mass flow can readily be calculated to 2326 kg/s and the rich solution to 2394 kg/s.

As the real system would require to pump both the lean and the rich solutions to the top of the absorber and stripper respectively, a set of pumps would be expected. As this system has not been build nor fully designed yet, the height of these vessels has not yet been determined. Thus the work needed by these pumps can not be precisely predicted, but according to Andersen (2009b) an elevation of 30 m would be a reasonable estimate. The effect needed for the pumps has been calculated through a simple energy balance seen in equation (9.11).

$$W_{pump} = \Delta z \cdot g \cdot \dot{m} \quad (9.11)$$

$W_{pump}$  being the work of the pump,  $\Delta z$  being the height difference,  $g$  being the acceleration due to gravity and  $\dot{m}$  being the mass flow. This is a simplified version of the standard energy balance, assuming an equal pressure, no heat loss and no difference in velocity before the pump and after the elevation. In other words, the stream that enters the pump, stream a on Figure 9.5, is identical to stream c in every aspect. The properties in the b part of the stream is not calculated in this model.

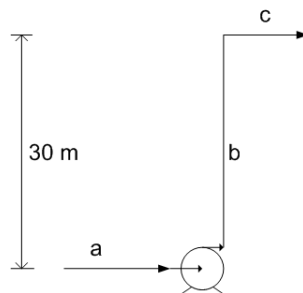


Figure 9.5: Pumping sketch

Throughout the system, heat exchangers must be prepared to handle possible phase shifts of the streams. As the quality of a given stream might be of interest, the model is build to be compatible with these shifts. For demonstration purposes, the heat exchangers has been modelled in different ways. One approach is to use the temperatures and heat capacities to determine the heat exchange. When using temperatures, one has to take the saturation temperature into account, as the temperature stays the same throughout the evaporation/condensation process, while the heat transfer is high. When using this approach, a convenient method of programming is using the "procedure" programming method of EES. This is a programming method that allows for chronologically executed scripts, which in turn allows for using IF-THEN-ELSE structures facilitating the possibility of executing different script parts dependent on the situation. The other approach, which is a

much simpler mathematical solution, is to use enthalpies, where the evaporation/condensation energy follows with no further programming from the enthalpies.

#### **9.4 CCS model conclusion**

The CCS model has been constructed on the basis of inadequate information prohibiting the construction of a full model of the CCS unit in the same way as done with the steam cycle. What goes on internally in the CCS unit is largely unmodelled and only the effect in the steam inlet from the steam cycle and on the utility cooling water has been modelled. Therefore the CCS model presents itself as an add-on to the steam cycle model.

The parameter values returned by the model are dependent on the inlet conditions of the streams. Therefore results of this model are not presented in this chapter but in Section 10.5 where actual inputs from the steam cycle model are used.



## Chapter 10

# CCS Integration

*In this chapter the integration study between the steam cycle model and the CCS model will be presented. The chapter will begin with a sensitivity analysis of the steam cycle model to find out what the steam cycle sensitivity is, in terms of efficiency, electricity production and heat production, when heat is removed at different points. At feasible points the steam cycle model and the CCS model will be combined to predict the effect of the CCS unit on the same parameters. Measures to regain waste heat from the CCS system will be considered and their effect on the same parameters will be presented. The different alternatives for integration and their effects on plant performance will be discussed in order to enable a conclusion pertaining to retrofitting a CCS unit at Nordjyllandsværket block 3.*

### 10.1 Sensitivity analysis

When integrating a system as the CCS unit into a power plant, there are many things to consider. First of all, the energy needed for the reboiler must be extracted from somewhere in the steam cycle. But as this energy has to be of a certain amount and quality, there are restrictions as to where the heat can be extracted. These restrictions will inevitably force the extraction closer to the boiler. Vattenfall has made a series of correlations between how the extracted steam pressure and temperature will affect the plant. Presented here is an example of one of these correlations for the IP1 turbine, Figure 10.1.

From the correlation can be seen, that the higher quality heat we extract for the CCS unit, the energy penalty will increase, due to the fact, that higher quality steam must be extracted closer to the boiler, thus yielding lower energy flow through the turbines further away from the boiler. In conclusion, the further away from the boiler the heat can be extracted the better. In this project it is not considered a possibility to alter the steam cycle components.

The steam cycle model may not be able to accept removal of the necessary amounts of heat for the CCS unit but nevertheless it can provide valuable information on the steam cycle behaviour as heat is removed. As will be seen during this section, the information obtained from a sensitivity analysis can form the basis of credible evaluations of efficiency, electricity and heat production.

Pressure	1,5	2	2,5	3
Steam(kg/s)	Bara	bara	bara	bara
76	-37	-44	-49	-53
78	-37	-44	-49	-54
80	-38	-44	-50	-54
82	-38	-45	-51	
84	-38	-47	-52	
86	-39	-48	-54	
88	-39	-49		
89	-40	-50		
90				

	Forbidden
	Turbine Design modification needed
	Acceptable

Figure 10.1: Power loss in MW due to extraction of steam from the IP1 turbine as a function of steam pressure and mass flow rate, (Andersen, 2009a)

In Chapter 8 limits of the steam cycle model when removing steam was found in certain points. The same points will be used for the sensitivity analysis since these points are the strongest candidates for heat removal for the CCS unit. Even though the limit of heat removal in certain cases was relatively low there is a sufficient range of possible heat removal for a sensitivity study at the selected points.

The selected points are as mentioned in Chapter 8 immediately after the boiler before the VHP turbine, at the I stream for the district heating and immediately after the IP0 turbine before the inlet of the IP1 and 2 turbines. In Figure 10.2 the steam cycle with red markings at these points can be seen.

A couple of comments can be attached to the chosen points for sensitivity analysis. First of all there are significant difficulties with extracting heat between the boiler and the VHP turbine. This is due to the fact that the heat removed here is not immediately replaceable by transferring more heat from the boiler. This is of course, due to the fact that more heat from the boiler means higher temperatures in the boiler and therefore also more heat transferred to the first and second reheaters. The reheaters are already at maximum temperature (580 °C) at normal boiler temperature and it is therefore a potential problem to raise the temperature due to the thermal stress limitations of the steel in the superheater tubes. It may be possible to adjust the temperature in the reheaters by injecting more cold feed water but this has not been studied. In Appendix A, the large boiler model presented is able to predict the effects of raising boiler temperature as well as the needed mass flow rate of injection to control steam temperature in the reheaters. This, however, requires some manual iterations making it too time consuming to do in this project. Therefore the heat is removed from the first point without adding more heat from the boiler.

In the second point at the I stream, which is the best candidate for heat removal, the heat removed affects only the district heating system, since this stream holds more heat than necessary for the CCS unit to function. Therefore it is possible to predict the loss of efficiency by hand at all levels of heat removal since it is merely a question of subtracting the heat from the district heating and calculating the new efficiency. However, this point is considerably more interesting when combining the steam cycle and CCS model and when recuperating waste heat from the CCS.

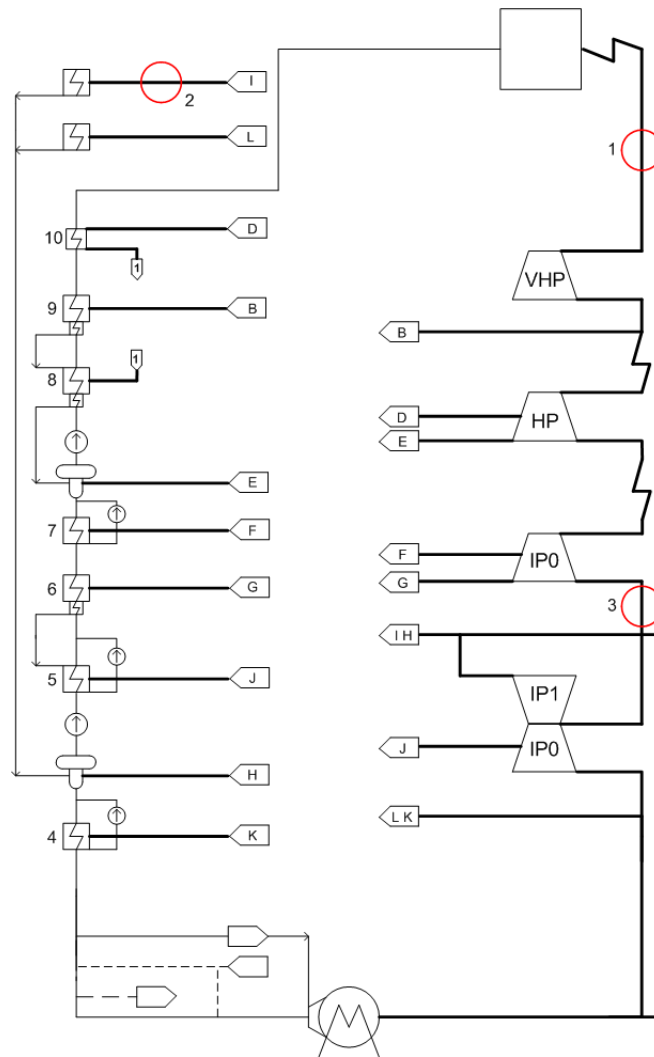


Figure 10.2: The selected points for sensitivity analysis in the steam cycle.

Therefore the sensitivity analysis at this point provides some preliminary indications of the effect of removing heat from the I stream to be further investigated in the following sections.

The last point immediately after the IP0 turbine is the point in which heat removal will have the most complicated effect on the steam cycle. Both the electricity and the heat production will be affected by removing heat here. This is therefore the most interesting point to do a sensitivity analysis, especially when considering that this is where the model diverges at the lowest heat removal.

It should be noted that the CCS unit demands 18.3874 MW of electricity to run pumps and compression of CO<sub>2</sub>. This value is subtracted from the electricity production when calculating efficiencies in order to make these more realistic in terms of integration with the CCS unit. Therefore the electricity productions presented in the following are what the power plant produces minus what is used for the CCS unit and these values are then used for calculating efficiencies. Therefore the efficiencies and electric production values are therefore slightly lower at no heat removal than predicted in Chapter 8.

### 10.1.1 Point 1

When heat is removed from the steam after the boiler before the VHP turbine the electricity production responds as can be seen in Figure 10.3.

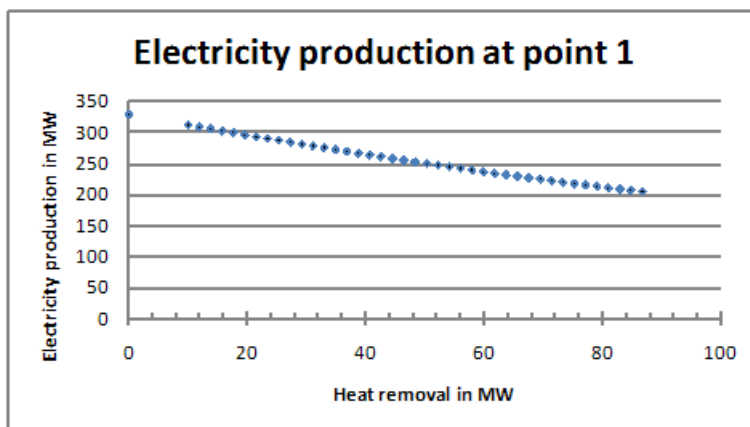


Figure 10.3: Electricity production under varying heat removal at point 1.

This tendency is as expected when removing heat just before the turbines. Removing 85 MW of heat makes the electricity production drop by 122 MW plus the 18 MW that are constant for the CCS unit. Linear extrapolation of this result to the 206 MW needed for the CCS unit returns an electricity production of only 32,5 MW. This is of course completely unacceptable and underlines the unfeasibility of point 1 as a potential spot for extracting heat.

Looking at the production of district heating a different behaviour is displayed, see Figure 10.4. As heat is removed from point 1 the district heating increases significantly. When 86 MW of heat is removed from the steam cycle the district heat is increased by 66 MW.

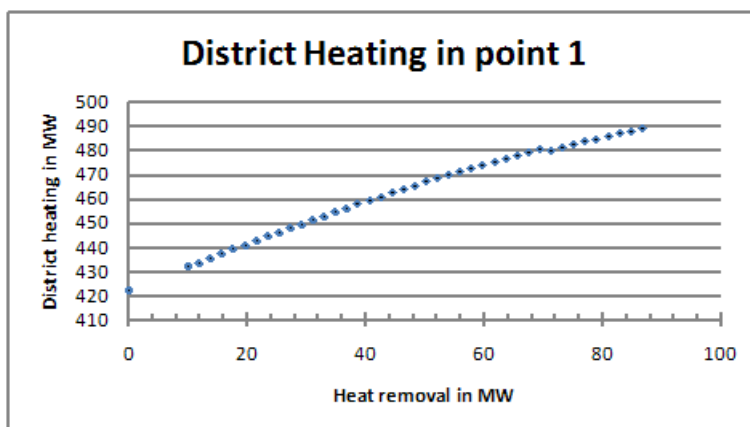


Figure 10.4: Heat production as a function of heat removal at point 1.

This behaviour is so far unexplained. The extra heat available for the district heating stems from a lower electricity production in all of the turbines making the IH stream hotter. Why the turbines all produce less energy is not known since the inlet conditions of the turbines after the second re-heating should be normal. It is therefore not known whether this is a physically correct result or a

consequence of the model structure. It would require a thorough study of model behaviour to conclude anything about this. The presented behaviour results in efficiencies as seen in Figure 10.5 and Figure 10.6.

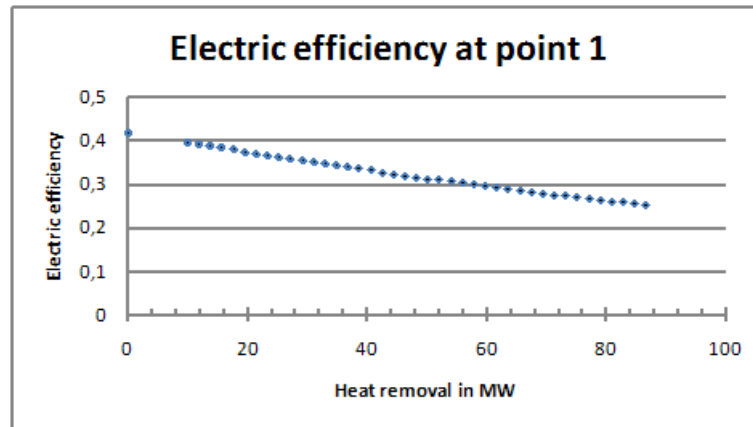


Figure 10.5: The electric efficiency as a function of heat removal at point 1.

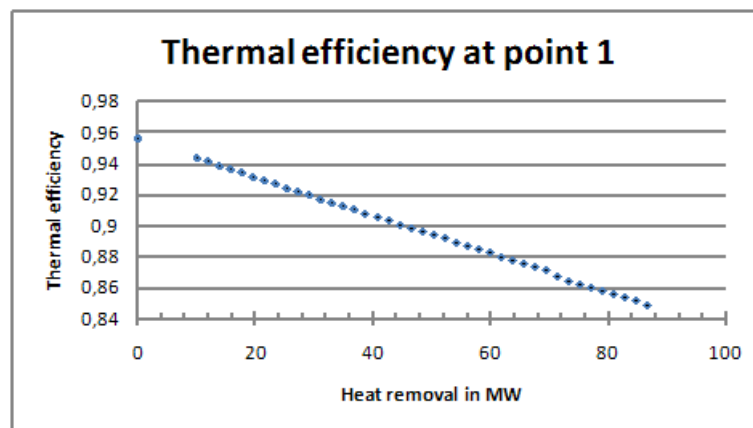


Figure 10.6: The thermal efficiency as a function of heat removal at point 1.

As can be seen in Figure 10.5 and Figure 10.6 both the electric and the thermal efficiency drops as heat is removed. While the electric efficiency drops 17 percentage points from approximately 42 % to 25 %, over the 86 MW of heat removed, the thermal efficiency drops 11 points from approximately 96 % to 85 %. This is as expected when the electricity and heat productions are taken into consideration. It must, however, be remembered that these efficiency drops are merely at removal rates of 86 MW which is nowhere near the over 200 MW necessary for the CCS unit to function.

The information obtained from the sensitivity analysis in point 1 is that it is not feasible to extract heat for the CCS unit here. There are several reasons for this. First of all it is not necessarily physically possible with the boiler type at NJV 3 but also the electricity production drops so rapidly that it would be unreasonable from an economic point of view to extract heat here.

### 10.1.2 Point 2

Removing the necessary heat from the I stream for the district heating is the best candidate for supplying the CCS unit with steam. This is because removing heat from this stream does not immediately affect the electric efficiency. Also, the I stream is the stream with the lowest energy quality it is still feasible to use for heating the reboiler. It should be noted however that removing heat from the district heating system also proposes a problem since Nordjyllandsværket is obliged to be able to deliver 422 MW of district heating. Removing between 0 and 206 MW of heat from the I stream results in the following curve of electricity production, see Figure 10.7.

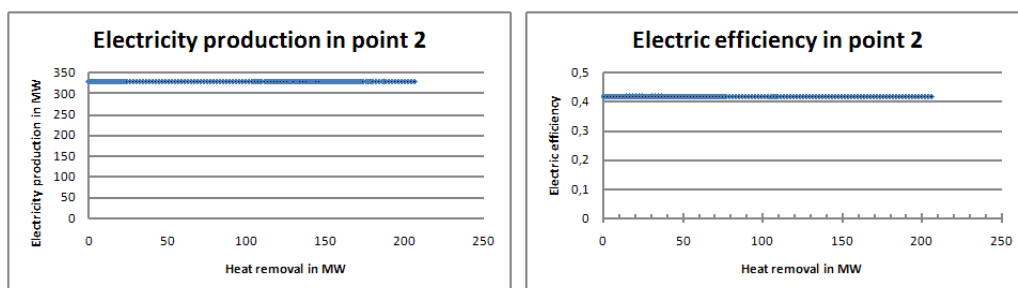


Figure 10.7: The electricity production and the electric efficiency as a function of heat removal in point 2.

It is obvious from Figure 10.7 that the electricity production is unaffected by removal of heat from the I stream. Therefore also is the electric efficiency as can also be seen in Figure 10.7. Therefore the effects on the steam cycle performance must be found in the district heating output. The district heat production when heat is removed at point 2 can be seen in Figure 10.8.

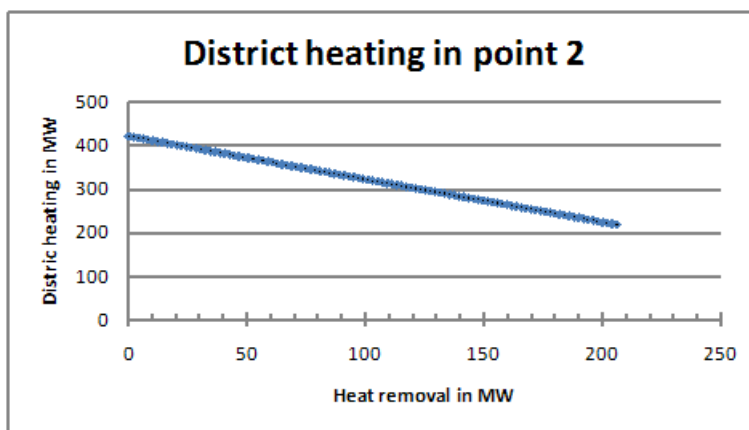


Figure 10.8: District heating production as a function of heat removal in point 2.

As heat is removed from the district heating stream I, the district heating naturally drops. When the full 206 MW of heat for the CCS unit is removed the district heating output drops by the same 206 MW. This has an effect on the thermal efficiency of the steam cycle as can be seen in Figure 10.9.

In Figure 10.9 it can be seen that the thermal efficiency of the plant drops by approximately 26 % point from 95.61 % to 69.39 % when removing 206 MW in stream I. This corresponds to removal of roughly half of the district heating effect. In general the steam cycle is very stable to the removal of heat in the I stream which has almost no effect on the steam cycle itself.

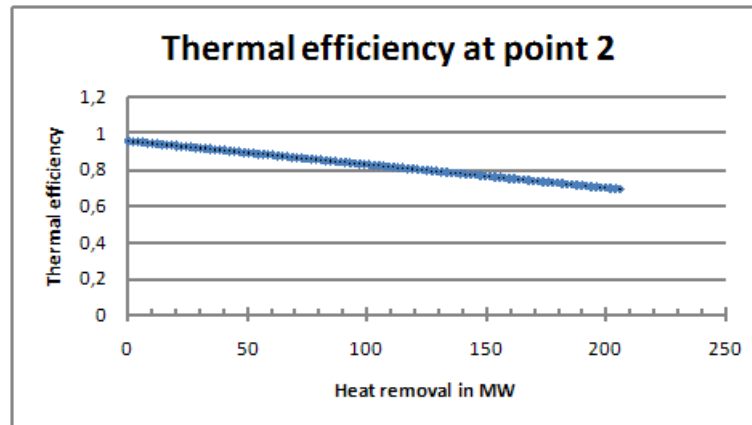


Figure 10.9: Thermal efficiency as a function of heat removal in point 2.

### 10.1.3 Point 3

Removing heat from the steam flow at point 3 after the IP0 turbine is expected to have effects on both the district heating and the electricity production. What should be seen is a drop in electricity production at the IP1 and IP2 turbines which together produce over 30 % of the steam cycle electricity. Also the same flow eventually provides heat for the district heating through both the I and L stream and therefore a drop in district heat production is also expected. It should be noted that this point only converges up to 14 MW of heat removal and that the sensitivity analysis in this case therefore is based on a shorter range.

In Figure 10.10 the development of the electricity production can be seen as a function of heat removal in point 3.

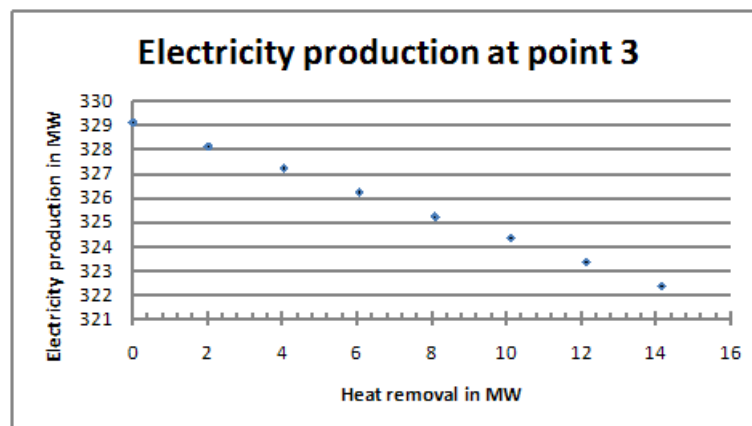


Figure 10.10: Electricity production as a function of heat removal in point 3.

In Figure 10.10 it can be seen that the electricity production of the steam cycle drops from 329 MW to 322 MW when 14 MW of heat is removed at point 3. This corresponds to a drop from 329 MW to 201.3 MW when 206 MW of heat is removed. This is significantly better than the 32.5 MW of electricity production obtained when removing 206 MW in point 1.

The district heat production sensitivity to heat removal at point 3 can be seen in Figure 10.11.

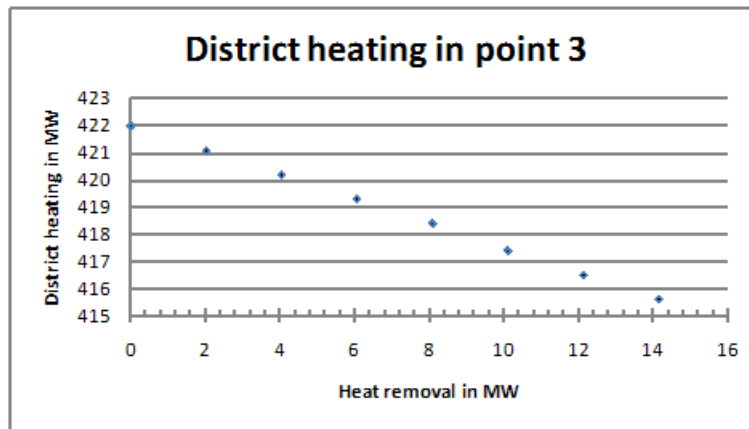


Figure 10.11: Production of district heating as a function of heat removal at point 3.

Looking at Figure 10.11 it is possible to see that the district heating output drops 6 MW from 422 MW at no heat removal to 416 MW at 14 MW heat removal. Extrapolating this result to 206 MW of heat removal means a drop in district heating output of 115.6 MW to an output of 306.4 MW.

These reductions in electricity production and district heating production can be seen in the electric and thermal efficiencies. In Figure 10.12 the electric efficiency can be seen as a function of heat removal in point 3.

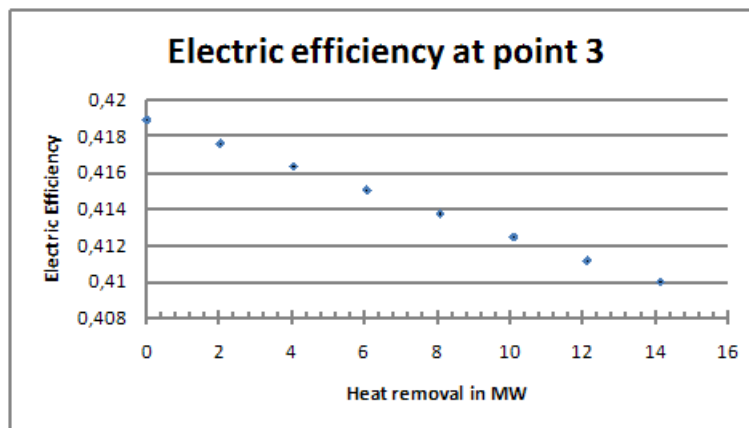


Figure 10.12: Electric efficiency as a function of heat removal in point 3.

In Figure 10.12 it can be seen that the electric efficiency drops 0.9 % point from 41.89 % to 40.99 %. This behaviour is completely as expected since it corresponds perfectly to the drop in electric production in Figure 10.10. Turning to the thermal efficiency, the combination of the drop in electric and district heat production can be seen in Figure 10.13.

The thermal efficiency drops 1.78 % points from 95.61 % to 93.83 % when removing 14 MW of heat. Extrapolating this result to 206 MW of heat removal returns a thermal efficiency of 69.69 %, a drop of 25.9 % points.

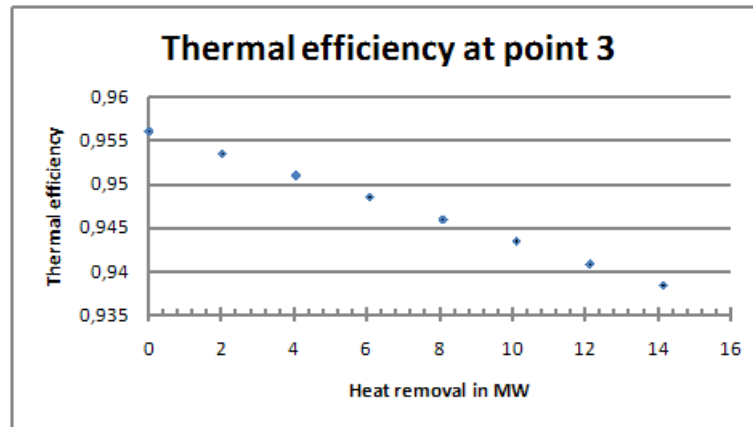


Figure 10.13: Thermal efficiency as a function of heat removal at point 3.

## 10.2 Sensitivity discussion

The sensitivity analysis provides a basis for evaluating the best candidates for places to remove heat for the CCS reboiler. It has not been possible to have converging results at all points for 206 MW of heat removal but the dependency on heat removal has been observed to be approximately linear in the cases presented here. Therefore extrapolations of the achieved results to 206 MW of heat removal are used to evaluate where the heat removal is most feasible. In Table 10.1 the extrapolated results for the three cases of heat removal can be seen.

case	El. prod. MW	Heat prod. MW	$\eta_{el}$ %	$\eta_{therm}$ %
No CCS	347.5	422.0	44.23	97.95
Point 1	32.5	583.5	1.67	70.10
Point 2	329.0	216.0	41.89	69.39
Point 3	201.3	306.4	28.72	69.69

Table 10.1: Key parameters for the steam cycle found by sensitivity analysis and extrapolated to a heat removal of 206 MW.

In Table 10.1 the first thing to notice is the difference between the electric production in the no CCS case and at point 2. This difference is the 18.5 MW it will take to run pumps and compressors in the CCS unit and is a default difference present in all of the heat extraction cases.

With this in mind we are able to comment on the extrapolated values in Table 10.1. Beginning with Point 1 it can be seen that the electric production drops to almost nothing if 206 MW is removed at point 1. This alone is enough to discard this point as a possibility for heat removal, but when looking at the district heat production this displays furthermore some odd behaviour that can be a result of steam cycle behaviour as well as the model flaws. This, along with the fact that it is also uncertain whether the boiler is physically able to transfer the amount of heat required for this configuration of the heat removal, makes the results of point 1 rather academic and the feasibility as a point for heat removal very low. Therefore point 1 is not considered for heat removal further in this report.

In point 2 the electricity production is unharmed, except for the power needed for CCS pumps and compressors, since all of the heat is taken from the district heating system. Therefore heat removal in point 2 returns the highest possible electric efficiency with a mere 2.34 % point drop from the no CCS case. On the other hand the thermal efficiency drops by 28.56 % points to 69.39 %. This value can only be improved by recovering waste heat from the CCS unit or the like.

Point 3 has approximately the same thermal efficiency as point 2, but another balance between reduction in electric and district heat production. In this case almost 150 MW is taken from the electricity production and a further 115 MW from the district heating. This is more than the total energy removed from electricity and district heating in point 2 and the resulting thermal efficiency must therefore originate from a lower intake of heat in the boiler and reheaters.

Choosing between point 2 and 3 as the most feasible place to extract heat for the CCS unit becomes a matter of prioritising between electricity production and production of district heating. As mentioned Nordjyllandsværket Unit 3 is obliged to be able to deliver 422 MW of district heating when demanded but by experience this demand only occurs in the coldest month of the year. Therefore it is possible to imagine a solution that enables the plant to continue to produce the maximum amount of electricity when running in district heating mode and taking the heat from the district heating. This would be possible in by far the largest part of the year when the plant is not required to produce maximum district heating.

### 10.3 Integration of the models

The steam cycle model and the CCS model are designed to function together in an intergrated model of electricity generation at NJV 3 with carbon capture. From the discussion on the performance on the steam cycle model it is known that convergence is not given when integrating the models. The choice of heat transfer interface (point of heat extraction) between the models is important for common convergence but merely integrating the models in itself can pose a problem too demanding for the EES solver to converge.

In this project, the most feasible extraction point has been chosen as the stream leaving the IP1 turbine for district heating. This stream contains enough energy in sufficient quality to supply the CCS unit. This point is also the only point that poses no convergence restrictions making sufficient heat transfer infeasible. Therefore the reboiler in the CCS unit will be supplied with heat from this point.

Multiple scenarios for the cooling of the CCS unit has been evaluated. It is not possible to cool with part of the steam cycle. The system therefore utilizes a utility coolant of 5 K, which could be water from the fjord. The waste heat of the this cooling is substantial, but unfortunately at low temperature. Due to this, and the fact that the flow in the low temperature areas of the steam cycle is very low, there is no suitable place for heat exchanging this waste heat with the steam cycle, even though this would be an obvious option for recovering some of the heat transferred to the CCS unit. Therefore, the system will turn out as seen in Figure 10.14.

This integration configuration of the steam cycle model and the CCS model corresponds exactly to the situation described in the sensitivity analysis point 2 and the results obtained by running the integrated model should therefore be the same in terms of efficiency and production.

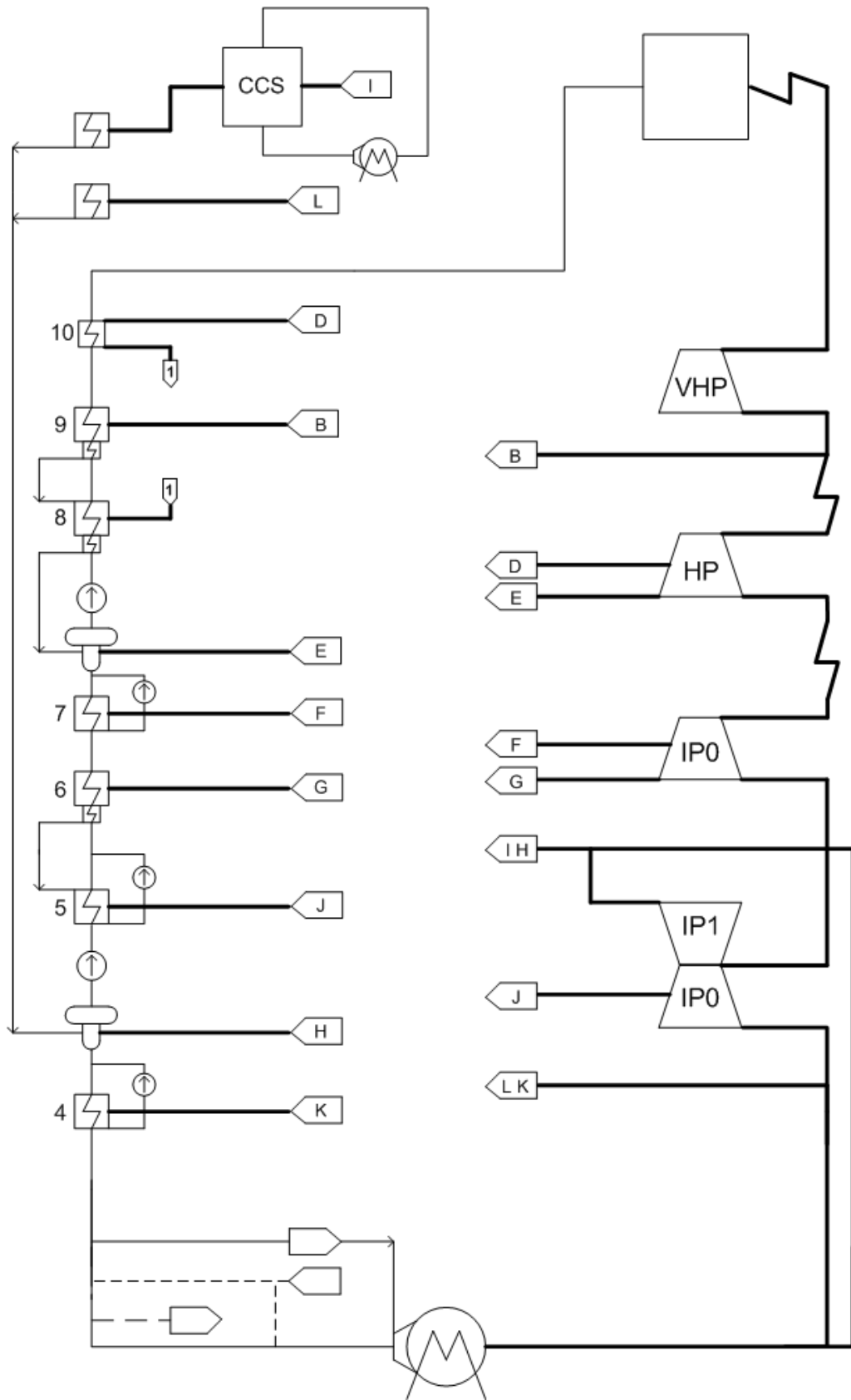


Figure 10.14: NJV3 with CCS system

## 10.4 Integration in EES

As the two systems were modelled independently, different methods of merging the models must be considered. The most simple method would be to copy-paste the code of one model into the code of the other. But as the models includes both guesses and limits for the variables, this method would include a tedious job of manually copying every guess and value from one model to another. As the models both contain a substantial number of variables, this method would be quite time consuming.

EES also has a build in function of merging two models. This function will import the code from one file directly to another at the cursor position. However, as EES has a certain structure of the files, this might cause problems. Furthermore, the method is not made for merging models of the size presented in this project, hence it is very memory consuming and in fact it requires more memory than available on the used equipment.

The last method is using the \$include function available in EES. This method will import the functions, procedures, modules and subprograms of the imported file including their guesses and limits. These will be imported and used as standard scripts, which is, they will be executed silently with none of their calculations showing in the solution windows. This method has been chosen in spite of the drawback of the silent execution. This is done, since the needed results are returned to the main program, thus their inner workings are not utilized.

Even though the CCS model is included in the steam cycle, a few modifications of the steam cycle is necessary to enable EES to compute the solution. Of course the I stream that originally went directly to the district heating heat exchanger must be modified to pass through the CCS unit. In modelling terms that means, that this stream now must enter the CCS unit, and a new stream will arise from the CCS unit to the heat exchanger. This is simply done by creating new variables for the new stream and changing the destination of the original stream.

Furthermore, the power consumption of the pumps and compressors in the CCS unit must be subtracted from the electric output of the plant as also done in the sensitivity analysis.

## 10.5 CCS Performance

When running the integrated CCS steam cycle model the CCS part of the model returns some results which are particular for the CCS model and which has so far not been presented. These results will be presented in this section before the key results of the integrated model.

The CCS unit as modelled in this project has been designed to extract 90 % of the carbon dioxide from the flue gas. By using the LG-ratio chosen for the system and the flue gas mass flow of the plant, this yields, as mentioned, a MEA mass flow of 2326 kg/s. To move this amount of fluid through the system the pumps will consume a total of 1.39 MW while the compression cycle will require 16.997 MW. The waste heat of the system will be a stream of 1120 kg/s of water at a temperature of 78.5 °C. The steam will leave the unit at a temperature of 100.8 °C and a quality of 0.04421. This results in an energy consumption from the steam of 205.947 MW. The values can be seen in Table 10.2

Parameter	Value
Flue gas mass flow	353.4 kg/s
CO <sub>2</sub> mass fraction	0.2137
CO <sub>2</sub> caption rate	90 %
CO <sub>2</sub> mass flow	67.97 kg/s
MEA mass flow	2326 kg/s
Cooling effect	309 MW
Pumping effect	1.39 MW
Boiler load per mass	3.03 MW/kg(CO <sub>2</sub> )
Boiler load	205.947 MW
Compression load	16.997 MW
Utility mass flow	1120 kg/s
Utility temperature	78.5 °C
Utility pressure	1 bar

Table 10.2: Results of the CCS unit

## 10.6 Integrated results

With the models integrated, the performance of the entire setup can be evaluated as compared to the steam cycle without CCS. The four key variables of performance are electric efficiency, thermal efficiency, district heating output and electric output. These key values are listed along with the original values in Table 10.3.

Parameter	No CCS	With CCS
Electric efficiency	44.23 %	41.89 %
Thermal efficiency	97.95 %	69.39 %
District heating output	422 MW	216 MW
Electric output	347.5 MW	329.1 MW

Table 10.3: Key variables of initial integration

As can be seen this integration effectively halves the district heating output and decreases the overall plant efficient by 28.56 percentage points. The electric output decreases by 18.4 MW which originate from the pumps and compressors of the CCS unit. These results are completely similar to the results obtained in the sensitivity analysis, which is a confirmation that the integration has been done correctly.

In general, the plant is severely affected by this sort of integration. Lower efficiency and insufficient district heating output is the inevitable results of retrofitting a CCS unit to the steam cycle. It is therefore prudent to consider measures of recovering as much heat as possible from the CCS unit since even slight improvements in steam cycle efficiency has considerable economical benefits for the plant.

## 10.7 Improvement idea

To improve the performance of the integrated plant, there are three main options. Firstly, the steam outlet could be moved in an attempt to lower the burden on the steam cycle. This has been tried in Section 10.1 and proven not to be feasible. Secondly, a more efficient solvent or a different set up of the CCS unit could prove beneficial in terms of improving efficiencies. There is a high probability that this would be able to lower the energy consumption of the system. However, studying such changes are beyond the scope of this project. Lastly, the waste heat of the CCS unit could, as already mentioned, be investigated for possible use.

As can be seen in Table 10.2, there are vast quantities of energy removed in the cooling cycle. The following sections have the purpose to try to exploit this stream to increase the efficiency of the plant. As described in Section 10.3 this is, however, heat of low quality not suitable for heat exchange with the steam cycle. To enable exploitation of this source, other methods than standard heat exchange must be investigated.

The principal idea of the attempt to recover waste energy from the CCS unit is to increase the quality of the energy to be able to exchange heat with the district heating system. Utilizing a heat pump could enable the low quality stream to transfer some of its contained energy to the district heating network, trying to regain some of the energy lost.

## 10.8 Heat pumps

In short, a heat pump is a thermodynamic machine extracting heat from a low temperature reservoir to a reservoir of higher temperature, by utilizing the different saturation temperatures at different pressures. That is, the working fluid enters an evaporator at low pressure, yielding a low saturation temperature. When the low pressure fluid has been fully evaporated and maybe even superheated, it is compressed. During the compression both the temperature and the pressure will rise. With the rise in pressure follows a rise in saturation temperature. The idea is to raise the saturation temperature beyond the wanted temperature in the fluid to be heated. This will allow the working fluid to release the entire condensation energy to the target fluid. Eventually the working fluid is expanded through a valve to reach the low pressure once again.

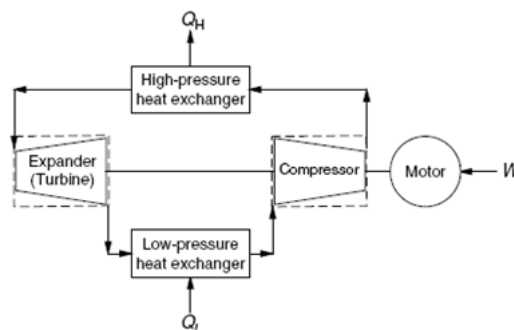


Figure 10.15: Conceptual drawing of a heat pump (Aye, 2007)

A general sketch of a heat pump can be seen in Figure 10.15. As can be seen in this sketch it is possible to use a turbine as the expander to increase efficiency. In this project, however, a very crude and simple model of the heat pump cycle has been modelled to give an estimate of what could be expected from an actual cycle. A sketch of the system modelled for this project can be seen in Figure 10.16.

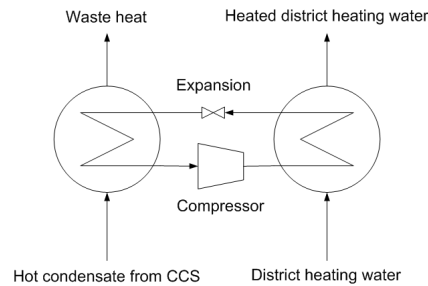


Figure 10.16: Conceptual drawing of the modelled system

As mentioned, the evaporated working fluid is compressed to reach a higher pressure to facilitate the heat transfer. In the model in this project, this is done by using simple isentropic compression. The total work required by the compressors for the two heat pumps amounts to 34.35 MW, that must be subtracted from the power generation of the plant.

The coefficient of performance (COP) of a heat pump is a measure of how much heat is transferred compared to the required energy for the compressor. It is calculated as seen in (10.1) or (10.2) (Çengel and Turner, 2005).

$$COP = \frac{Q_H}{W_{net,in}} \quad (10.1)$$

$$COP = \frac{Q_H}{Q_H - Q_L} = \frac{1}{1 - Q_L/Q_H} \quad (10.2)$$

$Q_H$  being the heat transfer from the working fluid to the hot reservoir,  $Q_L$  the heat transfer from the cold reservoir to the working fluid and  $W_{net,in}$  the energy for the compressor.

The idea of this project is to utilize the heated cooling stream from the CCS unit as a heat source. The same can be done with the excess heating steam from the unit. The energy in the excess heating stream is, however, considerably less, since it is a condensate of a quality of approximately 0.044. This will result in a heat output of approximately 195.33 MW transferred to the district heating system. The key values of the heat pump system can be seen in Table 10.4.

Parameter	Cooling water	Excess steam	Total
Heat transfer	182.4 MW	12.93 MW	195.33 MW
Pump work	33.86 MW	0.49 MW	34.35 MW
COP	5.39	26.38	5.69

Table 10.4: Key variables of heat pumps

As can be seen, the heat output is very high compared to the required energy input for the second heat pump. This results in a COP for this heat pump of 26.38, which is very high compared to

other cycles. The very high COP in this model is thought to be a result of the relatively high temperatures in this system and the low pressure ratio (approximately 2.44). Most heat pumps are designed to operate at considerably lower temperatures, as they are meant for household heating purposes, transferring heat from the outdoors at temperatures in the vicinity of 0 °C to inside a building. As the heat around zero degrees celsius is of very poor quality, a considerably higher compression load is to be expected, yielding a decreased COP value.

## 10.9 Integration of the model

Once decided on using heat pumps, the plant design must be evaluated. The two streams are of nearly identical temperature, but with the excess heating steam slightly higher. As to avoid exergy destruction, it is most effective to let the stream of lowest temperature exchange heat with a lower temperature. This yields a configuration in which the cooling fluid exchanges heat with the district heating coming from the remaining heat exchanger, and the excess steam exchanges heat with the stream exiting the first heat pump.

The cooling water was not originally part of the steam cycle and should remain as such. The stream could either be an isolated circuit or it could be water directly from the fjord. But the water from the fjord is salt water and may contain vegetation and other particles. Therefore it is not suitable for flowing through multiple heat exchangers. Thus the cooling water for the CCS unit is modelled as a closed circuit which is cooled by the water from the fjord in the same way as done in the steam cycle condenser. The heating steam was originally removed from the steam cycle, and to preserve the total fluid mass in the steam cycle, this should be lead back into the steam cycle. The proposed system can be seen in Figure 10.17

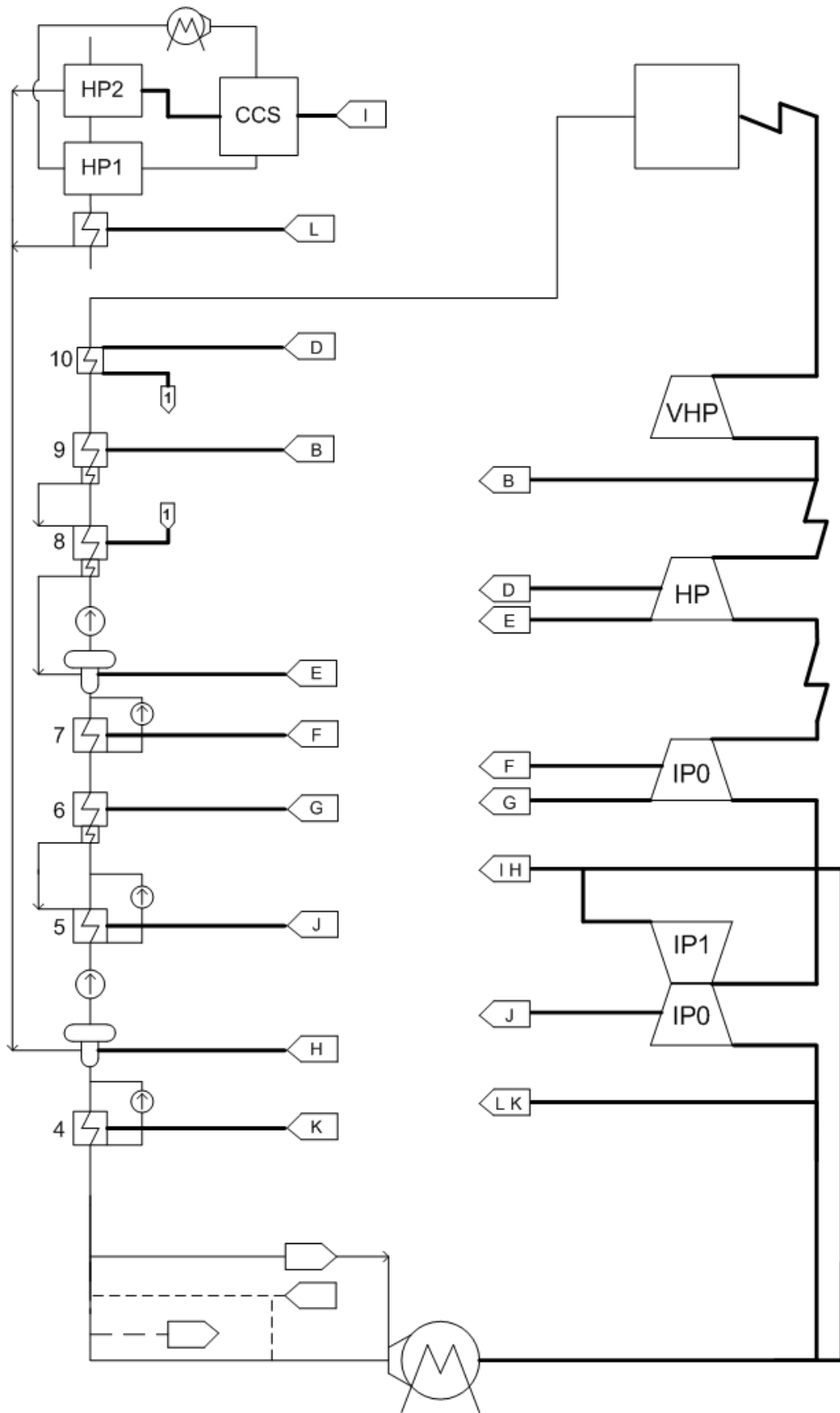


Figure 10.17: Sketch of the proposed system

## 10.10 Integration of heat pumps in EES

As for the previous integration of the CCS unit, the heat pumps has been merged with the existing model using the \$include function. The two heat pumps has been modelled seperately, as the target pressures of the working fluid are not the same, and are therefore included seperately as well.

To enable EES to solve the model a few modifications has to be done again. As for the CCS unit, the streams must be redirected to their new targets, and new streams must be defined. Furthermore, as the heat pumps contribute to the district heating in a different manner than the original heat exchanger, the heat transfer equation for the district heating system must be updated. As was the case for the CCS unit, the power consumption of the pumps must be subtracted from the electric output of the plant.

The system performance can again be evaluated by using the four key values of the plant. These can be seen in Table 10.5

Parameter	No CCS	With CCS	With CCS and HP
Electric efficiency	44.23 %	41.89 %	36.56 %
Thermal efficiency	97.95 %	69.39 %	86.72 %
District heating output	422 MW	216 MW	404.5 MW
Electric output	347.5 MW	329.1 MW	294.7 MW

Table 10.5: Key variables of second integration

As can be seen in the table, the electric efficiency and the electric output has dropped by 5.33 percentage points and 34.4 MW respectively compared to the CCS with no heat recuperation. This is due to the additional pump work required for the heat pumps. At the same time, the overall plant efficiency and the district heating output has increased dramatically by 17.33 percentage points and 188.5 MW owing to the recovered heat from the CCS unit. The difference in district heat output and total heat transfer between Table 10.5 and Table 10.4 respectively is a result of the fact that the 8 MW originally transferred from the I stream into the distrit heating is now fed into the heat pumps. These figures are not necessarily completely final as the heat pumps models are merely a first iteration and could hold potential for improvement or the opposite, if investigated further with respect to working fluid and pressures.

## 10.11 Flexibility

NJV 3 today is the most efficient coal fired power plant i Denmark. As such it is running at full capacity most of the time as it produces electricity and heat cheaper than other plants. Implementing a CCS unit will increase the cost of generation and reduce the capacity of the plant. As NJV 3 must be able to deliver high amounts of electricity in certain cases, and as they are obliged by contract to guarentee a district heating capacity of 422 MW, flexibility of the plant is important. The main problem with retrofiting CCS to an existing unit is, that the original capacity of the plant, which is an integrated part of a supply grid, will be altered, possibly causing problems for the plants ability to compete at the market.

For NJV 3 the obligation of district heating capacity offers a great challenge when implementing CCS. As can be seen in Table 10.5 the district heating capacity has decreased below the promised

capacity. There are several ways of dealing with this problem. A rebuild or replacing of the boiler and turbines could facilitate higher steam temperatures and thereby higher capacity of the cycle, but this is a very costly solution. Another way could be renegotiating the contract in order to lower the promised capacity. Lastly, an integration method allowing for a total bypass of the CCS system restoring the original steam cycle could be an option. A system of that sort would be configured as can be seen in Figure 10.18.

A system like this allows for a total shut off of the CCS unit, which will transfer the entire I stream through the district heating heat exchanger as originally intended. At the same time the power consumption of the CCS unit and the heat pumps will be zero, and thus, the plant will operate in the original designed cycle, generating power and heat as originally intended.

## 10.12 Chapter conclusion

The final integrated steam cycle with CCS and heat recovery model consists of approximately a thousand equations in complicated interrelationships. The models have been constructed individually and integrating them is quite a challenge if convergence is to be maintained. Even so, convergence of the integrated model has been obtained, with relevant and interesting results as a consequence.

As seen in Table 10.5, the power plant performance has, as expected, decreased. This decrease is caused by the energy consumed in boiling the MEA/CO<sub>2</sub> solution, and in the pumps and compressors for the CCS unit and the heat pumps. Through the heat pump system a considerable part of the waste heat from the CCS unit can be recovered and used in the district heating system. With the added heat pumps, the heat output will climb to 404.5 MW, which is still below the promised capacity. This calls for either further studies of how to integrate a CCS system, contract negotiation or as proposed the CCS shut down option.

This integration approach, yields a feasible solution to the CCS problem, though it does still offer some problems, that must be addressed if an actual carbon capture plant is to be built.

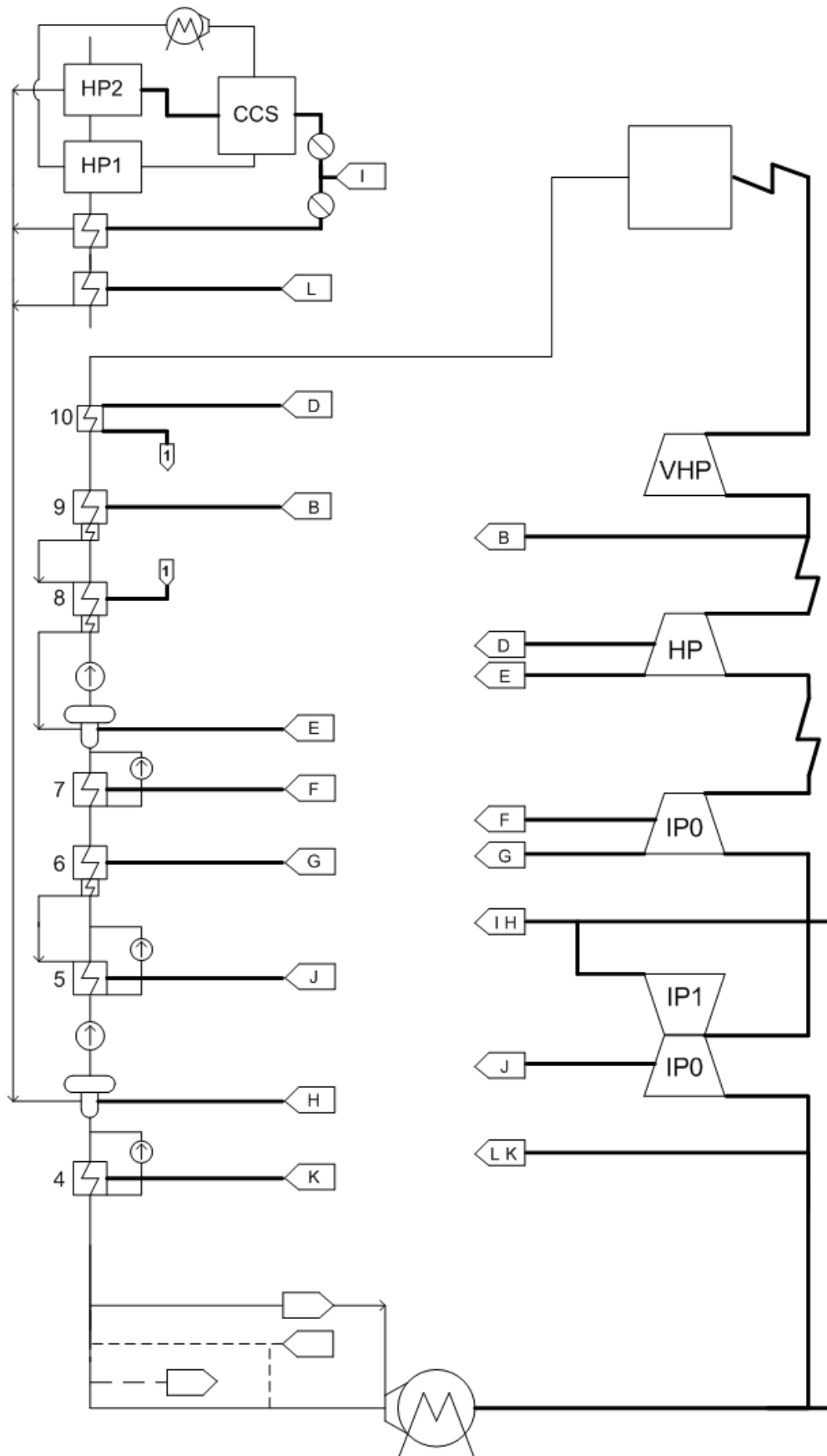


Figure 10.18: Sketch of plant with capability of switching of the CCS unit

# Chapter 11

## Conclusion

This report has been a study of CCS and the integration of a CCS unit at Nordjyllandsværket Unit 3. During this project available and future technologies of CCS has been studied through articles and in particular through participation in the 8th Annual Conference on Carbon Capture and Sequestration. Through this technology study it has been found that, while MEA is the solvent of choice for Vattenfall A/S, several other solvent technologies hold promise of a more efficient CCS process. Also other technologies applicable when constructing new power plants are under development.

A detailed model of the steam cycle at NJV 3 has been formulated along with a model of the CCS unit of 90 % CO<sub>2</sub> capture. The steam cycle model has proven to be very precise in all load cases but somewhat unstable to large changes in steam cycle conditions, due to solver problems with complex systems. The CCS model also predicts results in coherence with given design information but is not a stand alone model.

The models have been combined into a single model of the NJV Unit 3 with CCS. This model predicts values of thermal and electric efficiencies for the CCS integrated system. It has been found that the electric and thermal efficiency decreases by 2.34 % points and 28.56 % points respectively. In particular the district heating output drops by 51 %. In other words, the plant suffers considerably from the capture of CO<sub>2</sub>.

Through the use of waste heat from the CCS unit it has proven possible to recover some of the lost thermal efficiency. A configuration of CCS integration has been proposed utilising two heat pumps, that lifts the quality of the waste heat to levels useable in the district heating system. Two heat pumps has been modelled for this new integration suggestion and integrated into the steam cycle CCS model resulting in an entire model of the steam cycle with CCS and heat recovery.

With the heat recovery proposed in this project the loss of thermal efficiency reduces to 11.23 % points while the electric efficiency drops further making the total loss 7.67 % points. NJV 3 will, if this method of integration is carried out, be able to produce 294.7 MW of electricity and 404.5 MW of district heating in full district heating mode.

It can be concluded that this project has been succesfull in formulating models of steam cycle behaviour and CCS energy demands. Furthermore a valid suggestion for heat recovery has been proposed and modelled. This proposal enables NJV 3 to still produce almost equal district heating as without CCS, rendering the time needed for CCS bypass very limited. However it has also been

found that EES is not a recommendable tool for complex modelling and further studies should therefore be conducted via other software.

## **Part II**

# **Appendices**



# Appendix A

## The boiler model

The boiler model is the most complicated model of the component models. This is because the heat exchange in the boiler takes place in different locations in the flue gas flow resulting in complicated interrelationships between the different parts of the heat exchangers. In this chapter the model formulated to simulate the behaviour of the steam and the flue gas in the boiler component, is described.

### A.1 The boiler characteristics

The boiler at NJV Blok 3 is a forced-flow type boiler after the Benson-principle (Vølund A/S et al., 2001). This means that Benson-operation is used above 35 % maximum continuous rating (MCR or load) below which circulation operation is used. The heat exchange takes place at supercritical pressure at loads above approximately 50 %. The boiler is equipped with a double reheat system capable of reheating steam to a temperature of 580 °C. The fuel burned is coal or in certain cases oil, where the coal has an average LHV of 25000 kJ/kg (Vølund A/S et al., 2001).

In Figure A.1 a sketch of the boiler with heat exchangers can be seen. The preheated feed water enters at the top of the boiler with a temperature of 298 °C and flows into the economiser. From here it flows to the bottom of the boiler where it enters the walls of the boiler and rises through the spiral shaped tubes towards the top of the boiler. When it reaches the top of the boiler, it flows out of the walls and into the cyclone separator where water is separated from steam when operating in circulation mode, before the steam flows back into the boiler. Back in the boiler the feed water, now transformed into steam, flows through a set of screens just above the combustion chamber before it flows through the superheaters protected from radiation behind the screens.

In Figure A.1 it is also possible to see the first and second reheater. The first reheater flows into the boiler immediately below the economiser and flows through three stages in the boiler until it leaves the boiler between the first and the second superheater. The second reheater flows into the boiler below the first stage of the first reheater and flows through an additional stage before it leaves the boiler just above the outlet of the superheaters.

This configuration of heat exchangers in the boiler creates an integrated system containing the boiler and the first and second high pressure turbines in which it is difficult to alter a parameter in

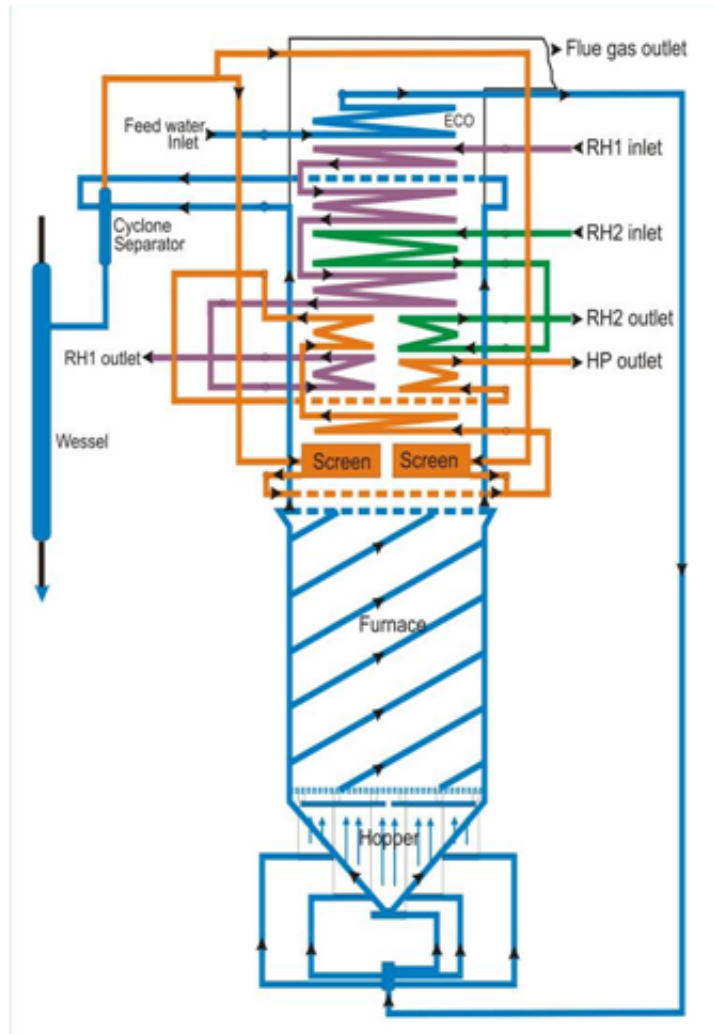


Figure A.1: Diagram of the flow through the boiler, (Grue, 2009b).

one position without influencing several other parameters. For example, lowering the temperature in the second superheater inlet means a larger heat exchange with the flue gas and therefore lower temperatures of the flue gas after this making the heat exchange with the first stage of the first reheater smaller.

## A.2 Model overview

From Figure A.1 it is possible to construct a model of the heat exchange in the boiler 1st run based on a series of heat exchangers. In Figure A.2 an overview of this series can be seen.

Each of the heat exchangers in this model are modeled via an  $\epsilon$ -NTU model. To serve the purpose of this investigation the term  $U \cdot A$  in (A.1), (Çengel and Turner, 2005), in the  $\epsilon$ -NTU model, is substituted with a thermal resistance  $1/R$ .

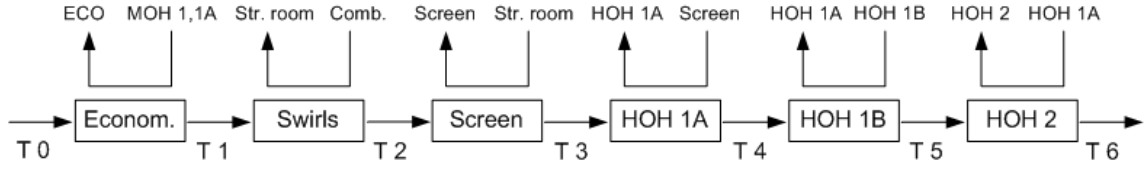


Figure A.2: An overview of the series of heat exchangers used in the boiler model 1st run. Steam flows from the left to the right.

$$NTU = \frac{U \cdot A_s}{C_{min}} = \frac{1}{R \cdot C_{min}} \quad (A.1)$$

This is done since no information on heat exchanger geometry or heat transfer area is available and therefore it is necessary to treat these variables as one. In this investigation all heat exchanger models are first run in "reverse" with fixed boundary conditions corresponding to different load cases to obtain the thermal resistance,  $R$ , in each heat exchanger for each load case. Setting  $R$  as a fixed value for each load case it is possible to use the heat exchanger models normally to obtain desired temperatures.

### A.3 The heat exchanger model

The alterations done to the  $\epsilon - NTU$  model yields the following equations for the  $\epsilon - NTU$  economiser model see (A.2) to (A.11).

$$Cp_{steam,ECO} = Cp \left( Steam; T = \frac{T_{steam,0} + T_{steam,1}}{2}; P = P_{steam,ECO} \right) \quad (A.2)$$

$$Cp_{flue,ECO} = Cp_{flue} \left( \frac{T_{flue,MOH1,1A} + T_{flue,ECO}}{2}; load \right) \quad (A.3)$$

$$C_{steam,ECO} = Cp_{steam,ECO} \cdot \dot{m}_{steam} \quad (A.4)$$

$$C_{flue,ECO} = Cp_{flue,ECO} \cdot \dot{m}_{flue} \quad (A.5)$$

$$C_{min,ECO} = MIN(C_{steam,ECO}; C_{flue,ECO}) \quad (A.6)$$

$$\dot{Q}_{ECO} = \epsilon_{ECO} \cdot (C_{min,ECO} \cdot (T_{flue,MOH1,1A} - T_{steam,0})) \quad (A.7)$$

$$\dot{Q}_{ECO} = C_{steam,ECO} \cdot (T_{steam,1} - T_{steam,0}) \quad (A.8)$$

$$\dot{Q}_{ECO} = C_{flue,ECO} \cdot (T_{flue,MOH1,1A} - T_{flue,ECO}) \quad (A.9)$$

$$NTU_{ECO} = HX('crossflow\_one\_unmixed'; \epsilon_{ECO}; C_{steam,ECO}; C_{flue,ECO}; 'NTU') \quad (A.10)$$

$$R_{ECO} = 1/(C_{min,ECO} \cdot NTU_{ECO}) \quad (A.11)$$

In (A.2) the specific heat capacity of the steam is found. This is done on the basis of an averaged temperature and a pressure. The application of an averaged temperature only yields approximate results and would only provide exact results provided that the specific heat capacity behaves linearly between the two. In Figure A.3 the development of the specific heat capacity of steam between 0 and 600 °C for a pressure of 330 bar can be seen.

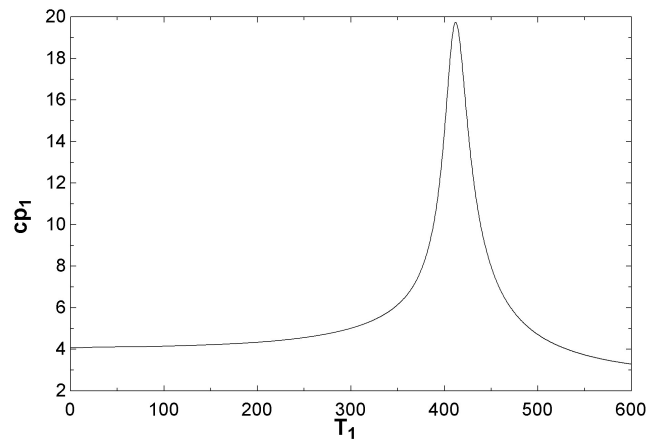


Figure A.3: The value of specific heat capacity for steam dependent on temperature.

In Figure A.3 it can be seen that the specific heat capacity of steam at 330 bar behaves very non-linearly meaning that application of averaged temperatures is less valid. However, runs of the finished model has been done for all load cases with the average specific heat capacities calculated as the integral of the specific heat capacity over the temperature divided by the temperature difference. These runs yielded improvements in the precision of the model results between 0.2 % and 0.4 % while the calculation time increased from approximately 2.5 seconds to over 20 minutes. With this in mind the assumption of linear heat capacities appear quite reasonable.

In the case of the specific heat capacity of the flue gas, see (A.3), the value of this is found much in the same way as for the steam, with averaged temperatures, but in this case it is based on a weighted average of heat capacity of the different compounds in the flue gas. The composition of the flue gas is given by (Vølund A/S et al., 2001) and is given without products of dissociation.

(A.4) to (A.6) are the intermediate equations in the  $\epsilon - NTU$  model that determines the minimum heat capacity of the two flows. These equations have required no specific assumptions in this investigation and are therefore of lesser interest here. Moving on to equations (A.7) to (A.9) these are the equations that provide the relationship between the heat fluxes between the flows and the temperature changes in the flow. When searching for the thermal resistance,  $R$ , of the heat exchanger, equation (A.9) determines the heat flux since temperatures are given from Vølund A/S et al. (2001). Equation (A.7) and (A.8) determines the efficiency,  $\epsilon$ , and the temperature change of the steam respectively.

The final two equations are completely determined from the previous equations and therefore add no degrees of freedom to the system when searching for the thermal resistance. Equation (A.10) is a function in EES that determines the number of transfer units (NTU) from the efficiency,  $\epsilon$ , and equation (A.11) finally determines the thermal resistance. When running the model as intended this value is determined while the heat flux is unknown. It should be noticed that equation (A.10) is used for a cross flow heat exchanger with the steam unmixed. When modeling the remaining heat exchangers in the model series this set of equations is the same, except for in a few special cases, as will be seen. It should also be noticed that the amount of steam flowing through the boiler heat exchangers increases at two points in the model. The reason for this is that steam at 25 °C

is injected into the steam cycle between the screens and the superheaters and again between the HOH 1B and HOH 2 heat exchangers at amounts of respectively 3.6 kg/s and 1.8 kg/s.

#### A.4 Radiation heat exchange

In boilers of the size found in NJV3 a considerable amount of the heat exchange is done through radiation. The geometry of the boiler at NJV3 is such that by far the largest part of the radiation heat transfer is done to the walls of the furnace and the screens, since the screens are in fact, as the name indicates, large screens with feed water in them that protects the superheaters from radiation. In the heat exchanger model used for the boiler in question it is assumed that all heat exchange via radiation is done with the furnace walls and that the heat is transferred into the swirls in these walls. This means of course that the temperature after the swirls,  $T_2$ , is overestimated and that the heat transfer with the screens are underestimated. However, these faults will compensate for each other so that the temperature after the screen,  $T_3$ , is reliable.

In this model the heat transfer by radiation is calculated simply as a forced flow of heat to the feed water in the swirls. The mentioned flow of heat by radiation can be determined from the LHV of the coal and the heat input of the intake air alone, since the temperature of the feed water is of lesser influence. This can be seen by the following simple calculation. The radiation from one body to another is given by (A.12), (Çengel, 2006).

$$\dot{Q} = A_s \cdot \sigma \cdot (T_2^4 - T_1^4) \quad (\text{A.12})$$

Letting the temperature of the flue gas be  $T_2 = 1500^\circ\text{C}$  and the temperature of the feed water be respectively  $T_1 = 400^\circ$  and  $T_1 = 450^\circ$ , one can obtain the relative decrease in  $\dot{Q}$  as the feed water temperature increases, (A.13).

$$\frac{\dot{Q}_{450}}{\dot{Q}_{400}} = 0,99694 \quad (\text{A.13})$$

As can be seen, changing the feed water temperature by 50 K, only changes the heat transfer by approximately 0,3 % making the assumption that the rate of heat transfer by radiation is a function of the flue gas temperatures alone valid. Therefore the following simple set of equations is all that is needed to calculate the heat flux by radiation.

$$\dot{Q}_{swirls} = \dot{Q}_{burned} - \dot{Q}_{flue,screen} \quad (\text{A.14})$$

$$\begin{aligned} \dot{Q}_{swirls} = \dot{m}_{steam,1} \cdot (&Enthalpy(Steam; T = T_{steam,2}; P = P_{steam,swirls1}) \\ &- Enthalpy(Steam; T = T_{steam,1}; P = P_{steam,swirls2})) \end{aligned} \quad (\text{A.15})$$

In (A.14) the  $\dot{Q}$ 's are enthalpy contents in the flue gas at different points in the boiler.  $\dot{Q}_{burned}$  is the enthalpy of the flue gas immediately after combustion and  $\dot{Q}_{flue,screen}$  is the enthalpy content at the screens. Since using equations (A.14) and (A.15) is all that is needed there is no use for the ordinary  $\epsilon - NTU$  model equations for the "swirls" heat exchanger.

## A.5 The flue gas side

When using this model as a part of the steam cycle in NJV3 the state of the flue gas is of lesser importance. However it is necessary in order to obtain the correct heat flux into the steam side, that the thermodynamic state of the flue gas is modeled in some detail. In Figure A.4 a flow diagram of the flue gas can be seen.

In Figure A.4 it can be seen that temperatures are given at outlets of the various heat exchangers corresponding to inlet temperatures of flue gas at different places in Figure A.2. It can also be seen that the flue gas sometimes flows over two heat exchangers at the same time making the mass flow for each heat exchanger half the total flue gas flow. It is also evident here that the outlet temperature of the flue gas at a heat exchanger is not necessarily the inlet temperature of the flue gas in the next heat exchanger in the coupling as seen in Figure A.2. This is the reason why it is necessary to model the two high pressure turbines and the two reheating processes, before being able to run the boiler model as intended. Luckily this is not the case when running in reverse for the thermal resistances and therefore the thermal resistances can be found for each part of a total boiler model by itself.

## A.6 The boiler model results

The original intent of the  $\epsilon - NTU$  model is to use two inlet temperatures and the thermal resistance in terms of  $U \cdot A$  to calculate the outlet temperatures. While this is also the intent for the present model, the thermal resistances must first be found. Therefore another boundary condition is provided at each heat exchanger, which is the outlet flue gas temperature. Thereby the heat exchanger models are able to predict both the thermal resistances and the output temperatures of the heat exchangers. As an extra feature the model is able to calculate the total heat transfer into the steam and the boiler efficiency.

The model is run for four different load cases corresponding to nominal load, 80 %, 60 % and 40 % load. In Table A.1 the predicted values for final output temperature, total heat transfer and their respective nominal values from the boiler documentation, (Vølund A/S et al., 2001), can be found along with values for relative error of these. In the boiler documentation it is shown that the different load cases makes no difference to the output temperature which is always 582 °C.

load	$T_{\text{predicted}}$	$T_{\text{nominal}}$	Error	$Q_{\text{predicted}}$	$Q_{\text{nominal}}$	Error
%	°C	°C	%	MW	MW	%
100	593,7	582	2,0	551,7	561,2	1,7
80	588,8	582	1,2	463,4	469,1	1,2
60	585,0	582	0,5	368,0	367,6	0,1
40	598,4	582	2,8	266,6	269,2	1,0

Table A.1: Comparison of predicted model values with nominal values from the boiler documentation.

In Table A.1 it can be seen that the precision of the boiler model for the output temperature varies from 0.5 % to 2.8 % depending on load case. The precision of the prediction of the total heat transfer varies from 0.1 % to 1.7 %. This is considered acceptable errors for the purpose of this model.

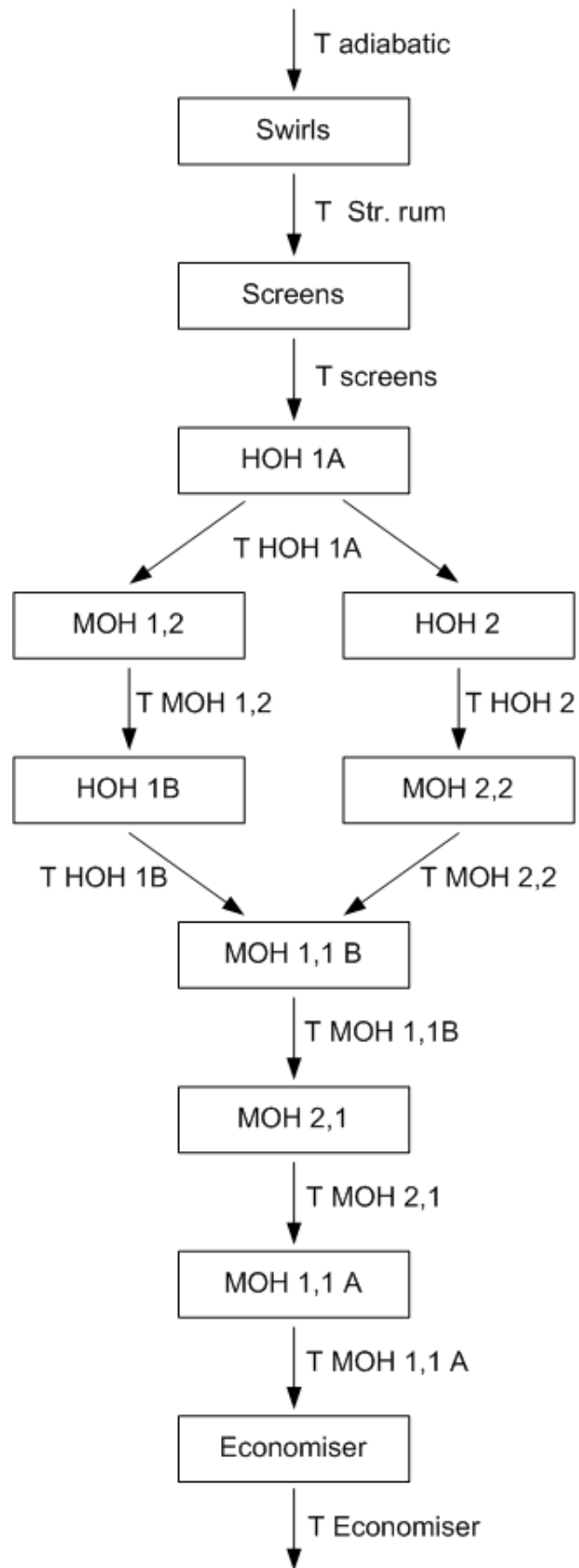


Figure A.4: Flow diagram of the flue gas through the boiler

As mentioned, it is also possible to calculate the efficiency of the first boiler circuit,  $\eta$ . In Table A.2 the predicted boiler efficiency for this circuit can be seen for varying load cases.

load	100 %	80 %	60 %	40 %
$\eta$	0.595	0.6084	0.6146	0.6121

Table A.2: Predicted first circuit boiler efficiency for varying load case.

This efficiency varies between 0.595 and 0.6146. The development of the first circuit boiler efficiency can be seen on Figure A.6.

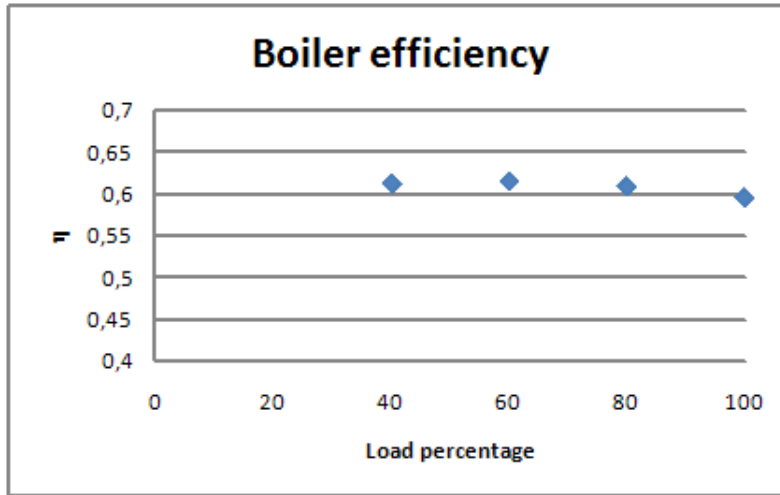


Figure A.5: Graph depicting efficiency of the first boiler circuit.

The expected behaviour of the boiler efficiency as the load decreases is to increase toward a maximum at a load between 10 and 20 % and then rapidly decreases. The efficiencies stated here should be added to the efficiencies of the first and second reheating to obtain the true efficiency of the boiler. It should be noticed that efficiencies below 35 % load, where the boiler ceases to operate in Benson mode, are not entirely comparable to those above the same load.

Finally it is now possible to state the thermal resistances, R, calculated for the heat exchanger series to be used when the boiler model is run as a part of a larger steam cycle model. The values of the different thermal resistances can be found in Table A.3, all values are in K/W.

load	Eco.	Screens	HOH 1A	HOH 1B	HOH 2
100 %	3,635E-6	2,728E-5	1,31E-5	9,506E-6	1,4E-5
80 %	4,108E-6	2,975E-5	1,436E-5	1,056E-5	1,509E-5
60 %	4,186E-6	3,265E-5	1,569E-5	1,177E-5	1,65E-5
40 %	4,79E-6	3,747E-5	1,754E-5	1,265E-5	1,698E-5

Table A.3: Thermal resistance, R, for different load cases. All values are in K/W.

There are two similar models for the first and second reheat that are not presented here.

## Appendix B

# Numerical methods in EES

*This appendix will explain the solver method used in EES and describe some of the strengths and weaknesses.*

EES is a numerical equation solver, build for solving multiple non-linear equations. A number of methods are implemented to increase the calculation speed and improve the chance of convergence. As EES is designed to solve larger equation systems, a method for dividing the system into as many smaller equation sets, called blocks, as possible is implemented.

When solving smaller linear system, the effect of a blocking system is limited. Using the standard Newton-Raphson iteration method will converge quickly anyway. But when solving complex system involving non-linear equations, the blocking routine becomes essential. EES utilizes the Tarjan Method (Klein, 2009). The algorithm is also known as Tarjan's strongly connected components algorithm. The aim of the algorithm is establish a sequence for solving the system. An example from Klein (2009) can be a system of three equations as seen in (B.1)

$$\begin{aligned}x_1 + 2x_2 + 3x_3 &= 11 \\5x_3 &= 10 \\3x_2 + 2x_3 &= 7\end{aligned}\tag{B.1}$$

Using Tarjan's method, these equations can be classified through a system of indecies, and ordered in a way that requires less computation to solve (Eppstein, 1996). This specific system can be split into three blocks, the first being the second equation. From this,  $x_3$  can be solved directly. The equation then constitutes block 1. When  $x_2$  is known, the third equation can easily be solved for  $x_3$ , constituting block 2. Knowing  $x_2$  and  $x_3$  the first equation can readily be solved, constituting block 3.

The general idea is, when following the dictated order, every block can be solved independently. In this example, each block only contains a single equation with one unknown. When operating with more complex system a block may consist of any number of equations. The equation in each block then form a system of equations, that can be solved either directly or through an iteration method.

Looking at the system in the example, the approach of solving this system directly using Newton-Raphson iteration properly will converge quickly as well, but when solving complex system, the blocking method increases both computation time and improves the chance of convergence.

When faced with a system, EES uses Newton-Raphson iteration. This method is based on updating the starting guess, using the function value and derivative in the guess point, see (B.2) (Weisstein, 009a).

$$x_1 = x_0 - \frac{f(x_0)}{f'(x_0)} \quad (\text{B.2})$$

In EES this method has been split up, to allow variable step sizes (Klein, 2009). In EES, the problem is rewritten in terms of residuals, and finds the derivative (B.3)

$$\begin{aligned} ax^2 + bx &= c \\ ax^2 + bx - c &= \epsilon \\ 2ax + b &= \frac{d\epsilon}{dx} = J \end{aligned} \quad (\text{B.3})$$

where  $\epsilon$  is the residual. EES then solves the equation using the supplied starting guesses. This will result in a residual,  $\epsilon$  and a derivative J, the Jacobian matrix.

To obtain the step size, EES uses the formula (B.4)

$$J\Delta x = \epsilon \quad (\text{B.4})$$

where  $\delta x$  is the step size. The idea is then to determine the new guess using  $x_1 = x_0 - \Delta x$ . To avoid instability and divergence, EES automatically test the new x before using it. If the residual from a new guess is worse, that is bigger, than the previous, the step size is halved. This test is done up to 20 times before accepting a new guess value (Klein, 2009). This method also limits the extreme step size that may be generated when the derivative is close to zero.

EES will keep on iterating and improving the guess till either the step size or the residual reaches a threshold.

The Newton-Raphson method is generally a quick way to solve an equation set. However, it is very reliant on the initial guesses. If the functions yields one or more extremes, with a derivative of zero, the iteration may stall, since if Jacobian matrice in (B.4) is zero, the step size can't be determined. This can be illustrated with a third order equation, as done in Klein (2009), following (B.5)

$$x^3 - 3.5x^2 + 2x = 10 \quad (\text{B.5})$$

The graphical solution can be seen in Figure B.1

If the initial guess, as shown on the graph, is set to 3, the system will quickly converge to the correct solution. But if the guess is set to 2, the derivative will yield (B.6)

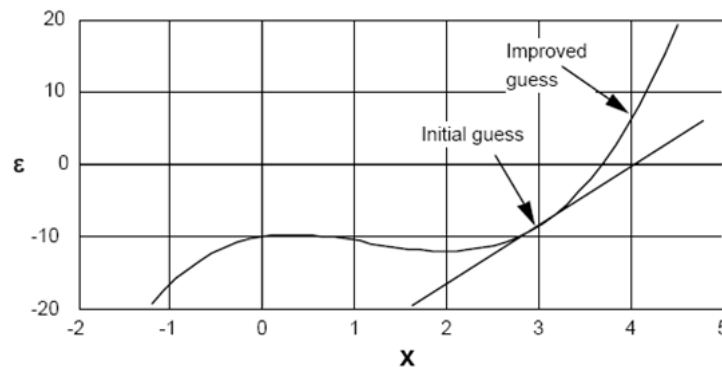


Figure B.1: Residual of  $x^3 - 3.5x^2 + 2x = 10$  (Klein, 2009)

$$f'(x) = 3x^2 - 7x + 2$$

$$f'(2) = 3 \cdot 2^2 - 7 \cdot 2 + 2 = 0 \quad (\text{B.6})$$

thus halting the iteration.

A couple of notes should be said about the Newton-Raphson method. The method converges quadratically, which is generally quite quick. But as seen, the method requires direct calculation of the derivative. When the formulas becomes sufficiently complicated, it may be hard or even impossible to obtain the derivative directly. In this case, the derivative can be approximated using the secant method. This method will estimate the slope of the function by calculating the function values in the actual point and a point nearby. The secant method improves the Newton-Raphson greatly and though it does require slightly more processing, the penalty is acceptably small (Weinstein, 009b).

Newton-Raphson iteration is as written highly dependant on the derivatives. If the initial guess is far from the true zero, it may not converge and is therefore refered to as a local technique. EES tries to avoid this problem by allowing the user to define upper and lower boundaries for each variable (Klein, 2009).

Lastly it should be noted, that when EES was coded, the intention was to build an easy-to-use study aid. EES is extremely good for simple systems, but when the systems grow larger and more complex, the software shows limitations and could with advantage be replace by a more specialized simulation software.



# Appendix C

## Steam tables

*This chapter will provide a brief introduction to steam tables, how they were produced and how some have been deemed obsolete today by the International Association for the Properties of Water and Steam (IAPWS).*

The information in this section is based on the release "Obsolete IAPWS Recommendations" (IAPWS, 2005) and "Revised Release on the IAPWS Industrial Formulation 1997 for the Thermodynamic Properties of Water and Steam" (IAPWS, 2007).

The intention of these tables were to list the thermodynamic properties of water and steam, such as pressure, enthalpy, volume and so on. The first skeleton tables were introduced in 1934 at the International Steam-Table Conference, including uncertainty estimations. With the advance in power plant technology these original tables became obsolete shortly after World War II. As advances in technologies and methods for measuring thermodynamic properties had presented new and more accurate data, a new set of skeleton values were approved in 1963, which were fairly accurate up to pressures of 100 MPa and 800 °C. In 1985 improved technology again offered more data with higher accuracy and a new set of skeleton values were approved, which in 1994 were revised to fit the International Temperature Scale of 1990, a standard calibration for measuring both Kelvin and Celsius (Preston-Thomas, 1989). The older version were based on the International Practical Temperature Scale. In the region between 0 °C and 800 °C the maximum difference is 0.36 K but the average is much smaller (Techware Engineering Applications, 2009)

As computers started to evolve during the sixties, a need for equations rather than tables lead to the formations of The International Formulation Committee, which purpose was to evolve equations for use in automated computing. In 1966 the first set of formulations were published. These were revised in 1967, now know as the IFC-67 formulation.

As the skeleton tables evolved, the IFC-67 formulation became obsolete. A new set of equations were released in 1997, IAPWS-IF97, which are the standard equations used today.

With the advances in computer technology the use of tables has diminished, finally leading to a withdraw of the steam tables in 2003. Today IAPWS solely recommend to use the equations.

In the same way, a set of standards for the transport properties has been evolved. The first set were accepted in 1964, matching the skeleton tables of 1963. These were replaced by equations

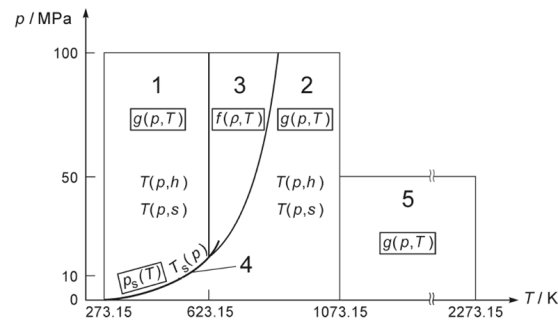


Figure C.1: The 5 regions in which the steam formulas are divided (IAPWS, 2007)

in 1975 and 1977, which were slightly modified in 1985 and 1997 to represent new standards for the thermodynamic properties and again in 2003 to correct minor inconsistencies.

In 1983 a guideline for properties in the vicinity of the critical point were introduced, later to be revised in 1992.

Today the formulas recommended are divided into 5 regions, see Figure C.1. For each region a set of equations and constants has been established. For example equation (C.1) (IAPWS, 2007) is the basic equation of region 1.

$$\frac{g(p, T)}{RT} = \gamma(\pi, \tau) = \sum_{i=1}^{34} n_i (7.1 - \pi)^{I_i} (\tau - 1.222)^{J_i} \quad (\text{C.1})$$

From this equation, describing Gibbs free energy ( $g$ ), all the thermodynamic properties can be derived from the dimensionless number  $\gamma$ . In the equation  $\pi$  and  $\tau$  are pressure and temperature ratios respectively between the state to be calculated and a reference state.  $R$  is the universal gas constant and  $n$ ,  $I$  and  $J$  are tabulated constants (IAPWS, 2007). The derived data has been tested for consistency and computation time before approval.

In short, the improvements from the old tables to the newer are improved calculation speed, improved accuracy, new temperature scale, new high temperature region and improved consistency at boundaries (Techware Engineering Applications, 2009).

# Bibliography

Alsthom

1993. List of heat balance diagrams.

Alsthom

2009. CO<sub>2</sub> Solutions at a Glance. Conference material.

Andersen, J. M.

2009a. Carbon Capture and Storage Technology (CCS). Slideshow.

Andersen, J. M.

2009b. Personal communication.

Andersen, J. M. and M. Köpcke

2007. Carbon Capture at NJV3 and AMV1.

Aye, L.

2007. Heat Pumps. Technical report, Dep. of Civil and Environmental Engineering, University of Melbourne.

Barillas, K.

2009. The CO<sub>2</sub>- and H<sub>2</sub>-Permeance of Membranes Composed of Highly CO<sub>2</sub>-Philic Polymers. Conference lecture.

Bhown, A.

2009. Assesment of post-combustion co<sub>2</sub> capture technologies. Conference lecture.

Bohl, W.

1994. *Strömungsmaschinen*, volume 1. Vogel Fachbuch.

Booer, A.

2009. The Global CCS Experience to Date... A Bank of Knowledge to Draw on to Support CCS in North America. Conference lecture.

Ciferno, J. P., M. Ramezan, T. J. Skone, N. ya Nsakala, and G. N. Liljedahl

2007. Carbon Dioxide Capture from Existing Coal-Fired Power Plants. Technical report, US Department of Energy.

Clarke, D., B. Debeljak, V. de Janeiro, G. Göttlicher, D. Graham, N. Kirgegaard, M. Madsen, S. Pasini, B. Stortelder, L. Strömberg, W. vom Berg, and V. Hamacher

2004. CO<sub>2</sub> Capture and Storage - VGB Report on the State of the Art. Technical report, VGB PowerTech e.V.

David, J. and H. Herzog

2000. The Cost of Carbon Capture. Technical report, Massachusetts Institute of Technology.

Djursing, T.

2007. Ingeniøren - Dongs forsøg på at rense røg for CO<sub>2</sub> halter gevaldigt. <http://ing.dk/>. Webpage.

Çengel, Y. A.

2006. *Heat and Mass Transfer, A Practical Approach -3ed.* McGraw-Hill.

Çengel, Y. A. and R. H. Turner

2005. *Fundamentals of Thermal-Fluid Sciences - 2ed.* McGraw-Hill.

## EPA

2009. Frequently asked questions about global warming and climate change: Back to basics. folder.

## EPA

2009a. US Environmental Protection Agency - 2009 Draft U.S. Greenhouse Gas Inventory Report. <http://epa.gov/>. Webpage.

## EPA

2009b. US Environmental Protection Agency - Temperature Changes. <http://epa.gov/>. Webpage.

## Eppstein, D.

1996. ICS 161: Design and Analysis of Algorithms. Lecture Notes.

## EPRI

2009a. Generation 2008, annual overview.

## EPRI

2009b. Integrated Gasification Combined-Cycle (IGCC) With CO<sub>2</sub> Capture and Storage Demonstration. Conference material.

## EPRI, N. Holt, A. Maxson, J. Parkes, J. Phillips, R. Trautz, J. Wheeldon, and J. Brehm

2008. Advanced Coal Power System with CO<sub>2</sub> Capture: EPRI's CoalFleet for Tomorrow Vision. Technical report, EPRI.

## Ericson, A.

2009. The role of CCS in Decarbonization of Power. Conference lecture.

## Favre, E., R. Bounaceur, and D. Roizard

2008. Biogas, membranes and carbon dioxide capture. Technical report, Laboratoire des Sciences Du Génie Chimique, Nancy-Université.

## Grue, J.

2009a. Brug af tal fra Alstom/BWE i rapporten. Mail correspondence.

## Grue, J.

2009b. Præsentation af projektforslag for AAU. Slideshow.

## Grue, J.

2009c. Vattenfall og NJV præsentation. Slideshow.

## Gupta, M., I. Coyle, and K. Thambimuthu

2003. CO<sub>2</sub> Capture Technologies and Opportunities in Canada. Technical report, CANMET Energy Technology Centre.

## Hammond, M.

2009. CCS with Alstom's Chilled Ammonia process at AEP's Mountaineer Plant. Conference lecture.

## Herzog, H. and D. Golomb

2004. Carbon Capture and Storage from Fossil Fuel Use. Technical report, Massachusetts Institute of Technology.

## Holton, S.

2009. KM-CDR Post-Combustion CO<sub>2</sub> Capture with KS-1<sup>tm</sup> Advanced Solvent. Conference lecture.

## Hultman, N. E.

2007. Carbon Sequestration. Technical report, Science, Technology and International Affairs, Georgetown University, Washington, USA.

## IAPWS

2005. Obsolete IAPWS Recommendations. Technical report, IAPWS.

## IAPWS

2007. Revised Release on the IAPWS Industrial Formulation 1997 for the Thermodynamic Properties of Water and Steam. Technical report, IAPWS.

- Klein, S. A.  
2009. *EES - Engineering Equation Solver for Microsoft Windows*. F-Chart Software.
- Liu, D. H. F. and B. G. Lipták  
1997. *Environmental Engineers' Handbook (2ed)*. Lewis Publishers.
- Luebke, D.  
2009. Ionic Liquids For Precombustion Capture of CO<sub>2</sub>: A Comparison of Membrane and Solvent Approaches. Conference lecture.
- Mahajan, O. P., R. Yarzab, and P. L. W. Jr  
1977. Unification of coal-char gasification reaction mechanisms. Technical report, Materials Science and Engineering Dep, Pennsylvania State University.
- Marion, J., N. ya Nsakala, T. Griffin, and A. Bill  
2008. Controlling Power Plant CO<sub>2</sub> Emissions: A Long Range View. Technical report, ALSTOM Power Technology Center.
- McLarnon, C.  
2009. Field Testing of Ammonia based CO<sub>2</sub> Capture Technology. Conference lecture.
- Mitsubishi  
2009. Mitsubishi CO<sub>2</sub> Capture Technology. Conference material.
- Northemann, A., G. Sieder, H. Garcia, and O. Spuhl  
2009. No Escape for CO<sub>2</sub>. Conference lecture. 8th Annual Conference on Carbon Capture and Sequestration.
- OSHA  
2009. Occupational Safety and Health Guideline for Ethanolamine. <http://www.osha.gov/>. Webpage.
- Park, Y. C., S.-H. Jo, S.-Y. Lee, C. K. Ryu, and C.-K. Yi  
2009. Field Test of A Potassium-Based Dry Sorbent CO<sub>2</sub> Capture Process Using Slip Stream of Coal-Fired Power Plant Flue Gas. Conference material.
- Preston-Thomas, H.  
1989. The International Temperature Scale of 1990 (ITS-90). Technical report, Comité Consultatif de Thermométrie.
- Rhee, J. S. and J. Iamchaturapatr  
2008. Carbon capture and sequestration by a treatment wetland. Technical report, Korea Institute of Science and Technology.
- Rochen, E.  
2008. False Hope - Why carbon capture and storage won't save the climate. Technical report, Greenpeace.
- Rubin, E. S. and A. B. Rao  
2002. A Technical, Economic and Environmental Assessment of Amine-based CO<sub>2</sub> Capture Technology for Power Plant Greenhouse Gas Control. Technical report, U.S. Department of Energy.
- Schatz, D. A.  
1978. Alternate Acid Gas Removal System Study. Technical report, Carnegie-Mellon University, Pittsburgh, Pennsylvania.
- Siriwardane, R.  
2009. Sorbent-Enhanced Water Gas Shift Reaction Studies. Conference lecture.
- Techware Engineering Applications  
2009. Background About IAPWS-IF97, the New Industrial Formulations for Steam Properties. <http://www.techwareeng.com/>. Webpage.
- Thomas, N.  
2009. Update on RTI's Dry Carbonate Process: Carbon Dioxide Capture from Power Plant Flue Gas. Conference lecture.

Turk, B.

2009. High Temperature CO<sub>2</sub> Capture from Syngas for Gasification Applications. Conference lecture.

Turns, S. R.

2006. *An introduction to Combustion - 2nd Edition*. McGraw-Hill.

Vattenfall

2008. Nordjylland Power Station Unit 3. Booklet.

Vattenfall

2009. Vattenfall.dk. <http://www.vattenfall.dk/>. Webpage.

Vølund A/S, Aalborg Ciser International A/S, and Burmeister & Wain A/S

2001. *Vendsysselværket, Blok 3, Anlægsdokumentation*.

Weissermel, K. and H.-J. Arpe

2003. *Industrial organic chemistry*. Wiley-VCH Verlag GmbH.

Weisstein, E. W.

2009a. Newton's Method. <http://mathworld.wolfram.com/>. Website.

Weisstein, E. W.

2009b. Secant Method. <http://mathworld.wolfram.com/>. Website.

Wildgust, N.

2009. Lessons Learned from IEA GHG R&D Program Supported Projects. Conference lecture.

WRI

2009. <http://earthtrends.wri.org/>. webpage.

Zachary, J.

2008. Options for reducing a coal-fired plant's carbon footprint: Part I. Technical report, Bechtel Power Corp.